

not necessarily represent all patients with HIV-1 infection in Japan. However, as above-mentioned, our clinic treats approximately 15% of the total HIV patients in Japan, and furthermore, characteristics of the patients with HIV-1 infection newly diagnosed and reported to the Japanese National HIV Registry in 2011 (n=1529) is very similar to those of the study population: 94% male, 64% infected through homosexual contact, and 59% in their 20s and 30s of age (http://api-net.ifap.or.jp/status/2011/11nenpo/hyo_02.pdf, in Japanese). Most HIV-1 infected patients reside in urban areas such as Tokyo metropolitan area as well. Thus, the discrepancy between the study patients and all HIV patients in Japan should not be too large. Second, the structured interview designed for data collection does not prevent underreporting of illicit drug use. However, underreporting to a certain degree is unavoidable with regard to issues such as illicit drugs [19].

In conclusion, the incidence of LTFU in illicit drug users was almost twice higher than that in non users among patients with HIV-1 infection in Japan. Multivariate analysis identified illicit drug use as a significant risk factor for LTFU, which influences prognosis of patients with HIV-1 infection. Little data is available for illicit drug use in Japan, especially among patients with HIV-1 infection. However, all relevant parties in relation to this issue need to recognize that illicit drug use has spread among patients with HIV-1 infection, and that illicit drugs

worsens adherence to HIV care in Japan. Appropriate measures for prevention and intervention of illicit drug use are urgently needed to ensure proper treatment and prevention of spread of HIV infection.

Acknowledgements

The authors thank Dr. Kiyoshi Wada, Department of Drug Dependence Research, National Institute of Mental Health, National Center of Neurology and Psychiatry, and Dr. Keishiro Yajima, AIDS Medical Center, National Hospital Organization Osaka National Hospital, for valuable comments for the manuscript. The authors also thank "coordinator nurses" who conducted the structured interviews (Ruiko Yakuwa, Beni Ito, Yuko Sugino, Miki Koyama, Kenji Takeda, Megumi Shimada, Jongmi Seo, Yuki Yamada, Kyoko Ishigaki), and all other clinical staff at the AIDS Clinical Center for their help in completion of this study.

Author Contributions

Conceived and designed the experiments: TN HG HK MT SO. Performed the experiments: MO KI. Analyzed the data: TN HK HG MT SO. Contributed reagents/materials/analysis tools: MO KI SO. Wrote the manuscript: TN HG MT SO.

References

- Egger M, May M, Chêne G, Phillips AN, Ledergerber B et al. (2002) Prognosis of HIV-1-infected patients starting highly active antiretroviral therapy: a collaborative analysis of prospective studies. *Lancet* 360: 119-129. doi:10.1016/S0140-6736(02)09411-4. PubMed: 12126821.
- Lohse N, Hansen AB, Pedersen G, Kronborg G, Gerstoft J et al. (2007) Survival of persons with and without HIV infection in Denmark, 1995-2005. *Ann Intern Med* 146: 87-95. doi:10.7326/0003-4819-146-2-200701160-00003. PubMed: 17227932.
- Hogg RS, Heath KV, Yip B, Craib KJ, O'Shaughnessy MV et al. (1998) Improved survival among HIV-infected individuals following initiation of antiretroviral therapy. *JAMA* 279: 450-454. doi:10.1001/jama.279.6.450. PubMed: 9466638.
- Wood E, Hogg RS, Yip B, Harrigan PR, O'Shaughnessy MV et al. (2004) The impact of adherence on CD4 cell count responses among HIV-infected patients. *J Acquir Immune Defic Syndr* 35: 261-268. doi:10.1097/00126334-200403010-00006. PubMed: 15076240.
- Dalal RP, Macphail C, Mqhayi M, Wing J, Feldman C et al. (2008) Characteristics and outcomes of adult patients lost to follow-up at an antiretroviral treatment clinic in Johannesburg, South Africa. *J Acquir Immune Defic Syndr* 47: 101-107. doi:10.1097/QAI.0b013e31815b833a. PubMed: 17971708.
- Bygrave H, Kranzer K, Hilderbrand K, Whittall J, Jouquet G et al. (2010) Trends in loss to follow-up among migrant workers on antiretroviral therapy in a community cohort in Lesotho. *PLOS ONE* 5: e13198. doi:10.1371/journal.pone.0013198. PubMed: 20976289.
- Brennan AT, Maskew M, Sanne I, Fox MP (2010) The importance of clinic attendance in the first six months on antiretroviral treatment: a retrospective analysis at a large public sector HIV clinic in South Africa. *J Int AIDS Soc* 13: 49. doi:10.1186/1758-2652-13-S4-O49. PubMed: 21134297.
- Lawn SD, Myer L, Harling G, Orrell C, Bekker LG et al. (2006) Determinants of mortality and nondeath losses from an antiretroviral treatment service in South Africa: implications for program evaluation. *Clin Infect Dis* 43: 770-776. doi:10.1086/507095. PubMed: 16912954.
- Mugavero MJ, Lin HY, Willig JH, Westfall AO, Ulett KB et al. (2009) Missed visits and mortality among patients establishing initial outpatient HIV treatment. *Clin Infect Dis* 48: 248-256. doi:10.1093/cid/cin5705. PubMed: 19072715.
- Giordano TP, Gifford AL, White AC Jr., Suarez-Almazor ME, Rabeneck L et al. (2007) Retention in care: a challenge to survival with HIV infection. *Clin Infect Dis* 44: 1493-1499. doi:10.1086/516778. PubMed: 17479948.
- Giordano TP (2011) Retention in HIV care: what the clinician needs to know. *Top Antivir Med* 19: 12-16. PubMed: 21852711.
- Wood E, Montaner JS, Tyndall MW, Schechter MT, O'Shaughnessy MV et al. (2003) Prevalence and correlates of untreated human immunodeficiency virus type 1 infection among persons who have died in the era of modern antiretroviral therapy. *J Infect Dis* 188: 1164-1170. doi:10.1086/378703. PubMed: 14551887.
- Strathdee SA, Palepu A, Cornelisse PG, Yip B, O'Shaughnessy MV et al. (1998) Barriers to use of free antiretroviral therapy in injection drug users. *JAMA* 280: 547-549. doi:10.1001/jama.280.6.547. PubMed: 9707146.
- Malta M, Magnanini MM, Strathdee SA, Bastos FI (2010) Adherence to antiretroviral therapy among HIV-infected drug users: a meta-analysis. *AIDS Behav* 14: 731-747. doi:10.1007/s10461-008-9489-7. PubMed: 19020970.
- Horstmann E, Brown J, Islam F, Buck J, Agins BD (2010) Retaining HIV-infected patients in care: Where are we? Where do we go from here? *Clin Infect Dis* 50: 752-761. PubMed: 20121413.
- Weber R, Huber M, Rickenbach M, Furrer H, Elzi L et al. (2009) Uptake of and virological response to antiretroviral therapy among HIV-infected former and current injecting drug users and persons in an opiate substitution treatment programme: the Swiss HIV Cohort Study. *HIV Med* 10: 407-416. doi:10.1111/j.1468-1293.2009.00701.x. PubMed: 19490174.
- Milloy MJ, Marshall BD, Kerr T, Buxton J, Rhodes T et al. (2012) Social and structural factors associated with HIV disease progression among illicit drug users: a systematic review. *AIDS* 26: 1049-1063. doi:10.1097/QAD.0b013e32835221cc. PubMed: 22333747.
- Porter K, Babiker A, Bhaskaran K, Darbyshire J, Pezzotti P et al. (2003) Determinants of survival following HIV-1 seroconversion after the introduction of HAART. *Lancet* 362: 1267-1274. doi:10.1016/S0140-6736(03)14570-9. PubMed: 14575971.
- Magnani R, Sabin K, Saidel T, Heckathorn D (2005) Review of sampling hard-to-reach and hidden populations for HIV surveillance. *AIDS* 19 Suppl 2: S67-S72. doi:10.1097/01.aids.0000167353.02289.b9. PubMed: 15930343.
- Wada K (2011) The history and current state of drug abuse in Japan. *Ann N Y Acad Sci* 1216: 62-72. doi:10.1111/j.1749-6632.2010.05914.x. PubMed: 21272011.
- Tominaga M, Kawakami N, Ono Y, Nakane Y, Nakamura Y et al. (2009) Prevalence and correlates of illicit and non-medical use of psychotropic drugs in Japan: findings from the World Mental Health Japan Survey 2002-2004. *Soc Psychiatry Psychiatr Epidemiol* 44: 777-783. doi:10.1007/s00127-009-0499-1. PubMed: 19190833.
- Wada K, Greberman SB, Konuma K, Hirai S (1999) HIV and HCV infection among drug users in Japan. *Addiction* 94: 1063-1069. doi:10.1046/j.1360-0443.1999.947106311.x. PubMed: 10707444.
- Vandenbroucke JP, von Elm E, Altman DG, Gøtzsche PC, Mulrow CD et al. (2007) Strengthening of Reporting of Observational Studies in Epidemiology (STROBE): explanation and elaboration. *Epidemiology* 18: 805-835. doi:10.1097/EDE.0b013e3181577511. PubMed: 18049195.
- Ndiaye B, Ould-Kaci K, Salleron J, Bataille P, Bonnevie F et al. (2009) Incidence rate and risk factors for loss to follow-up in HIV-infected patients from five French clinical centres in Northern France - January 1997 to December 2006. *Antivir Ther* 14: 567-575. PubMed: 19578242.
- Rice BD, Delpech VC, Chadborn TR, Elford J (2011) Loss to follow-up among adults attending human immunodeficiency virus services in England, Wales, and Northern Ireland. *Sex Transm Dis* 38: 685-690. PubMed: 21844719.
- Hidaka Y, Ichikawa S, Koyano J, Urao M, Yasuo T et al. (2006) Substance use and sexual behaviours of Japanese men who have sex with men: a nationwide internet survey conducted in Japan. *BMC Public Health* 6: 239. doi:10.1186/1471-2458-6-239. PubMed: 17002800.
- Giordano TP, Hartman C, Gifford AL, Backus LI, Morgan RO (2009) Predictors of retention in HIV care among a national cohort of US veterans. *HIV Clin Trials* 10: 299-305. doi:10.1310/hct1005-299. PubMed: 19906622.
- Qian HZ, Stinnette SE, Rebeiro PF, Kipp AM, Shepherd BE et al. (2011) The relationship between injection and noninjection drug use and HIV disease progression. *J Subst Abuse Treat* 41: 14-20. doi:10.1016/j.jsat.2011.01.007. PubMed: 21349679.
- McCroft A, Kirk O, Aitlins P, Chies A, Blaxhult A et al. (2008) Loss to follow-up in an international, multicentre observational study. *HIV Med* 9: 261-269. doi:10.1111/j.1468-1293.2008.00557.x. PubMed: 18400074.
- Lebouc'hé B, Yazdanzpanah Y, Gérard Y, Sissoko D, Ajana F et al. (2006) Incidence rate and risk factors for loss to follow-up in a French clinical cohort of HIV-infected patients from January 1985 to January 1998. *HIV Med* 7: 140-145. doi:10.1111/j.1468-1293.2006.00357.x. PubMed: 16494627.
- Latkin CA, Knudtson AR, Sherman S (2001) Routes of drug administration, differential affiliation, and lifestyle stability among cocaine and opiate users: implications to HIV prevention. *J Subst Abuse* 13: 89-102. doi:10.1016/S0899-3289(01)00070-0. PubMed: 11547627.
- Langenau SE, Teti M, Silva K, Jackson Bloom J, Harocopos A et al. (2012) Initiation into prescription opioid misuse amongst young injection drug users. *Int J Drug Policy* 23: 37-44. doi:10.1016/j.drugpo.2011.05.014. PubMed: 21689917.
- Pollini RA, Banta-Green CJ, Cuevas-Mota J, Metzner M, Teshale E et al. (2011) Problematic use of prescription-type opioids prior to heroin use among young heroin injectors. *Subst Abuse Rehabil* 2: 173-180. PubMed: 23293547.
- Wada K (2010) [Epidemiology of drug abuse and dependence]. *Nihon Rinsho* 68: 1437-1442. PubMed: 20715473.
- Forrest DW, Metsch LR, LaLota M, Cardenas G, Beck DW et al. (2010) Crystal methamphetamine use and sexual risk behaviors among HIV-positive and HIV-negative men who have sex with men in South Florida. *J Urban Health* 87: 480-485. doi:10.1007/s11524-009-9422-z. PubMed: 20101468.
- Kurtz SP (2005) Post-circuit blues: motivations and consequences of crystal meth use among gay men in Miami. *AIDS Behav* 9: 63-72. doi:10.1007/s10461-005-1682-3. PubMed: 15812614.
- Mansergh G, Shouse RL, Marks G, Guzman R, Rader M et al. (2006) Methamphetamine and sildenafil (Viagra) use are linked to unprotected receptive and insertive anal sex, respectively, in a sample of men who have sex with men. *Sex Transm Infect* 82: 131-134. doi:10.1136/sti.2005.017129. PubMed: 16581738.
- Halkitis PN, Green KA, Mourges P (2005) Longitudinal investigation of methamphetamine use among gay and bisexual men in New York City: findings from Project BUMPS. *J Urban Health* 82: 118-125. doi:10.1093/urban/ji020. PubMed: 15738324.

Pharmacokinetics of Rifabutin in Japanese HIV-Infected Patients with or without Antiretroviral Therapy

Junko Tanuma^{1*}, Kazumi Sano², Katsuji Teruya¹, Koji Watanabe¹, Takahiro Aoki¹, Haruhito Honda¹, Hirohisa Yazaki¹, Kunihisa Tsukada¹, Hiroyuki Gatanaga¹, Yoshimi Kikuchi¹, Shinichi Oka¹

1 AIDS Clinical Center, National Center for Global Health and Medicine, Tokyo, Japan, **2** Department of Drug Metabolism and Disposition, Meiji Pharmaceutical University, Tokyo, Japan

Abstract

Objective: Based on drug-drug interaction, dose reduction of rifabutin is recommended when co-administered with HIV protease inhibitors for human immunodeficiency virus (HIV)-associated mycobacterial infection. The aim of this study was to compare the pharmacokinetics of rifabutin administered at 300 mg/day alone to that at 150 mg every other day combined with lopinavir-ritonavir in Japanese patients with HIV/mycobacterium co-infection.

Methods: Plasma concentrations of rifabutin and its biologically active metabolite, 25-*O*-desacetyl rifabutin were measured in 16 cases with HIV-mycobacterial coinfection. Nine were treated with 300 mg/day rifabutin and 7 with 150 mg rifabutin every other day combined with lopinavir-ritonavir antiretroviral therapy (ART). Samples were collected at a median of 15 days (range, 5–63) of rifabutin use.

Results: The mean C_{max} and AUC_{0-24} of rifabutin in patients on rifabutin 150 mg every other day were 36% and 26% lower than on 300 mg/day rifabutin, while the mean C_{max} and AUC_{0-24} of 25-*O*-desacetyl rifabutin were 186% and 152% higher, respectively. The plasma concentrations of rifabutin plus its metabolite were similar between the groups within the first 24 hours, but it remained low during subsequent 24 to 48 hours under rifabutin 150 mg alternate day dosing.

Conclusion: Rifabutin dose of 150 mg every other day combined with lopinavir-ritonavir seems to be associated with lower exposure to rifabutin and its metabolite compared with rifabutin 300 mg/day alone in Japanese patients. Further studies are needed to establish the optimal rifabutin dose during ART. The results highlight the importance of monitoring rifabutin plasma concentration during ART.

Trial registration: UMIN-CTR (<http://upload.umin.ac.jp/cgi-open-bin/ctr/ctr.cgi?function=search&action=input&language=E>) UMIN00001102

Citation: Tanuma J, Sano K, Teruya K, Watanabe K, Aoki T, et al. (2013) Pharmacokinetics of Rifabutin in Japanese HIV-Infected Patients with or without Antiretroviral Therapy. PLoS ONE 8(8): e70611. doi:10.1371/journal.pone.0070611

Editor: Omar Sued, Fundacion Huesped, Argentina

Received: February 26, 2013; **Accepted:** June 19, 2013; **Published:** August 5, 2013

Copyright: © 2013 Tanuma et al. This is an open-access article distributed under the terms of the Creative Commons Attribution License, which permits unrestricted use, distribution, and reproduction in any medium, provided the original author and source are credited.

Funding: This work was supported by the Health Labour Sciences Research Grant (#H18-AIDS-008 and #H21-AIDS-006) from the Ministry of Health, Labour and Welfare of Japan. The funders had no role in study design, data collection and analysis, decision to publish, or preparation of the manuscript.

Competing Interests: The authors have declared that no competing interests exist.

* E-mail: jtanuma@acc.ncgm.go.jp

Introduction

Rifabutin is commonly used for human immunodeficiency virus (HIV)-associated mycobacterial infections, especially during combination antiretroviral therapy (cART) containing HIV protease inhibitors (PIs), since it is less likely to induce hepatic microsomal enzymes than rifampicin [1–4]. Conversely, rifabutin and its active metabolite, 25-*O*-desacetyl rifabutin, are substrates of CYP 3A4 and concomitant use of PIs can elevate blood concentrations of rifabutin and 25-*O*-desacetyl rifabutin [3–8]. Such rise can increase the risk of side effects such as anterior uveitis [2,9–12]. Thus, a lower dose of rifabutin has been recommended in patients treated with PIs.

The previously recommended dose of rifabutin in combination with ritonavir-boosted PI (PI/r) [13] of 150 mg every other day, was associated with low rifabutin plasma concentrations and increases rate of acquired rifampicin resistance [14–17].

Furthermore, the Tuberculosis Trials Consortium (TBTC)/US Public Health Service Study 23 [14] suggested that AUC_{0-24} of 4.5 $\mu\text{g}/\text{mL}$ is the cutoff value for risk of emergence of resistance to rifampicin. On the other hand, the combination of rifabutin at 150 mg thrice weekly with atazanavir-ritonavir provides exposure to rifabutin comparable to that of rifabutin 300 mg alone [11]. Thus, although 150 mg/day is the current recommended dose for rifabutin during PI/r-based cART [4], the optimal dose of rifabutin when used with a PI/r regimen remains to be established.

Ethnic differences, including body weight, renal clearance and various genetic factors like single nucleotide polymorphism (SNP), haplotype or DNA methylation [18,19], may alter the dose required to achieve a particular concentration of the drug in the circulation. Thus, pharmacokinetic studies involving different ethnic groups are needed to determine the recommended dose that take such factors into account. To our knowledge, there are no such pharmacokinetic studies for rifabutin use in Asians, who

are characterized by lower body weight compared with other ethnic groups. The present study was conducted to evaluate the pharmacokinetics of rifabutin in Japanese patients with HIV-1-related mycobacterial infection when used alone at 300 mg/day without cART and at 150 mg every other day when used in combination with lopinavir/ritonavir.

Methods

Ethics Statement

The study protocol was approved by the Ethics Committee of the National Center for Global Health and Medicine (NCGM-H20-580; approved on 7th February 2008). All participants provided their written informed consent before enrollment as indicated in the protocol.

The protocol for this study and supporting CONSORT checklist are available as supporting information; see File S1 for English translation of the protocol and File S2 for the Japanese original protocol and File S3 for CONSORT checklist.

Study design

Consecutive patients with HIV-1-related mycobacterial infection who received rifabutin-containing therapy at the National Center for Global Health and Medicine, Tokyo, Japan, between February 2008 and March 2009, were eligible for the study. After their written informed consent was provided, clinical history, physical examinations and laboratory tests (e.g., blood chemistry and complete blood cell count) were carried out within one week prior to the pharmacokinetic study. Patients were excluded if they were over 20 years of age or if they had abnormal liver function tests [aspartate aminotransferase (AST), alanine aminotransferase (ALT) or total bilirubin (>3 times the upper limit of normal: ULN)], or severe renal dysfunction (creatinine clearance <30 ml/min), and in the case of female patients if they were pregnant or

breastfeeding. Rifabutin was administered while fasting at 300 mg/day and the dose was adjusted when used with cART as recommended by the treatment guideline at the time of the study [13]. Medications administered concomitantly or within 2 weeks before the first study day were recorded. To evaluate the impact of rifabutin plasma concentration on treatment efficacy and adverse events, participants were followed up for at least 2 years after stopping rifabutin. Any side effect noted during rifabutin use or within four weeks after stopping rifabutin, its association with rifabutin was assessed.

Pharmacokinetic assays

Pharmacokinetic sampling commenced after 5 days of rifabutin-containing anti-mycobacterial therapy without (Group I) or with (Group II) cART. Sequential enrollment of a patient into both groups was accepted. Blood samples were collected just before rifabutin administration and then 0.5, 1, 2, 4, 6, 8 and 24 hours afterward. Patients of Group II treated with 150 mg of rifabutin every other day underwent additional sampling at 48 hours. The plasma concentrations of rifabutin and its major metabolite, 25-*O*-desacetyl rifabutin [20–23] were determined simultaneously by validated high-pressure liquid chromatography (HPLC). Blood samples were taken in heparin-containing tubes, placed on ice and centrifuged at 3000 \times g for 10 min. Then, the obtained plasma was deproteinized by using three times volume of methanol and centrifuged 15,000 \times g for 5 min, and the supernatant was used for assay. The HPLC standard for rifabutin and 25-*O*-desacetyl rifabutin were kindly provided by Pfizer Co. (Pfizer, Inc., NY). The HPLC system consisted of Agilent 1100 series (Agilent Technologies, Santa Clara, CA). Isocratic elution was performed using the Inertsil ODS-3 column (5 μm , 4.6 mm I.D. \times 150 mm; GL Sciences Inc, Tokyo, Japan) with a guard column (5 μm , 4.6 mm I.D. \times 10 mm; GL Sciences Inc). The UV detection wavelength was 280 nm. The mobile phase consisted of 9 mM

Table 1. Characteristics of study subjects.

	All (n=16)	Group I (without cART, n=9)	Group II (with cART, n=7)	p value ^a
Male sex, n	16	9	7	
Age, median years (range)	36 (23–60)	36 (23–55)	35 (23–60)	0.53
Body weight, median kg (range)	57.3 (44–66)	58.0 (46–64)	56.5 (44–66)	0.98
Mycobacterium, multiple choice, n				
<i>M. tuberculosis</i>	13	7	6	1.00
<i>M. avium</i>	4	3	1	0.94
<i>M. kansasii</i>	1	0	1	0.85
CD4 count, median cells/mm ³ (range)	63 (2–164)	63 (2–164)	63 (19–135)	0.84
Plasma viral load, median log copies/ml (range)	4.97 (3.43–6.62)	4.98 (4.18–6.62)	4.95 (3.43–5.18)	0.10
AST, median IU/L (range)	29 (16–70)	25 (16–59)	30 (17–51)	0.65
ALT, median IU/L (range)	27 (13–70)	26 (23–70)	29 (19–70)	0.31
Time on rifabutin, median days (range)	15 (5–63)	7 (5–20)	29 (10–63)	0.017
Time on cART, median days (range)	14 (10–29)	–	14 (10–29)	–
Concomitant medications, n				
lopinavir-ritonavir	7	–	7	–
clarithromycin	3	2	1	1.00
fluconazole	1	0	1	0.85

^aBy Fisher's exact test for categorical data and Mann Whitney's U test for continuous variables. cART, combination antiretroviral therapy; AST, aspartate aminotransferase; ALT, alanine aminotransferase; IU, international unit. doi:10.1371/journal.pone.0070611.t001

phosphate buffer (pH 6.8)-acetonitrile (30:70, v/v). The flow-rate was set at 1.0 ml/min and all separations were performed at 30°C in column oven.

Statistical and pharmacokinetic analyses

The area under the curve (AUC) was calculated using non-compartmental techniques (WinNonlin, ver. 5, Pharsight Corp., Mountain View, CA) based on the obtained values (AUC 0–24 h for all, AUC 0–48 h for Group II). The maximum plasma concentration (C_{max}) and time of C_{max} (T_{max}) were determined directly from the data.

Statistical analyses were performed using SPSS software package for Windows, version 17.0J (SPSS Japan Inc, Tokyo). Differences between groups were determined by using the Fisher's exact test for categorical data and the Mann-Whitney's test for continuous variables. For all statistical analyses, differences were considered significant if the p value was less than 0.05.

Results

Patient characteristics

A total of 15 patients were enrolled in the study and 5 of 15 participated in both Group I and II. In total, twenty sampling was

done for rifabutin pharmacokinetic analysis; 11 in Group I and 9 in Group II. Data from two sampling in Group I and 2 in Group II were excluded from the analysis because samples at 24-hour were unavailable or sampling was conducted earlier than 5 days of rifabutin use. As a result, data from 9 sampling in Group I and 7 sampling in Group II were used for analysis. The baseline characteristics of the 16 sampling cases are summarized in Table 1. All 7 patients of Group II were being treated with lopinavir/ritonavir as their cART, and thus rifabutin was administered at 150 mg every other day based on the guidelines at the time of the study [13]. Two cases of Group I and 1 of Group II were being treated with clarithromycin (CAM) [20] for systemic mycobacterial infection caused by *M. avium* or *M. intracellulare* (*M. avium* Complex: MAC). Five patients of Group I, in whom ART had been delayed several weeks after anti-mycobacterial therapy to prevent the immune reconstitution inflammatory syndrome (IRIS), were later enrolled in the study as patients of Group II (Figure 1). Accordingly, the median time of rifabutin use was longer in Group II than in Group I. There was no significant difference between the groups with regard to gender, age, body weight, CD4 counts, HIV-RNA load, type of mycobacteria and concomitant use of clarithromycin or fluconazole. All were Japanese and the median body weight was 57.3 kg. All patients completed their anti-

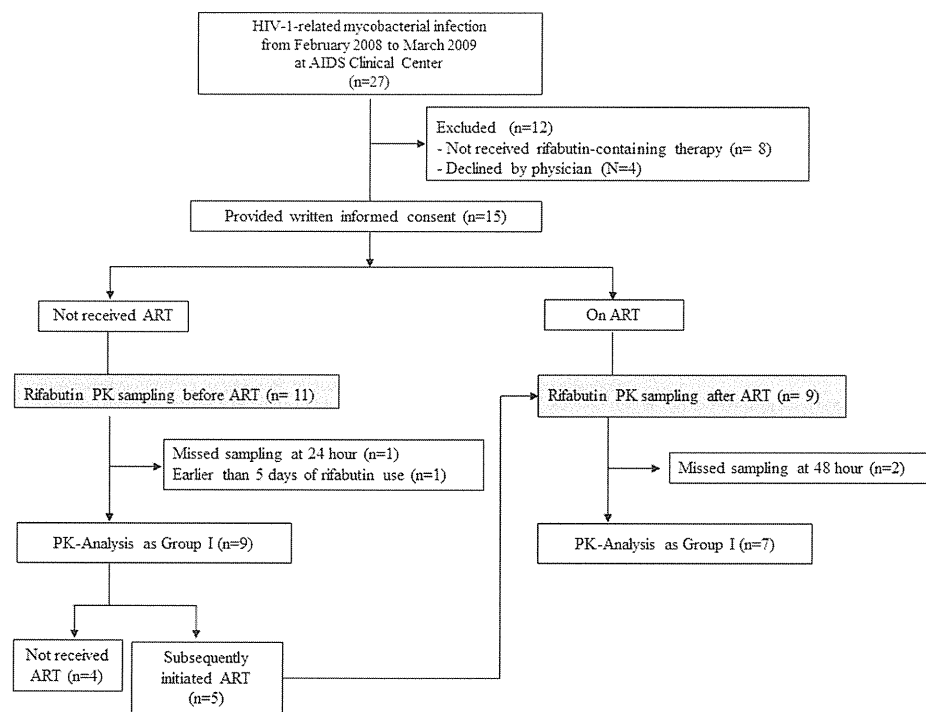


Figure 1. Flow chart of participants through the study. PK, pharmacokinetic; ART, antiretroviral therapy. doi:10.1371/journal.pone.0070611.g001

Table 2. Pharmacokinetic parameters for rifabutin and 25-O-desacetyl rifabutin.

	Group I (without combination antiretroviral therapy, n = 9)		Group II (with combination antiretroviral therapy, n = 7)		P value ^a
	Median (range)	Mean (90% CI)	Median (range)	Mean (90% CI)	
Rifabutin					
C_{max} (μ g/mL)	0.46 (0.15–0.86)	0.44 (0.39–0.49)	0.28 (0.10–0.44)	0.29 (0.25–0.33)	0.10
AUC _{0–24} (μ g h/mL)	2.79 (1.32–15.7)	4.86 (3.83–5.90)	3.00 (1.13–5.43)	3.38 (2.92–3.84)	0.38
AUC _{0–48} (μ g h/mL) ^b	5.59 (2.63–31.3)	9.71 (7.62–511.8)	4.21 (1.76–6.90)	4.58 (3.38–5.78)	0.32
T_{max} (h)	2.0 (2.0–4.0)	2.9 (2.6–3.1)	6.0 (2.0–12.0)	4.8 (4.1–5.1)	0.03
25-O-desacetyl rifabutin					
C_{max} (μ g/mL)	0.00 (0.00–0.30)	0.05 (0.03–0.08)	0.13 (0.05–0.23)	0.14 (0.12–0.16)	0.05
AUC _{0–24} (μ g h/mL)	0.00 (0.00–3.69)	0.82 (0.45–1.20)	1.52 (0.44–3.64)	2.07 (1.62–2.52)	0.12
AUC _{0–48} (μ g h/mL) ^b	0.00 (0.00–7.38)	1.64 (0.89–2.39)	5.93 (0.44–7.21)	4.32 (3.27–5.38)	0.15
T_{max} (h)	6.0 (2.0–8.0)	5.3 (4.6–6.0)	6.0 (2.0–12.0)	5.7 (4.6–6.9)	0.87
Rifabutin plus 25-O-desacetyl rifabutin					
C_{max} (μ g/mL)	0.47 (0.15–0.99)	0.49 (0.40–0.52)	0.42 (0.16–0.56)	0.39 (0.34–0.44)	0.54
AUC _{0–24} (μ g h/mL)	3.36 (1.32–19.3)	5.49 (4.18–6.76)	6.23 (1.57–7.92)	5.27 (4.48–6.07)	0.93
AUC _{0–48} (μ g h/mL) ^b	6.72 (2.63–38.7)	10.9 (8.35–13.5)	6.80 (2.20–14.1)	7.95 (6.40–9.49)	0.46

^aBy the Mann-Whitney's U test.

^bIn Group I, AUC_{24–48} is assumed the same as AUC_{0–24} and AUC_{0–48} is calculated as double of AUC_{0–24} for comparison with Group II. C_{max} , maximum plasma concentration; AUC, area under the curve; T_{max} , time of C_{max} ; CI, confidence interval. doi:10.1371/journal.pone.0070611.t002

mycobacterial treatment with clinical resolution of mycobacterial infections. None of the participants had treatment failure or relapse within more than 3 years of observation. Worsening of intra-abdominal lymphadenitis was observed in one patient with systemic *M. avium* infection at 8 months after stopping the 2-year rifabutin-containing anti-mycobacterial therapy, which excluded treatment failure or relapse. All patients confirmed complete adherence to anti-mycobacterial therapy and cART.

Pharmacokinetic parameters of rifabutin and its 25-O-desacetyl metabolite

The pharmacokinetic parameters of rifabutin and 25-O-desacetyl rifabutin are summarized in Table 2 and their mean plasma concentration-time data of 48 hours are illustrated in Figure 2A and 2B. For calculation of AUC_{0–48}, the data from 24 to 48 hours in Group I was assumed to be the same as that for 0–24 hours because rifabutin was administered once a day at the same dosage. As shown in Table 2, the mean values of C_{max} and AUC_{0–24} of rifabutin were 36% and 26% lower in Group II than in Group I, while the mean values of C_{max} and AUC_{0–24} of 25-O-desacetyl rifabutin were 186% and 152% higher in Group II than in Group I. However, the differences in the above values between the two groups were not statistically different. The low rifabutin concentration and high metabolite concentration in Group II may reflect the induction of rifabutin metabolism due to the longer duration of rifabutin use. Since 25-O-desacetyl rifabutin is microbiologically active against mycobacterium, total rifabutin activity might include rifabutin plus this metabolite. Figure 2C illustrates the mean plasma concentration of rifabutin plus the metabolite over time. Patients of Groups I and II had similar plasma concentrations of rifabutin plus the metabolite within the first 24 hours. However, the level of rifabutin plus the metabolite during the subsequent 24–48 hours was considerably lower in Group II than in Group I (dotted line in Figure 2C; Group I during 0–24 hours), whereas the AUC_{0–48} was not statistically

different between the groups. Notably, 6 (67%) cases of Group I and 5 (71%) of Group II failed to achieve the AUC_{0–24} value suggested as risk for emergence of rifamycin-resistant *M. tuberculosis* [14] (4.5 μ g h/mL). Neither C_{max} nor AUC_{0–24} of rifabutin and 25-O-desacetyl rifabutin were associated with age, body weight, body mass index, or CD4 count.

Rifabutin-associated side effects

Of the 15 participants, three patients developed side effects possibly related to rifabutin during the observational period; two of Group I developed skin rash and the other of Group II developed grade 2 rise in liver enzymes (ALT or AST 2.6–5.0 times of ULN). The skin rash appeared on day 11 of rifabutin-containing regimen in one patient and on day 28 in the other, and was resolved in both patients within several days after withdrawal of rifabutin. The rise in liver enzymes was detected after two months of rifabutin-containing regimen in combination with cART, and improved soon after discontinuation of rifabutin. Notably, the median CD4 counts in the three patients with rifabutin toxicity were significantly lower than in patients without rifabutin toxicity (12 vs 76, cells/mm³, $p = 0.028$). However, rifabutin toxicity did not correlate with rifabutin AUC_{0–24}, C_{max} , or the concurrent use of cART (rifabutin AUC_{0–24}: $p = 0.37$, rifabutin C_{max} : $p = 0.86$, cART use: $p = 0.21$).

Discussion

In the present study, a low dose of rifabutin (150 mg every other day), in combination with lopinavir/ritonavir-containing cART, yielded comparable AUC_{0–24} of rifabutin and 25-O-desacetyl rifabutin to the commonly used dose of rifabutin of 300 mg/day. The advantage of the low-dose rifabutin included lower exposure to rifabutin and metabolite during the subsequent 24 to 48 hours in Japanese patients with HIV-mycobacteria co-infection. Since many participants started their cART after at least 1 month of

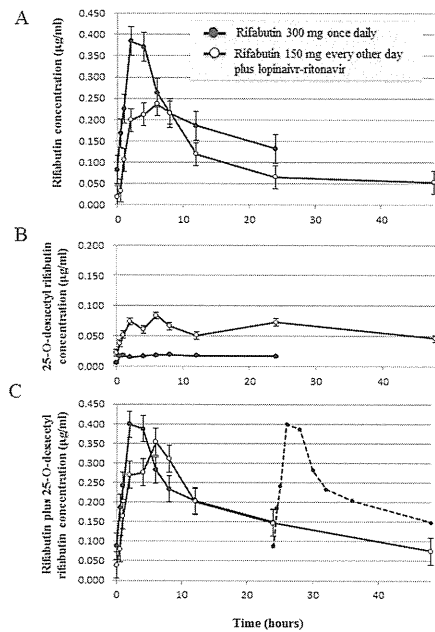


Figure 2. Mean plasma concentrations-versus-time plots of rifabutin (A), 25-O-desacetyl rifabutin (B), and rifabutin plus 25-O-desacetyl rifabutin (C). Nine patients of Group I received 300 mg of rifabutin and 7 patients of Group II received 150 mg of rifabutin every other day with lopinavir/ritonavir-containing antiretroviral therapy. Solid circles: Group I, open circles: Group II. Data are mean \pm 1 standard errors. Dotted line in Figure C represents data of Group I during 0–24 hour for reference. RBT, rifabutin; PI/r, ritonavir-boosted protease inhibitor. doi:10.1371/journal.pone.0070611.g002

anti-mycobacterial therapy in order to avoid deterioration by immune-reconstitution syndrome, the metabolism of rifabutin was induced upon the commencement of cART. This led to lower rifabutin concentration and higher 25-O-desacetyl rifabutin concentration in Group II but provided similar concentrations of rifabutin plus its active metabolite. However, on the day without medication, plasma concentrations of rifabutin and its active metabolite were lower in Group II, which were less than the susceptibility breakpoint level for *M. tuberculosis* proposed by others [20]. This suggests increased risk of emergence of rifamycin-resistant *M. tuberculosis* during the day without medication under low-dose rifabutin therapy, and that the currently recommended dosage 150 mg daily with PI/r is reasonable to this population as well. In this regard, Zhang et al. [11] reported that treatment with 150 mg/day rifabutin with atazanavir-ritonavir resulted in high risk of severe neutropenia. Furthermore, their post-hoc simulation showed that rifabutin 150 mg thrice weekly with atazanavir-ritonavir provided a comparable exposure to rifabutin compared with rifabutin 300 mg daily. Considering the risk of rifamycin-resistance and rifabutin toxicity, monitoring of rifabutin plasma

concentration should be considered until the optimal rifabutin dosing during PI/r-based cART is fully established.

Although none of the patients showed treatment failure or relapse in this study, the rifabutin AUC₀₋₂₄ observed in the study was in general close to the low end of the value reported in previous studies [7,14] and many participants [6 (67%) of Group I and 5 (71%) of Group II] failed to achieve AUC₀₋₂₄ 4.5 µg/h/mL, the cutoff value suggested as risk for emergence of rifamycin-resistant *M. tuberculosis* [14]. One of the reasons for this discordant result might be the limitation of our study of small sample size involving several MAC and *M. kansasii* infections. Since acquisition of rifamycin-resistance *M. tuberculosis* was not frequent enough in this study group, it was difficult to evaluate the association with rifabutin pharmacokinetics and emergence of rifamycin-resistance. Other reasons may be the biological characteristics of rifabutin. Rifabutin has long postantibiotic effect against *M. tuberculosis* and MAC [20], shows extensive distribution in various tissues [21,22], and readily penetrates cell membranes of leucocytes [21,22]. These characteristics and their variations among patients can considerably influence the outcome of rifabutin-containing anti-mycobacterial therapy and therefore might be one of the explanations of favorable efficacy despite lower plasma concentrations of rifabutin in our study. Another limitation of this study is that plasma concentration of isoniazid was not measured, although low isoniazid plasma concentration is known to be independently related to treatment failure of HIV/TB co-infection [24]. Additionally, although there was no difference in rifabutin concentration among the patients with or without use of clarithromycin or fluconazole, those drugs can increase the rifabutin AUC and possibly affect the results. Since our study was enrolling patients with heterogeneous backgrounds in the real clinical setting, such as timing of sampling or different combination of anti-mycobacterial drugs, it was difficult to completely eliminate those impacts from the analysis. These conditions should be taken into account in the assessment of treatment outcome and associated factors in this study.

Among 15 study participants, 3 patients developed side effects related to rifabutin therapy, including skin rash and rise in liver enzymes. Notably, their CD4 counts were lower than those who did not show rifabutin toxicity, although rifabutin plasma concentrations and the concurrent use of cART were similar in the two groups. This is the first report implicating low CD4 count as a risk factor for rifabutin-related side effects. However, like other side effects of rifabutin, such as uveitis and leukocytopenia, which have been reported to be related to high-dose rifabutin or high rifabutin plasma concentrations [9–12], careful assessment involving larger population samples are needed to evaluate the association between high plasma concentrations of rifabutin and the related skin rash and hepatotoxicity.

In conclusion, in Japanese patients with HIV-mycobacteria co-infection, the plasma concentrations of rifabutin and active metabolite within the first 24 hours of treatment with low-dose rifabutin (150 mg every other day) combined with lopinavir-ritonavir, were similar to those encountered with 300 mg/day rifabutin alone. However, these concentrations decreased on the day without medication. Our findings could help determine the optimal dose of rifabutin during cART. Further studies are needed to establish the optimal dose of rifabutin during cART. Monitoring of rifabutin plasma concentration should be considered in patients with HIV-mycobacteria co-infection.

Supporting Information

Protocol S1 Summary in English. English translation of the protocol Summary. (DOCX)

Protocol S1 Protocol and IC form in Japanese. The full version of the study protocol and the informed consent form in Japanese. (PDF)

CONSORT Checklist S2. (DOC)

References

- American Thoracic Society, Centers for Disease Control and Prevention and the Infectious Diseases Society. (2003) American Thoracic Society/ Centers for Disease Control and Prevention/ Infectious Diseases Society of America: treatment of tuberculosis. *Am J Respir Crit Care Med* 6: 605–662.
- Pfizer, Inc. Mycobutin (rifabutin) prescribing information. Pfizer, Inc., New York, NY. Available: http://www.pfizer.com/files/products/usp_mycobutin.pdf. Accessed 2012 August 21.
- Centers for Disease Control and Prevention. (2009) Guidelines for Prevention and Treatment of Opportunistic Infections in HIV-Infected Adults and Adolescents. *MMWR* 58: 1–207.
- Panel on Antiretroviral Guidelines for Adults and Adolescents. Guidelines for the use of antiretroviral agents in HIV-1-infected adults and adolescents. Department of Health and Human Services. Available: <http://aidsinfo.nih.gov/contentfiles/rguidelines/AdultandAdolescentGL.pdf>. Accessed 2012 August 21.
- Kraft WK, McCrea JB, Winchel GA, Carides A, Lowry R, et al. (2004) Indinavir and rifabutin drug interactions in healthy volunteers. *J Clin Pharmacol* 44: 305–313.
- Ford SL, Chen YC, Lou Y, Borland J, Min SS, et al. (2008) Pharmacokinetic interaction between fosamprenavir-ritonavir and rifabutin in healthy subjects. *Antimicrob Agents Chemother* 52: 534–538.
- Boulangier C, Hollender E, Farrell K, Stambaugh JJ, Maassen D, et al. (2009) Pharmacokinetic evaluation of rifabutin in combination with lopinavir-ritonavir in patients with HIV infection and active tuberculosis. *Clin Infect Dis* 49: 1305–1311.
- Zhang X, Fetterer S, Zwanziger E, Rowell L, Salgo M, et al. (2011) Pharmacokinetic interaction study of ritonavir-boosted saquinavir in combination with rifabutin in healthy subjects. *Antimicrob Agents Chemother* 55: 680–687.
- Centers for Disease Control and Prevention. (1994) Uveitis associated with rifabutin therapy. *MMWR* 43: 658.
- Shafraun SD, Singer J, Zarovny DP, Deschênes J, Phillips P, et al. (1998) Determinants of rifabutin-associated uveitis in patients treated with rifabutin, clarithromycin, and ethambutol for *Mycobacterium avium* complex bacteremia: a multivariate analysis. *Candian HIV Trials Network Protocol 010 Study Group. J Infect Dis* 177: 252–255.
- Zhang J, Zhu L, Stonier M, Coumbis J, Xu X, et al. (2011) Determination of rifabutin dosing regimen when administered in combination with ritonavir-boosted atazanavir. *J Antimicrob Chemother* 66: 2075–2082.

Acknowledgments

We thank all the staff of the AIDS Clinical Center for the care of patients.

Author Contributions

Conceived and designed the experiments: JT. Performed the experiments: JT KS. Analyzed the data: JT. Contributed reagents/materials/analysis tools: JT KS. Wrote the paper: JT. Technical advice: YK. Patients' recruitment: KW TA HH HY K. Tsukada. Technical advice: K. Teruya HG SO.

OPEN

SUBJECT AREAS:
INFECTION
HIV INFECTIONS
RETROVIRUS
VIRAL MEMBRANE FUSION

Arginine insertion and loss of N-linked glycosylation site in HIV-1 envelope V3 region confer CXCR4-tropism

Kiyoto Tsuchiya¹, Hiroataka Ode^{2,3}, Tsunefusa Hayashida^{1,4}, Junko Kakizawa¹, Hironori Sato², Shinichi Oka^{1,4} & Hiroyuki Gatanaga^{1,4}

¹AIDS Clinical Center, National Center for Global Health and Medicine, 1-21-1 Toyama, Shinjuku-ku, Tokyo 162-8655, Japan, ²Pathogen Genomics Center, National Institute of Infectious Diseases, 4-7-1 Gokuen, Musashimurayama-shi, Tokyo 208-0011, Japan, ³Clinical Research Center, National Hospital Organization Nagoya Medical Center, 4-1-1 Sannomaru, Naka-ku, Nagoya 460-0001, Japan, ⁴Center for AIDS Research, Kumamoto University, 2-2-1 Honjo, Chuo-ku, Kumamoto 860-0811, Japan.

Received 12 April 2013

Accepted 24 July 2013

Published 8 August 2013

Correspondence and requests for materials should be addressed to H.G. (higatana@acc.ncgm.go.jp)

The third variable region (V3) of HIV-1 envelope glycoprotein gp120 plays a key role in determination of viral coreceptor usage (tropism). However, which combinations of mutations in V3 confer a tropism shift is still unclear. A unique pattern of mutations in antiretroviral therapy-naïve HIV-1 patient was observed associated with the HIV-1 tropism shift CCR5 to CXCR4. The insertion of arginine at position 11 and the loss of the N-linked glycosylation site were indispensable for acquiring pure CXCR4-tropism, which were confirmed by cell-cell fusion assay and phenotype analysis of recombinant HIV-1 variants. The same pattern of mutations in V3 and the associated tropism shift were identified in two of 53 other patients (3.8%) with CD4⁺ cell count <200/mm³. The combination of arginine insertion and loss of N-linked glycosylation site usually confers CXCR4-tropism. Awareness of this rule will help to confirm the tropism prediction from V3 sequences by conventional rules.

Since the introduction of maraviroc, a specific CCR5 antagonist, into clinical practice, scientific and clinical studies have focused on the coreceptor usage of human immunodeficiency virus type 1 (HIV-1). Evidence indicates the presence of a homogeneous population of predominantly CCR5-tropic variants^{2,3} early in HIV-1 infection^{4,5}. CXCR4-tropic variants^{6,7}, against which specific CCR5 antagonists are inefficient, can be distinguished from R5-tropic variants by their tendency for higher replication kinetics and a broader target cell range⁸. Their presence *in vivo* has been associated with accelerated fall in CD4⁺ cell count and rapid disease progression^{9,10}. CXCR4-tropic variants evolve from CCR5-tropic ones in the natural course of HIV-1 infection, though the exact mechanism of viral tropism evolution is not known yet. Long-term observation of natural course, which is indispensable for understanding the mechanism of tropism evolution, is usually difficult, because early use of antiretroviral therapy (ART) is highly recommended¹¹. In this study, untreated natural course of one hemophiliac, who acquired HIV-1 infection through contaminated blood product before 1985 and exhibited slow disease progression, was followed until a rapid fall in CD4⁺ cell count in 2007. The sequence change in the HIV-1 envelope (Env) glycoprotein gp120 V3 region (V3), the main determinant of HIV-1 tropism¹², was analyzed between 2003 and 2007. The results identified a unique change in 2007 associated with change in HIV-1 tropism. The same kind of sequence change in V3 was also identified in two other patients and in some of the registered sequences in the Los Alamos HIV sequence database.

Results

V3 sequence changes in Case 1. Case 1 was an ART-naïve Japanese hemophiliac who acquired HIV-1 subtype B infection through contaminated blood product before 1985 and exhibited a slow disease progression. We reported previously the emergence of an escape mutation in HIV-1 Pol from cytotoxic T-lymphocyte (CTL) response in association with a mild increase in viral load in 1999 in this patient (KI-127)¹³. The HIV-1 viral load was steady around 10⁴ copies/mL between 2002 and 2006 (Figure 1a). However, at the end of 2006, the viral load began to increase, coupled with a rapid fall in CD4⁺ cell count. Since the emergence of CXCR4-tropic variants was suspected, changes in the V3 region were analyzed at five time points (June 2003, April 2006, and January, April, and November 2007) by sequencing 19–27 clones. Originally, most of the clones had identical or resembled V3

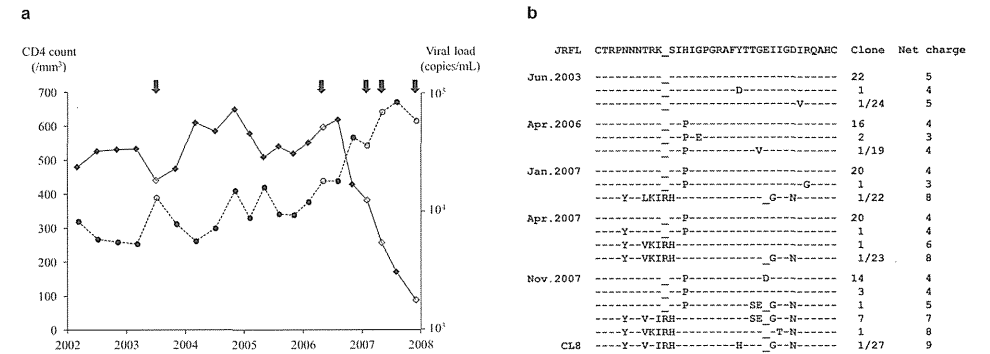


Figure 1 | (a). Clinical course of Case 1. The CD4⁺ cell count (diamonds and solid lines) and HIV-1 load (circles and broken lines) from 2002 to 2008 are plotted. Arrows at the top indicate the five time points when V3 sequences were analyzed. Open diamonds and circles indicate the CD4⁺ cell counts and HIV-1 loads at the same five time points. (b). V3 sequence changes in Case 1. Cloned sequences analyzed at the five time points are shown. The V3 sequence of HIV-1 JRFL is shown at the top column as a reference. Amino acids identical to those of HIV-1 JRFL are indicated as dashes. The numbers of clones harboring the corresponding V3 sequences are shown on the right.

sequences with CCR5-tropic HIV-1 JRFL (Figure 1b). Interestingly, a unique clone, harboring arginine insertion at position 11 of V3 (Ins11R), one amino acid deletion at position 25 (Del25), and other multiple amino acid substitutions, was identified at a frequency of 1/22 in January 2007, and the frequency of the same kind of the clones subsequently increased to 2/23 in April 2007, and 9/27 in November 2007, which was considered to be associated with the rapid fall in CD4⁺ cell count.

Insertion and deletion confer CXCR4-tropism. In the next step, cell-cell fusion assay was performed to analyze the effect of the observed V3 changes on viral tropism, using Env-expressing 293 T cells and CD4⁺ and CCR5⁺/CXCR4⁺ COS-7 cells. One V3 clone

harboring Ins11R and Del25 identified in November 2007, named CL8-V3 (Figure 1b), was incorporated into JRFL Env-expressing plasmid. The cell-cell fusion assay demonstrated that CL8-V3 was purely CXCR4-tropic whereas JRFL was purely CCR5-tropic (Figure 2a). Ins11R occurred by the insertion of 'ACA' between 'G' and 'T' of 'AGT' at position 11 at nucleotide sequence level, and therefore, the substitution of serine (S) with histidine (H) at position 12 (S12H) was also associated with Ins11R in Case 1 ('AGT' → 'AGACAT' at nucleotide level; 'S' → 'RH' at amino acid level [Ins11R/S12H]). To identify the determinant of observed tropism change, the plasmids harboring Ins11R/S12H, Del25, and Ins11R/S12H/Del25 were also constructed using JRFL backbone. In the cell-cell fusion assay, Ins11R/S12H decreased CCR5-tropism of

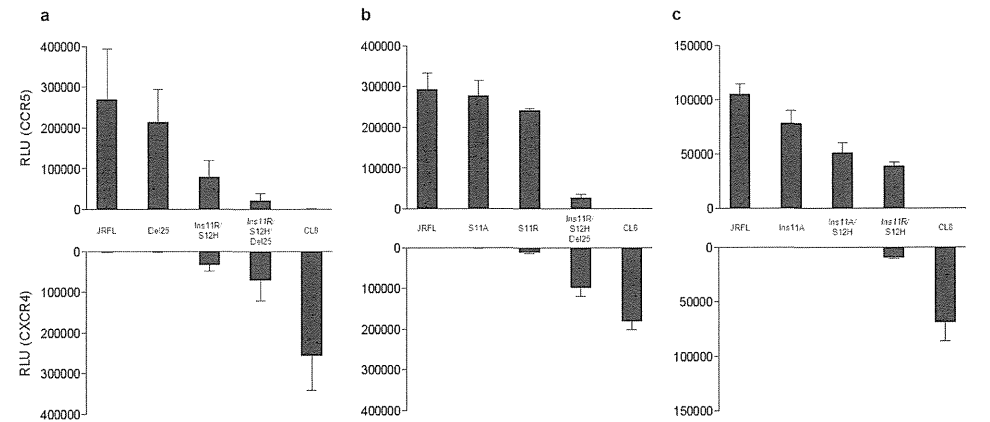


Figure 2 | Effect of Ins11R/S12H and Del25 in cell-cell fusion assay (a). Cell-cell fusion assay was performed using Env-expressing 293 T cells and CD4⁺ and CCR5⁺/CXCR4⁺ COS-7 cells. Data are mean ± SD values in relative luminescent unit (RLU) of six experiments (performed in duplicate and repeated three times). Analysis of two elements of Ins11R in cell-cell fusion assay (b and c). Effects of placing R at position 11 (b) and one amino acid elongation of V3 (c) were analyzed. Cell-cell fusion assay was performed using Env-expressing 293 T cells and CD4⁺ and CCR5⁺/CXCR4⁺ COS-7 cells. Data are mean ± SD values in relative luminescent unit (RLU) of six experiments (performed in duplicate and repeated three times).

JRFL-V3 and conferred CXCR4-tropism, resulting in dual-tropic (Ins11R/S12H vs. JRFL). Del25 further decreased the CCR5-tropism of Ins11R/S12H-V3 and increased CXCR4-tropism (Ins11R/S12H/Del25 vs. Ins11R/S12H), though Del25 alone did not significantly change the JRFL-V3 tropism (Del25 vs. JRFL). Considered together, the results suggest that Ins11R/S12H is indispensable for CXCR4-tropism of CL8-V3 and that Del25 strengthened the CXCR4-tropism in the presence of Ins11R/S12H. However, their combination was not enough to confer JRFL-V3 pure CXCR4-tropism (Ins11R/S12H/Del25-V3-expressing 293 T cells still fused with CD4⁺/CCR5⁺ COS-7 cells at low level), and some other mutations were necessary for pure CXCR4-tropism of CL8-V3.

Which is important, substitution or elongation? The above results suggested that Ins11R/S12H was indispensable for CXCR4-tropism of CL8-V3. According to the 11/25 rule, a basic amino acid residue (R or lysine [K]) at either position 11 or 25 of V3 is associated with CXCR4-tropism, whereas acidic or neutral amino acid residues at these positions are associated with CCR5-tropism^{12,14,15}. Ins11R/S12H has two elements: one is to place R at position 11 and the other is one amino acid elongation of V3. To determine whether positioning R at 11 is sufficient for conferring CXCR4-tropism or whether V3 elongation is also necessary for this process, S at position 11 of JRFL-V3 was substituted with R (S11R) and alanine (A) (S11A) as reference. However, both substitutions did not alter the pure CCR5-tropism of JRFL (Figure 2b), indicating that not only R at position 11 but also one amino acid elongation was indispensable for dual tropism caused by Ins11R/S12H.

Is one amino acid elongation sufficient to induce CXCR4-tropism or is positioning R at 11 is also necessary? To answer this question, two V3-expressing plasmids were constructed; one harbored Ins11A only and the other harbored Ins11A and S12H (Ins11A/S12H). The cell-cell fusion assay indicated that Ins11A decreased and Ins11A/S12H further decreased infectivity with CCR5 though neither of them conferred CXCR4-tropism (Figure 2c). These results indicate that not only one amino acid elongation of V3 but also positioning R at 11 is indispensable for dual tropism caused by Ins11R/S12H.

Effect of net charge of V3. Ins11R/S12H conferred CXCR4-tropism and Del25 strengthened it. However, Ins11R/S12H/Del25-V3 was still dual-tropic, though CL8-V3 was purely CXCR-4 tropic. The next question was which mutation is necessary for Ins11R/S12H/Del25-V3 to become purely CXCR4-tropic, like CL8-V3 (to lose CCR5-tropism)? There are six amino acid substitutions in CL8-V3 (substitution of asparagine [N] with tyrosine [Y] at position 5 [N5Y], substitution of threonine [T] with valine [V] at position 8 [T8V], substitution of K with isoleucine [I] at position 10 [K10I], substitution of Y with H at position 22 [Y22H], substitution of V with glycine [G] at position 26 [V26G], and substitution of aspartic acid [D] with N at position 29 [D29N]), compared with Ins11R/S12H/Del25-V3. According to the net charge rule, the higher net charge of V3 is associated with CXCR4-tropism when calculated by subtracting the number of negatively charged amino acid residues (D and glutamic acid [E]) from the number of positively charged ones (K and R)^{12,14}. D29N was the only amino acid substitution that increased the net charge of V3 among the six amino acid substitutions described above. Therefore, we analyzed the effect of D29N by adding D29N to Ins11R/S12H/Del25-V3 (Ins11R/S12H/Del25/D29N) and reverting it in CL8-V3 (CL8/N29D). In the cell-cell fusion assay, D29N reduced CCR5-tropism of Ins11R/S12H/Del25-V3 though it remained dual-tropic (Ins11R/S12H/Del25/D29N vs. Ins11R/S12H/Del25), and the reversion of D29N did not change CL8-V3 tropism (CL8/N29D vs. CL8) (see Supplementary Figure S1). These results indicate that D29N does not cause tropism difference between Ins11R/S12H/Del25-V3 and CL8-V3, indicating that the net charge rule did not work well.

In silico prediction of the effect of substitutions. Adding D29N failed to alter the tropism of Ins11R/S12H/Del25-V3 from dual-tropic to purely CXCR4-tropic. There were five other amino acid substitutions between Ins11R/S12H/Del25-V3 and CL8-V3. Because the V3 conformation is important for coreceptor interactions¹⁶ and because conformation of V3 loop is sensitive to V3 mutations^{17,18}, we examined how these V3 mutations could influence conformation of V3 in solution using molecular dynamics (MD) simulation¹⁹. In our MD simulation study, V3-loops of JRFL and Del25 (both CCR5-tropic) were placed in the opposite direction from the β 20- β 21 loop (Figure 3a), while CL8-V3 loop (CXCR4-tropic) was closed to and in the same direction from the β 20- β 21 loop (Figure 3c). The results were consistent with those obtained with gp120_{1A1} recombinant outer domains containing CCR5-tropic and CXCR4-tropic V3 loop, respectively^{17,18}. The loops of dual-tropic Ins11R/S12H-V3 and Ins11R/S12H/Del25 were located between Del25-V3 and CL8-V3 (Figure 3b). In fact, when the structural differences at the tip of the V3 tip region, i.e., the 'GPGR' amino acid residues were quantitatively measured with the root mean square deviation (RMSD) of the main chain¹⁷, CL8-V3 was found to be located far from the loop of JRFL-V3 and Del25-V3, while those of Ins11R/S12H-V3 and Ins11R/S12H/Del25-V3 were between them (Table 1). These results suggest that our MD simulation could predict the V3 tropism based on the magnitude of the RMSD values of the V3 loop tip. In the next step, each of the six amino acid substitutions of CL8-V3 was incorporated into Ins11R/S12H/Del25-V3, and the location and conformation of the constructed loop was analyzed. When D29N was incorporated, the RMSD from JRFL-V3 decreased and that from CL8-V3 increased (Table 2), and the loop orientation was still similar to that of Ins11R/S12H/Del25 (Figure 3d), suggesting that D29N does not seem to change the tropism, compatible with the results of the cell-cell fusion assay (see Supplementary Figure S1). Among other single amino acid substitutions, only T8V was found to increase the RMSD from JRFL-V3 and decrease that from CL8-V3 (Table 2), and caused a positional shift of the V3 resembling that of the CL8-V3 (Figure 3e). N5Y did not change the orientation of the V3 loop (see Supplementary Figure S2a) though the RMSD from CL8-V3 increased and that from JRFL-V3 decreased (Table 2). K10I, Y22H, and V26G decreased the RMSD from JRFL-V3 and increased that from CL8-V3 (Table 2), and the V3 loop orientation was distinct from both Ins11R/S12H/Del25-V3 and CL8-V3 (see Supplementary Figure S2b, S2c, and S2d). These results suggest that among the six amino acid substitutions, T8V has the greatest impact on the tropism shift toward CXCR4-tropic.

Impact of T8V. Our *in silico* modeling predicted that T8V could alter the tropism of Ins11R/S12H/Del25-V3. In the next series of experiments, we incorporated T8V into JRFL-V3 (JRFL/T8V) and Ins11R/S12H/Del25-V3 (Ins11R/S12H/Del25/T8V), and analyzed the effect of such incorporation on their tropism using the cell-cell fusion assay. The incorporation of T8V into JRFL-V3 increased CCR5-tropism though it did not confer CXCR4-tropism (Figure 4a and 4b). However, T8V abrogated CCR5-tropism of Ins11R/S12H/Del25-V3 and converted it to purely CXCR4-tropic, although it did not increase CXCR4-tropism and Ins11R/S12H/Del25/T8V-V3 still had smaller CXCR4-tropism than CL8-V3 (Figure 4a). The combination of Ins11R/S12H/T8V was sufficient to confer CXCR4-tropism, although Del25/T8V did not (Figure 4b). T8V breaks the N-linked glycosylation motif 'NXT' at position 6-8 of V3, the loss of which was reported with tropism shift towards CXCR4-tropic^{20,21}. Our results indicated that T8V was indispensable for pure CXCR4-tropism of CL8, which seemed to support the previous findings of the importance of the loss of N-linked glycosylation motif for CXCR4-tropism. The loss of the glycan moiety in V3 stem might lead to change gp120 interaction surface for coreceptor binding and influence coreceptor

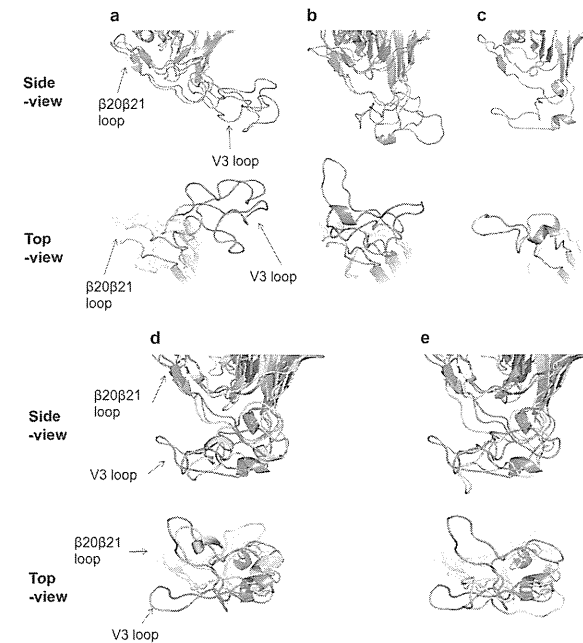


Figure 3 | Structural models of V3 loops on HIV-1 gp120 outer domains (a, b and c). MD simulations were performed for the HIV-1 JRFL gp120 outer domain with various V3 loops for CCR5 (a), dual (b), and CXCR4 (c) tropism. The most frequently appeared structures during 5–10 ns of MD simulations were extracted, and the top and side views of the structures around V3 loops are highlighted. (a) JRFL (gray) and Del25 (navy). (b) Ins11R/S12H/Del25 (gray) and Ins11R/S12H (navy). (c) CL8 (gray). Structural models of V3 loops of Ins11R/S12H/Del25-derived mutants (d and e). MD simulations were performed for the HIV-1 Ins11R/S12H/Del25 gp120 outer domain with D29N (d) or T8V (e) substitution in V3 loop. The most frequently appeared structures during 5–10 ns of MD simulations were extracted and superimposed with those of Ins11R/S12H/Del25 and CL8. (d) Superimposition of D29N (green), Ins11R/S12H/Del25 (gray), and CL8 (navy). (e) Superimposition of Ins11R/S12H/Del25/T8V (green), Ins11R/S12H/Del25 (gray), and CL8 (navy). Top and side views of the structures around V3 loops are shown.

tropism. However, available structural information was against this possibility, because the glycosylation site was exposed toward an opposite direction from the putative coreceptor binding site on V3^{16,22,23}. Accordingly, presence or absence of the glycan moiety in V3 stem did not cause significant differences in V3 configuration in our MD simulation system^{17,24}. Probably, amino acid substitution itself altered V3 configuration and coreceptor tropism.

GHOST cell infection assay. Our cell-cell fusion assay indicated that Ins11R/S12H and T8V were indispensable for pure CXCR4-tropism of CL8. The next series of experiments were designed to confirm the findings using HIV-1 infection assay in GHOST cells^{25,26}. HIV-1 JRFL and the recombinant HIV-1 variants harboring Del25-V3 and T8V-V3 had the same level of CCR5-tropism, although none could infect CXCR4⁺ GHOST cells (Figure 4c). In comparison, Ins11R/S12H-V3- and Ins11R/S12H/Del25-V3-harboring variants had lower levels of CCR5-tropism. The latter variant, but not the former, infected CXCR4⁺ GHOST cells though at low level. The Ins11R/S12H/Del25/T8V-V3-harboring variant lost the CCR5-tropism and acquired CXCR4-tropism, although the level of CXCR4-tropism was still lower than those of CL8-V3-harboring variant and HIV-1 NL4-3 (a CXCR4-tropic experimental strain). These results were compatible with the above-mentioned results of the cell-cell fusion assay, though the CCR5-tropism of Ins11R/S12H/Del25-V3 seemed stronger in the cell infection assay. Dual-tropic Ins11R/S12H/Del25-V3 might have decreased susceptibility to AMD3100 used in the CCR5⁺ GHOST Hi5 assay compared with pure CXCR4-tropic CL8-V3 and NL4-3-V3.

Same V3 pattern in two other cases. The analysis of V3 sequence changes in Case 1 demonstrated that Ins11R and the loss of N-linked

Table 1 | Overall structural differences between the two V3 loop tips of various HIV-1 variants

ID of V3	RMSD (Å)*			
	JRFL	Del25	Ins11R/S12H	Ins11R/S12H/Del25
Del25	13.8	-	-	-
Ins11R/S12H	17.4	8.6	-	-
Ins11R/S12H/Del25	29.4	28.7	23.6	-
CL8	38.9	37.5	33.1	14.2

*RMSD values of the main chain atoms at V3 tips (GPGR) of two gp120 outer domain models from MD simulations. A smaller RMSD value means a closer conformation between two gp120s.

Table 2 | Effect of a single amino acid substitution on overall structure of the gp120 V3 tip

ID of V3	Added mutations*	RMSD (Å) ^a	
		JRFL	CL8
Ins11R/S12H/Del25	None	29.4	14.2
Ins11R/S12H/Del25/N5Y	N5Y	32.5	14.1
Ins11R/S12H/Del25/T8V	T8V	33.6	12.6
Ins11R/S12H/Del25/K10I	K10I	26.3	39.4
Ins11R/S12H/Del25/Y22H	Y22H	28.6	27.0
Ins11R/S12H/Del25/V26G	V26G	28.4	19.6
Ins11R/S12H/Del25/D29N	D29N	28.4	17.0

*Added amino acid substitution in the V3 loop of the Ins11R/S12H/Del25 gp120.

^aRMSD values of the main chain atoms at V3 tips (GPGR) of two gp120 outer domain models from MD simulations.

glycosylation site indispensably contribute to a shift toward CXCR4-tropism. To determine whether this finding was true only in Case 1 or could be generalized to other cases, HIV-1 subtype B V3 sequences were analyzed in 53 other treatment-naïve patients with CD4⁺ cell count < 200/mm³. The same pattern of mutations was identified in two cases (3.8%). In one case (Case 2), four of twenty analyzed sub-clones of V3 sequences harbored Ins11R associated with S12H, Del25, and N6A resulting in the loss of N-linked glycosylation site, compared with JRFL-V3 (Figure 5). In the other case (Case 3), three of twenty-two sub-clones harbored Ins11R associated with S11R, Del25, and T8V, resulting in the loss of N-linked glycosylation site. To delineate the tropism of the V3 abovementioned clones, two V3 clones in each case, one harboring Ins11R and the loss of N-linked glycosylation site (KF6 in Case 2, T16 in Case 3 [see Figure 5]) and the other harboring none of them (KF8 in Case 2, T02 in Case 3 [see Figure 5]), was incorporated into JRFL Env-expressing plasmid. As expected, cell-cell fusion assay indicated that the clones harboring Ins11R and the loss of N-linked glycosylation site (KF6 and T16) were purely CXCR4-tropic, although the clones harboring none of them (KF8 and T02) were purely CCR5-tropic (Figure 6a and 6b). The results of the GHOST cell infection assay using V3-incorporated HIV-1 JRFL (Figure 6c) were similar to those of the cell-cell fusion

assay. Accordingly, it was concluded that the findings of the indispensability of Ins11R and the loss of N-linked glycosylation site for CXCR4-tropism were not only true in Case 1 but also in other cases.

Discussion

The phenotypic assay TrofileTM (Monogram Bioscience, South San Francisco, CA), which is based on recombinant virus technology, has been the most widely used diagnostic test for the detection of CXCR4-tropic HIV-1 variants²⁷. However, this method has logistical and technical limitations that make it far from convenient as a diagnostic test in clinical practice. Genotypic methods based on V3 sequence represent a more feasible alternative²⁸ and are progressively replacing phenotypic assays, though their clinical use requires good genotypic-phenotypic correlations. The 11/25 rule and the net charge rule were proposed for the tropism prediction from V3 sequence^{12,14,15}, although they show only a moderate correlation with the results of phenotypic assays^{12,15,28}. The results of specific genotypic tools, such as geno2pheno (Max-Planck Institute, Munich, Germany)^{29,30} and position-specific scoring matrix (PSSM)^{31,32} are comparable to those of phenotypic assays, suggesting that there should be some more genetic determinations for viral tropism. In this study, we successfully demonstrated two rules other than the 11/25 rule and the net charge rule on the association with CXCR4-tropic variants. One was that R insertion at position 11 of V3, not just placing R at position 11 but also one amino acid elongation, strongly shifted the HIV-1 tropism towards CXCR4-tropic. The other was that the loss of N-linked glycosylation site in V3 also shifted viral tropism towards CXCR4-tropic, which was previously described in some reports^{20,21}. In the V3 analysis in our index case, R insertion at position 11 conferred dual-tropism to originally CCR5-tropic V3, and the loss of N-linked glycosylation site altered it totally CXCR4-tropic (see Supplementary Figure S3). We identified these mutation patterns not only in the index case but also in two other cases. When we surveyed V3 sequences with tropism confirmed by phenotypic assay registered at the Los Alamos HIV sequence database (Los Alamos National laboratory, Los Alamos, NM) (<http://www.hiv.lanl.gov>, as of September 25, 2012), 28 sequences had R insertion at position 11; 7 of 199 (3.5%) CXCR4-tropic, 14 of 513

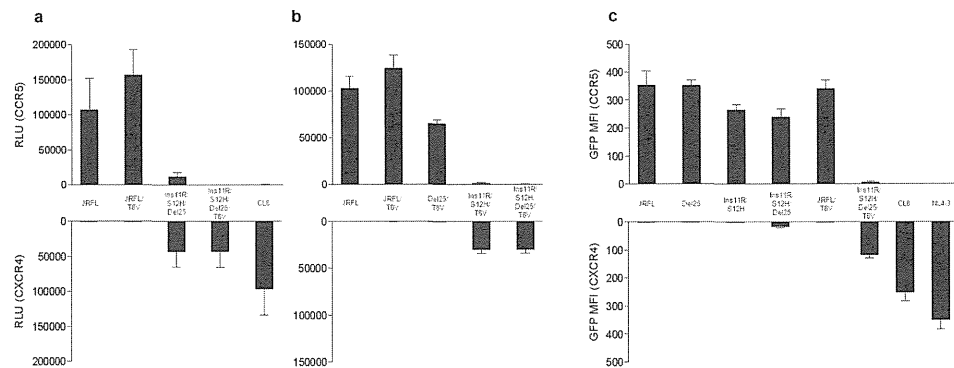


Figure 4 | Effects of T8V in cell-cell fusion assay (a and b). The effects of T8V were analyzed in combination with Ins11R/S12H/Del25 (a), and Del25 and Ins11R/S12H (b). Cell-cell fusion assay was performed using Env-expressing 293T cells and CD4⁺ and CCR5⁺/CXCR4⁺ COS-7 cells. Data are mean ± SD values in relative luminescent unit (RLU) of six experiments (performed in duplicate and repeated three times). Tropism of recombinant HIV-1 variants harboring mutations identified in Case 1 (c). Tropism of HIV-1 variants was assessed in CCR5⁺ GHOST Hi5 and CXCR4⁺ GHOST CXCR4 cells. The mean fluorescent intensity (MFI) of infected cells expressing green fluorescent protein (GFP) was measured. Data are mean ± SD values of six experiments (performed in duplicate and repeated three times).

	JRFL	CTRPNNNTRK_SIHIGPGRAFYTTGEIIGDIRQAHC	Clone	Net charge
Case2	KF8	-----G--M-----F-DN-----K---	12	6
		-----R G--M-----F-DN-----K---	2	6
		-----G--M-----G--F-DN-----K---	1	5
		-----G--M-----F-DN-----K-Y-	1	5
	KF6	---AI-K-RHF-----NN_KV---K---	2	10
	---AI-KRRHF-----NK--V---K---	1	9	
	---AI-K-RHF-----N_KV---K---	1/20	10	
Case3	T02	-----FA-D-----N--K-Y-	16	6
		-----FA-D-----K-Y-	2	5
		-----FA-D-----K-Y-	1	5
	T16	-----KVIRRR-----VA-D_TT---K-Y-	3/22	7

Figure 5 | Cloned V3 sequences in Cases 2 and 3. The V3 sequence of HIV-1 JRFL is shown at the top column as a reference. Amino acids identical to those of HIV-1 JRFL are indicated as dashes. The numbers of clones harboring the corresponding V3 sequences are shown on the right.

(2.7%) dual-tropic, and 7 of 3301 (0.2%) CCR5-tropic sequences. Their frequency was significantly higher in CXCR4-tropic and dual-tropic sequences than CXCR5-tropic ones ($p < 0.0001$; Chi-square test). (All of the 7 CCR5-tropic sequences with R insertion at position 11 were sub-clones derived from one pair of a transmitter mother and her transmitted child³³, and the sequences were so unique that it was actually difficult to determine the exact site of one amino acid insertion). Interestingly, all of the 28 V3 sequences with R insertion at position 11, had lost the N-linked glycosylation site and had one amino acid deletion in the C-terminal half of V3 (one amino acid deletion at position 24 or 25 in 18 sequences [64.3%]), similar to our three cases. No other amino acid elongation patterns were found in the N-terminal half of V3 in the Los Alamos database. There were 3,301 CCR5-tropic V3 sequences registered in the database. Among them, 18 sequences had a basic amino acid residue at position 11 and therefore they were misjudged as CXCR4-tropic by the 11/25 rule. Only 7 of them had R insertion and the other 11 were recognized as CCR5-tropic by our rules. Therefore using our rules increased the

specificity from 99.5% [(3,301-18)/3,301] to 99.8% [(3,301-7)/3,301] in identifying CXCR4- or dual-tropic V3 sequences in the Los Alamos database.

Considered together, amino acid elongation may be a rare event, but R insertion at position 11 sometimes occurs. The occurrence of such insertion seems to be always accompanied by loss of the N-linked glycosylation site and deletion of one amino acid in the C-terminal half of V3. The combination of these mutations usually confers CXCR4-tropism. Awareness of this rule will help to confirm the tropism prediction from V3 sequences by conventional rules.

Methods

Patients. Case 1 was an ART-naïve Japanese hemophilic who acquired HIV-1 subtype B infection through contaminated blood product before 1985 and exhibited slow disease progression, as described previously (K1-127)³⁴. The study also included 53 other treatment-naïve HIV-1 subtype B-infected patients with CD4⁺ cell count < 200/mm³, who were newly diagnosed in 2008. The ethics committee of The National Center for Global Health and Medicine approved the study and all participants provided written informed consent.

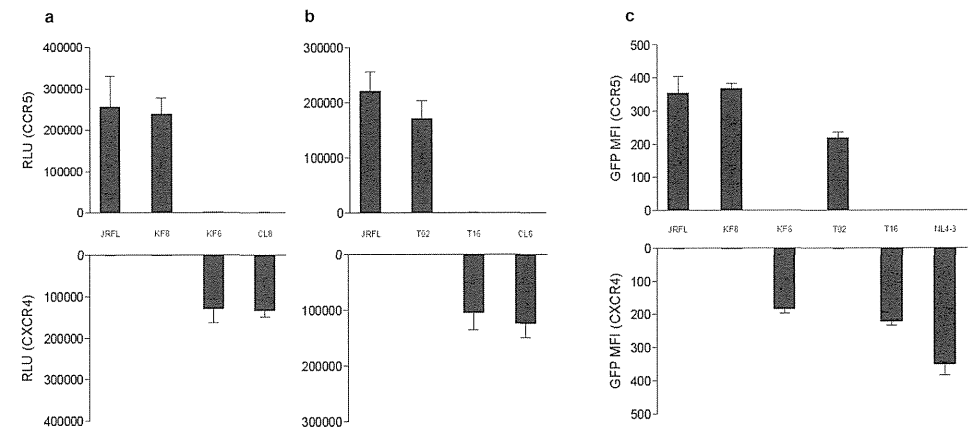


Figure 6 | Tropism of cloned V3 incorporated into JRFL gp120 backbone (a and b). Two distinct V3 clones from each of Case 2 (a) and Case 3 (b) were analyzed with the reference of JRFL-V3 and CL8-V3. Cell-cell fusion assay was performed using Env-expressing 293T cells and CD4⁺ and CCR5⁺/CXCR4⁺ COS-7 cells. Data are mean ± SD values in relative luminescent unit (RLU) of six experiments (performed in duplicate and repeated three times). Tropism of recombinant HIV-1 variants harboring V3 sequences derived from Cases 2 and 3 (c). Tropism of HIV-1 variants was assessed in CCR5⁺ GHOST Hi5 and CXCR4⁺ GHOST CXCR4 cells. The mean fluorescent intensity (MFI) of infected cells expressing green fluorescent protein (GFP) was measured. Data are mean ± SD values of six experiments (performed in duplicate and repeated three times).

Cells. The 293 T and COS-7 cells were cultured in Dulbecco's modified Eagle's medium (DMEM; Gibco, Grand Island, NY) with 10% fetal bovine serum (FBS; Equitech-Bio, Kerrville, TX). Parental GHOST cells³⁴ were cultured in DMEM supplemented with 10% FBS, 500 µg/ml G418 and 100 µg/ml hygromycin B. CCR5⁺ GHOST H15 and CXCR4⁺ GHOST CXCR4 cells³⁴ were cultured in DMEM supplemented with 10% FBS, 500 µg/ml G418, 100 µg/ml hygromycin B and 1 µg/ml puromycin.

Amplification, cloning and sequencing of Env V3 region. Total RNA was extracted from 200 µl of plasma using High Pure Viral RNA Kit (Roche, Indianapolis, IN) according to the instructions supplied by the manufacturer. HIV-1 cDNA was obtained by reverse transcriptase-polymerase chain reaction (RT-PCR) using the One Step RNA PCR kit (TaKaRa Bio, Kyoto, Japan). The DNA fragments were amplified by using the Ex Taq Hot Start Version (TaKaRa Bio) with the primer sets as follows. The Env fragment containing V3 region was amplified by RT-PCR with primers of C2 (5' - AATGTCCAGACAGTACAATGTACAC - 3') and C3 (5' - ACAATTTCTGG GTCCCCCTCTGAGGA - 3'). S1 (5' - ATGGAAATFAGGCAGTAGT - 3') and A1 (5' - CTCITCAATTTTATAACTATC - 3') primer sets were used for nested PCR. The amplified PCR products were purified using QIAquick PCR purification kit (Qiagen, Valencia, CA) and cloned by using the TOPO TA Cloning Kit (Invitrogen, Carlsbad, CA) according to the protocol provided by the manufacturer. At least 19 colonies were selected, inoculated into 4 ml of L broth, and incubated at 37°C overnight under vigorous agitation. In the next step, plasmids were isolated by using the QIAprep Spin Miniprep Kit (Qiagen). The purified plasmids were sequenced by using the ABI BigDye Terminator v3.1 Cycle Sequencing Ready Reaction Kit (Applied Biosystems, Foster City, CA) and processed with an automated ABI 3730 DNA Analyzer (Applied Biosystems).

Plasmid construction. The pcDNA6.2-CCR5 and pcDNA6.2-HIV-tat plasmids were constructed as described previously³⁵. Briefly, the entire human CCR5 gene including a stop codon was amplified using pZeoSV-CCR5³⁶ as a template. The PCR product was ligated into pcDNA6.2/Lucio-DEST vector (Invitrogen), cloned using the method recommended by the manufacturer, and termed as pcDNA6.2-CCR5. The CD4 expression vector (pcDNA6.2-CD4) and CXCR4 expression vector (pcDNA6.2-CXCR4) were generated using the same method. The CCR5-tropic HIV-1 JRFL³⁷ Env expression vector (pCXN-JRenv) and pLTR-LucE were used as described previously³⁵. The full length Env and part of the Nef encoding regions of the HIV-1 genome was amplified using pHIV-1 JRFL. The PCR product was ligated into pGEM-T Easy Vector System (Promega, Madison, WI), cloned using the protocol supplied by the manufacturer, and termed as pGEM-T Easy-Env. Amino acid substitutions, insertion and deletion were introduced into the V3 region of pGEM-T Easy-Env using the Quickchange Site-directed Mutagenesis Kit (Stratagene, La Jolla, CA) and applying the protocols supplied by the manufacturer. The V3 regions of pGEM-T Easy-Env containing mutations were digested with *StuI* and *XhoI*, and the obtained fragments were introduced into pCXN-JRenv or pHIV-1 JRFL.

Cell-cell fusion assay. The assay was conducted as described in detail previously³⁵. Briefly, the JRFL Env expression vector (WT or mutant) and Tat expression vector (0.5 µg each) were cotransfected into 293 T cells (2×10^5) using Lipofectamine 2000 (Invitrogen), while the CD4, CCR5 or CXCR4 expression vector and a reporter (luciferase) gene containing plasmid, pLTR-LucE (0.5 µg each) were cotransfected into COS-7 cells (2×10^5). On the next day, both cotransfected cells were harvested and mixed in a well of 96-well plates (2×10^4 cells each). The cotransfected cells were incubated further for 6 hrs and the luciferase activity in each well was detected using Bright-Glo Luciferase Assay System (Promega) and its luminescence level was measured using Wallace ARVO Sx 1420 multilabel counter (Perkin-Elmer, Waltham, MA).

MD simulation. MD simulation of gp120 outer domain containing V3 loop was performed as described previously^{17,18} with some modifications. Initially, the gp120 outer domain structures with various V3 elements were constructed by homology modeling^{38,39} using the Molecular Operating Environment (MOE) ver. 2008.10 (Chemical Computing Group Inc., Montreal, Quebec, Canada), as described previously^{17,18}. As a modeling template, we used the crystal structure of HIV-1 gp120 containing the entire V3 element (PDB code: 2B4C)¹⁹. Subsequently, MD simulations were performed for individual models using the SANDER module in the AMBER 9 program package^{40,41}. Heating calculations were achieved for 100 picoseconds until 310 K and MD simulations were subsequently executed at 310 K for 10 nanoseconds. The time step was set to 2.0 femtoseconds. The AMBER ff03ua force field⁴² and the GB implicit solvent function by Hawkins, Cramer, and Truhlar^{43,44} were applied. The "no cutoff" calculation was applied for the non-bonded energy calculation. In this study, we analyzed most frequently observed conformation among 5,000 snapshots obtained from 5.0–10.0 ns of MD simulation, which was selected by the Bayesian clustering algorithm⁴⁵.

Calculation of the RMSD. We compared the orientation of V3 loop between two gp120 outer domain models by the following procedure. We first superimposed two models by coordinating main chain atoms (N, C α , and C) in amino acid residues other than those in the V3 loop using PyMOL ver. 0.99 rc6 (Schrodinger LLC, Portland, OR, <http://www.pymol.org/>). Subsequently, the RMSD values for the V3 loop tip (GPGR) between the two models were calculated using the coordinates of the main chain atoms using the in-house program.

Viral tropism assay. The wild type CCR5-tropic HIV-1 strain, pHIV-1 JRFL, CXCR4-tropic HIV-1 strain, pHIV-1 NL4-3⁴⁶, and each pHIV-1 JRFL Env derived from mutations containing the V3 region of pGEM-T Easy-Env were transfected into 293 T cells with Lipofectamine 2000 (Invitrogen), and the obtained infectious clonal viruses were harvested 48 hrs after transfection and stored at -80°C until use. The GHOST cell infection assay^{34,47} was performed by incubating 1 ml containing 20 ng of p24 antigen of each virus with GHOST cells (2×10^4). Parental GHOST, CCR5⁺ GHOST H15, and CXCR4⁺ GHOST CXCR4 cells were infected for 72 hrs and then harvested. The mean fluorescent intensity (MFI) of infected cells expressing green fluorescent protein (GFP) was measured on a flow cytometer (FACS-Calibur, BD Bioscience, San Jose, CA). GHOST cells express low levels of CXCR4 and therefore infection of GHOST H15 alone was performed in presence of the CXCR4 antagonist AMD3100 (Sigma-Aldrich, St. Louis, MO) at dose of 1 µM.

- Parra, J. *et al.* Clinical utility of maraviroc. *Clin. Drug Invest.* **31**, 527–542 (2011).
- Alkhatib, G. *et al.* CC CKR5: a RNATES, MIP-1 α , MIP-1 β receptor as a fusion cofactor for macrophage-tropic HIV-1. *Science* **272**, 1955–1958 (1996).
- Dragic, T. *et al.* HIV-1 entry into CD4⁺ cells is mediated by the chemokine receptor CC-CKR-5. *Nature* **381**, 667–673 (1996).
- van't Wout, A. B. *et al.* Macrophage-tropic variant initiate human immunodeficiency virus type 1 infection after sexual, parenteral and vertical transmission. *J. Clin. Invest.* **94**, 2060–2067 (1994).
- Zhu, T. *et al.* Genotypic and phenotypic characterization of HIV-1 in patients with primary infection. *Science* **261**, 1179–1181 (1993).
- Björndal, A. *et al.* Coreceptor usage of primary human immunodeficiency virus type 1 isolates varies according to biological phenotype. *J. Virol.* **71**, 7478–7487 (1997).
- Scarlatti, G. *et al.* In vivo evolution of HIV-1 co-receptor usage and sensitivity to chemokine mediated suppression. *Nat. Med.* **3**, 1259–1265 (1997).
- Blaak, H. *et al.* In vivo HIV-1 infection of CD45RA⁺ CD4⁺ T cells is established primarily by synctium-inducing variants and correlates with the rate of CD4⁺ T cell decline. *Proc. Natl. Acad. Sci. U. S. A.* **97**, 1269–1274 (2000).
- Connor, R. I., Sheridan, K. E., Ceradini, D., Choe, S. & Landau, N. R. Change in coreceptor use correlates with disease progression in HIV-1-infected individuals. *J. Exp. Med.* **185**, 621–628 (1997).
- Koot, M. *et al.* Prognostic value of human immunodeficiency virus type 1 biological phenotype for rate of CD4⁺ cell depletion and progression to AIDS. *Ann. Intern. Med.* **118**, 681–688 (1993).
- The HHS Panel on Antiretroviral Guidelines for Adults and Adolescents. Guidelines for the Use of Antiretroviral Agents in HIV-1-Infected Adults and Adolescents. *U.S. Department of Health and Human Services* (2011).
- Poveda, E. *et al.* Genotype determination of HIV tropism – clinical and methodological recommendations to guide the therapeutic use of CCR5 antagonists. *AIDS Rev.* **12**, 135–148 (2010).
- Kawashima, Y. *et al.* Long-term control of HIV-1 in hemophiliacs carrying slow-progressing allele HLA-B*5101. *J. Virol.* **84**, 7151–7160 (2010).
- Delobel, P. *et al.* Population-based sequencing of the V3 region of env for predicting the coreceptor usage of human immunodeficiency virus type 1 quasisppecies. *J. Clin. Microb.* **45**, 1572–1580 (2007).
- Vandekerckhove, L. P. *et al.* European guidelines on the clinical management of HIV-1 tropism testing. *Lancet Infect. Dis.* **11**, 394–407 (2011).
- Huang, C. C. *et al.* Structures of the CCR5 N terminus and of a tyrosine-sulfated antibody with HIV-1 gp120 and CD4. *Science* **317**, 1930–1934 (2007).
- Yokoyama, M., Naganawa, S., Yoshimura, K., Matsushita, S. & Sato, H. Structural dynamics of HIV-1 envelope gp120 outer domain with V3 loop. *PLoS One* **7**, e37530 (2012).
- Naganawa, S. *et al.* Net positive charge of HIV-1 CRF01_AE V3 sequence regulates viral sensitivity to humoral immunity. *PLoS One* **3**, e3206 (2008).
- Huang, C. C. *et al.* Structure of a V3-containing HIV-1 gp120 core. *Science* **310**, 1025–1028 (2005).
- Clevestig, P., Pramanik, L., Leitner, T. & Ehrnst, A. CCR5 use by human immunodeficiency virus type 1 is associated closely with the gp120 V3 loop N-linked glycosylation site. *J. Gen. Virol.* **87**, 607–612 (2006).
- Van Baelen, K. *et al.* HIV-1 coreceptor usage determination in clinical isolates using clonal and population-based genotypic and phenotypic assays. *J. Virol. Methods* **146**, 61–73 (2007).
- Schnur, E. *et al.* The conformation and orientation of a 27-residue CCR5 peptide in a ternary complex with HIV-1 gp120 and a CD4-mimic peptide. *J. Mol. Biol.* **410**, 778–797 (2011).
- Pejchal, R. *et al.* A potent and broad neutralizing antibody recognizes and penetrates the HIV glycan shield. *Science* **334**, 1097–1103 (2011).
- Kuwata, T. *et al.* Conformational epitope consisting of the V3 and V4 loops as a target for potent and broad neutralization of simian immunodeficiency viruses. *J. Virol.* **87**, 5424–5436 (2013).
- Cecilia, D. *et al.* Neutralization profiles of primary human immunodeficiency virus type 1 isolates in the context of coreceptor usage. *J. Virol.* **72**, 6988–6996 (1998).
- Brown, B. K. *et al.* Biologic and genetic characterization of a panel of 60 human immunodeficiency virus type 1 isolates, representing clades A, B, C, D, CRF01_AE, and CRF02_AG, for the development and assessment of candidate vaccines. *J. Virol.* **79**, 6089–6101 (2005).

- Whitcomb, J. M. *et al.* Development and characterization of a novel single-cycle recombinant-virus assay to determine human immunodeficiency virus type 1 coreceptor tropism. *Antimicrob. Agents Chemother.* **51**, 566–575 (2007).
- Jensen, M. A. & van't Wout, A. B. Predicting HIV-1 coreceptor usage with sequence analysis. *AIDS Rev.* **5**, 104–112 (2003).
- Sing, T. *et al.* Predicting HIV coreceptor usage on the basis of genetic and clinical covariates. *Antivir. Ther.* **12**, 1097–1106 (2007).
- Jensen, M. A. *et al.* Improved coreceptor usage prediction and genotypic monitoring of R5-to-X4 transition by motif analysis of human immunodeficiency virus type 1 env V3 loop sequences. *J. Virol.* **77**, 13376–13388 (2003).
- Low, A. J. *et al.* Current V3 genotyping algorithms are inadequate for predicting X4 co-receptor usage in clinical isolates. *AIDS* **21**, E17–24 (2007).
- Poveda, E. *et al.* Design and validation of new genotypic tools for easy and reliable estimation of HIV tropism before using CCR5 antagonists. *J. Antimicrob. Chemother.* **63**, 1006–1010 (2009).
- Arroyo, M. A. *et al.* Virologic risk factors for vertical transmission of HIV type 1 in Puerto Rico. *AIDS Res. Hum. Retroviruses* **18**, 447–460 (2002).
- Mörner, A. *et al.* Primary human immunodeficiency virus type 2 (HIV-2) isolates, like HIV-1 isolates, frequently use CCR5 but show promiscuity in coreceptor usage. *J. Virol.* **73**, 2343–2349 (1999).
- Maeda, K. *et al.* Involvement of the second extracellular loop and transmembrane residues of CCR5 in inhibitor binding and HIV-1 fusion: insights into the mechanism of allosteric inhibition. *J. Mol. Biol.* **381**, 956–974 (2008).
- Maeda, Y., Foda, M., Matsushita, S. & Harada, S. Involvement of both the V2 and V3 regions of the CCR5-tropic human immunodeficiency virus type 1 envelope in reduced sensitivity to macrophage inflammatory protein 1 α . *J. Virol.* **74**, 1787–1793 (2000).
- Koyanagi, Y. *et al.* Dual infection of the central nervous system by AIDS viruses with distinct cellular tropisms. *Science* **236**, 819–822 (1987).
- Marti-Renom, M. A. *et al.* Comparative protein structure modeling of genes and genomes. *Annu. Rev. Biophys. Biomol. Struct.* **29**, 321–325 (2000).
- Baker, D. & Sali, A. Protein structure prediction and structural genomics. *Science* **294**, 93–96 (2001).
- Kollman, P. J. *et al.* Calculating structures and free energies of complex molecules: combining molecular mechanics and continuum models. *Acc. Chem. Res.* **33**, 889–897 (2000).
- Pearlman, D. A. *et al.* AMBER, a package of computer programs for applying molecular mechanics, normal mode analysis, molecular dynamics and free energy calculations to simulate the structural and energetic properties of molecules. *Comp. Phys. Commun.* **91**, 1–41 (1995).
- Hsieh, M. J. & Luo, R. Balancing Simulation Accuracy and Efficiency with the Amber United Atom Force Field. *J. Phys. Chem. B* **114**, 2886–2893 (2010).
- Hawkins, G. D., Cramer, C. J. & Truhlar, D. G. Parametrized models of aqueous free energies of solvation based on pairwise descreening of solute atomic charges from a dielectric medium. *J. Phys. Chem.* **100**, 19824–19839 (1996).
- Hawkins, G. D., Cramer, C. J. & Truhlar, D. G. Pairwise solute descreening of solute charges from a dielectric medium. *Chem. Phys. Lett.* **246**, 122–129 (1995).
- Shao, J., Tanner, S. W., Thompson, N. & Cheatham, T. E. 3rd. Clustering molecular dynamics trajectories: 1. Characterizing the performance of different clustering algorithms. *J. Chem. Theory Comput.* **3**, 2312–2334 (2007).

- Westervelt, P., Gendelman, H. E. & Ratner, L. Identification of a determinant within the human immunodeficiency virus 1 surface envelope glycoprotein critical for productive infection of primary monocytes. *Proc. Natl. Acad. Sci. U. S. A.* **88**, 3097–3101 (1991).
- Jekle, A. *et al.* Coreceptor phenotype of natural human immunodeficiency virus with nef deleted evolves in vivo, leading to increased virulence. *J. Virol.* **76**, 6966–6973 (2002).

Acknowledgments

We thank Dr. Kenji Maeda, Experimental Retrovirology Section, HIV and AIDS Malignancy Branch, National Cancer Institute, National Institutes of Health, for providing plasmids and helpful suggestion, and Drs. Hiroaki Mitsuya and Hirotoomi Nakata, Department of Infectious Diseases, Kumamoto University School of Medicine, for providing GHOST cell lines. We also thank the clinical and laboratory staffs of the AIDS Clinical Center, National Center for Global Health and Medicine, for their helpful support. This work was supported by a Grant-in-Aid for AIDS research from the Japanese Ministry of Health, Labour and Welfare (H23-AIDS-001), and the Global Center of Excellence Program (Global Education and Research Center Aiming at the Control of AIDS) from the Japanese Ministry of Education, Science, Sports, and Culture.

Author contributions


K.T. designed and performed the research, analyzed the data and wrote the manuscript. H.O. and H.S. performed MD simulation and calculation of the RMSD, wrote the manuscript. T.H. and J.K. performed the cloning and sequencing. S.O. designed and supervised the study. H.G. designed the study, analyzed the data, wrote and edited the manuscript. All authors read and approved the final manuscript.

Additional information

Supplementary information accompanies this paper at <http://www.nature.com/scientificreports>

Competing financial interests: S.O. has received honorariums and research grants from MSD, Janssen Pharmaceutical, Abbott, Roche Diagnostics, and Pfizer; has received honorariums from Viiv Healthcare, Torii Pharmaceutical, Bristol-Myers, Astellas Pharmaceutical, GlaxoSmithKline, Taiho Toyama Pharmaceutical, Daiinippon Sumitomo Pharma, and Daiichisankyo. The remaining authors declare to have no conflict of interest.

How to cite this article: Tsuchiya, K. *et al.* Arginine insertion and loss of N-linked glycosylation site in HIV-1 envelope V3 region confer CXCR4-tropism. *Sci. Rep.* **3**, 2389; DOI:10.1038/srep02389 (2013).

 This work is licensed under a Creative Commons Attribution-NonCommercial-ShareAlike 3.0 Unported License. To view a copy of this license, visit <http://creativecommons.org/licenses/by-nc-sa/3.0/>

RESEARCH

Open Access

Viral protein R of human immunodeficiency virus type-1 induces retrotransposition of long interspersed element-1

Kenta Iijima^{1†}, Noriyuki Okudaira^{1,2,11†}, Masato Tamura¹, Akihiro Doi^{1,2}, Yoshikazu Saito¹, Mari Shimura¹, Motohito Goto³, Akihiro Matsunaga¹, Yuki I Kawamura⁴, Takeshi Otsubo⁴, Taeko Dohi⁴, Shigeki Hoshino¹, Shigeyuki Kano^{2,5}, Shotaro Hagiwara⁶, Junko Tanuma⁷, Hiroyuki Gatanaga⁷, Masanori Baba⁸, Taku Iguchi^{9,12}, Motoko Yanagita⁹, Shinichi Oka⁷, Tadashi Okamura^{3,10} and Yukihito Ishizaka^{1*}

Abstract

Background: Viral protein R (Vpr), a protein of human immunodeficiency virus type-1 (HIV-1) with various biological functions, was shown to be present in the blood of HIV-1-positive patients. However, it remained unclear whether circulating Vpr in patients' blood is biologically active. Here, we examined the activity of blood Vpr using an assay system by which retrotransposition of long interspersed element-1 (L1-RTP) was detected. We also investigated the *in vivo* effects of recombinant Vpr (rVpr) by administering it to transgenic mice harboring human L1 as a transgene (hL1-Tg mice). Based on our data, we discuss the involvement of blood Vpr in the clinical symptoms of acquired immunodeficiency syndrome (AIDS).

Results: We first discovered that rVpr was active in induction of L1-RTP. Biochemical analyses revealed that rVpr-induced L1-RTP depended on the aryl hydrocarbon receptor, mitogen-activated protein kinases, and CCAAT/enhancer-binding protein β . By using a sensitive L1-RTP assay system, we showed that 6 of the 15 blood samples from HIV-1 patients examined were positive for induction of L1-RTP. Of note, the L1-RTP-inducing activity was blocked by a monoclonal antibody specific for Vpr. Moreover, L1-RTP was reproducibly induced in various organs, including the kidney, when rVpr was administered to hL1-Tg mice.

Conclusions: Blood Vpr is biologically active, suggesting that its monitoring is worthwhile for clarification of the roles of Vpr in the pathogenesis of AIDS. This is the first report to demonstrate a soluble factor in patients' blood active for L1-RTP activity, and implies the involvement of L1-RTP in the development of human diseases.

Keywords: HIV-1, Vpr, Blood, Retrotransposition, LINE-1, ORF1

Background

Viral protein R (Vpr), an accessory gene of human immunodeficiency virus type-1 (HIV-1), encodes a virion-associated nuclear protein of ~15 kDa [1]. Vpr has a variety of biological functions, including cell cycle abnormalities at the G₂/M phase and apoptosis of T cells and neuronal cells (for a recent review, see ref. [2]). Notably, it was shown that Vpr was present

in the blood of HIV-1-positive patients [3], and we previously reported that 20 of 52 blood samples from HIV-1-positive patients examined were positive for Vpr [4]. Blood Vpr was detected in patients with high titres of HIV-1 and, interestingly, was also detected in patients with low viral titres [4]. On the other hand, purified recombinant Vpr protein (rVpr) functions as a trans-acting factor [5,6], and rVpr activated viral replication in latently infected cells by increasing production of interleukin-6 (IL-6) by monocytes [7]. Further analyses revealed that rVpr-induced IL-6 production depended on p38, a mitogen-activated protein kinase (MAPK), and CCAAT/enhancer-binding protein β (C/EBP- β) [7]. These

observations suggest that blood Vpr could induce various clinical symptoms, but it remained unclear whether blood Vpr is biologically active.

Long interspersed element-1 (LINE-1, L1) and Alu are major endogenous retroelements, accounting for ~17 and ~10% of the human genome, respectively [8,9]. As an autonomous retroelement, L1 can retrotranspose not only itself but also other retroelements, such as Alu and SVA (short interspersed element-variable number tandem repeat-Alu, SINE-VNTR-Alu). Intriguingly, a single human cell contains more than 5×10^5 copies of L1, 80–100 of which are competent for retrotransposition (L1-RTP) [10]. During early embryogenesis, L1-RTP incidentally disrupts gene structures, leading to the development of inborn errors [11,12]. Of note, approximately 100 types of inheritable diseases have been identified as sporadic cases caused by mutagenic RTP of L1 or Alu [12]. Although most studies of L1-RTP have focused on early embryogenesis [13–16], recent lines of evidence suggest that L1-RTP is also induced in somatic cells [17–20]. In tumors of epithelial-cell origins and hepatomas, *de novo* L1 insertions were detected in the vicinity of tumor suppressor genes, suggesting that L1-RTP is actively involved in carcinogenesis [21,22]. Because L1-RTP alters cellular properties by causing various genetic alternations, including gene deletions [23,24], DNA damage [25], apoptosis [26] and immune responses [27], deregulation of L1-RTP in somatic cells likely functions as a trigger of various diseases.

Here we present evidence that Vpr is active for induction of L1-RTP, and further demonstrate that 6 of 15 blood samples from HIV-1 patients were positive for Vpr-induced L1-RTP. Interestingly, rVpr reproducibly induced L1-RTP in various organs, including the kidney, when administered to mice that harbored human L1 as a transgene (hL1-Tg mice) [28,29]. Clinically, HIV-1-associated nephropathy (HIVAN), which is mainly observed among African-Americans [30], is an end-stage renal deficiency that is found without apparent correlation with the viral load [31,32]. In view of reports that Vpr is a candidate molecule responsible for HIVAN [33,34], we propose that monitoring blood levels of Vpr is important for determining its involvement in the pathogenesis of HIVAN.

Results

rVpr induces L1-RTP

We initially performed a colony formation assay using purified rVpr and pCEP4/L1*neo1*/ColE1 (pL1-Neo^R) (Figure 1A and B) [28,35–37]. When HuH-7 human hepatoma cells were treated with rVpr, L1-RTP occurred in approximately 50 of 10^5 cells (Figure 1C, $P < 0.02$). rVpr caused no apparent cytotoxicity (Additional file 1: Figure S1). The activity of rVpr was also confirmed by a PCR-based assay using pEF06R [37,38], in which the

signal intensity of the 140 bp band, which corresponds to a product of L1-RTP, was increased by treatment with rVpr (Figure 1B, lower panel for the rationale of the PCR-based assay and 1D, lane 2). A quantitative PCR (qPCR) analysis was also carried out using a TaqMan probe designed to detect a junction point of two exons of the *EGFP* gene (Figure 1B, bottom; see also Additional file 2: Figure S2 for standard qPCR curves). Data revealed that rVpr significantly increased the frequency of L1-RTP (Figure 1E, $P < 0.05$). Notably, rVpr-induced L1-RTP was completely blocked by 8D1 and C217, monoclonal antibodies (mAbs) against Vpr (Figure 1D, lanes 5 and 6) [4], but not by an irrelevant mAb against a spike protein of severe acute respiratory syndrome coronavirus (Figure 1D, lane 4, SARS). Vpr-induced L1-RTP was also observed in HEK293T cells, in which the activity of ~1 ng/mL rVpr was detected (Figure 1E, lanes 10–12; Additional file 3: Figure S3).

Taking advantage of the high sensitivity of the PCR-based assay performed using HEK293T cells, we explored the activity of L1-RTP in blood samples from HIV-1-positive patients. Among 15 samples analyzed by a PCR assay, 6 were positive for L1-RTP induction (Figure 2A, upper panel; patients' clinical information is summarized in Additional file 4: Table S1). Notably, L1-RTP activity was selectively blocked by 8D1, indicating that the L1-RTP activity in HIV-1 patients is attributable to Vpr (Figure 2B and C). Interestingly, Vpr-induced L1-RTP was detected in patients with low HIV-1 titres (Figure 2D and Additional file 4: Table S1). To confirm this, we carried out immunoprecipitation followed by Western blot analysis (IP-WB analysis), and successfully detected Vpr in one of two blood samples that were positive for L1-RTP (no. 15; Additional file 5: Figure S4, arrowhead). Estimated concentration of the blood Vpr, when compared to the signals of standard rVpr, would be approximately 5 ng/mL (Additional file 5: Figure S4). In contrast, we could not detect Vpr in another sample (no. 1).

rVpr induces L1-RTP *in vivo*

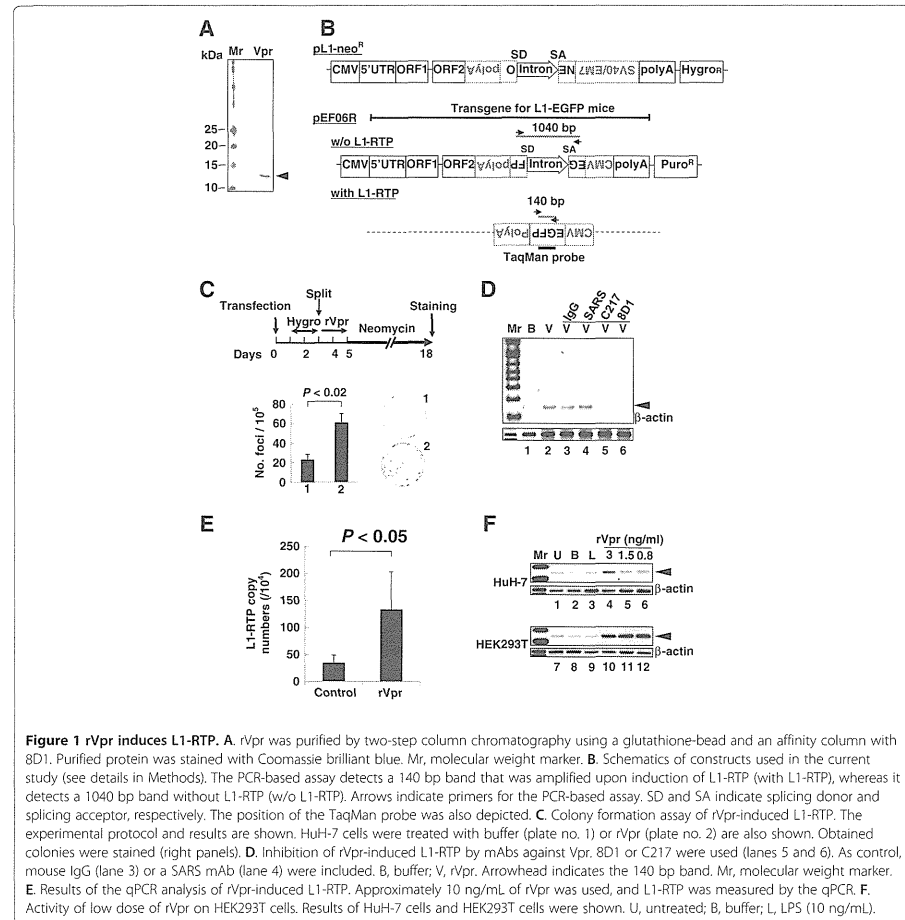
To determine the effects of rVpr *in vivo*, we next investigated L1-RTP after administration of rVpr to hL1-Tg mice (Figure 1B, solid line). As shown in Figure 3A, L1-RTP was detected in organs including the lymph nodes, liver, thymus and spleen upon intraperitoneal administration of ~200 ng of rVpr three times every 2 days (Additional file 6: Table S2). Interestingly, the qPCR analysis detected L1-RTP in the kidney after six intravenous administrations of 10 ng of rVpr (Figure 3B). To demonstrate that rVpr-induced L1-RTP was dependent on the reverse transcriptase activity of ORF2 [9], we first carried out *in vitro* experiments to examine whether rVpr-induced L1-RTP was blocked by nucleotide analogue

* Correspondence: zakay@i.rncgm.go.jp

[†]Equal contributors

¹Department of Infectious Diseases, Research Institute, National Center for Global Health and Medicine, 1-21-1 Toyama, Shinjuku-ku, Tokyo 162-8655, Japan

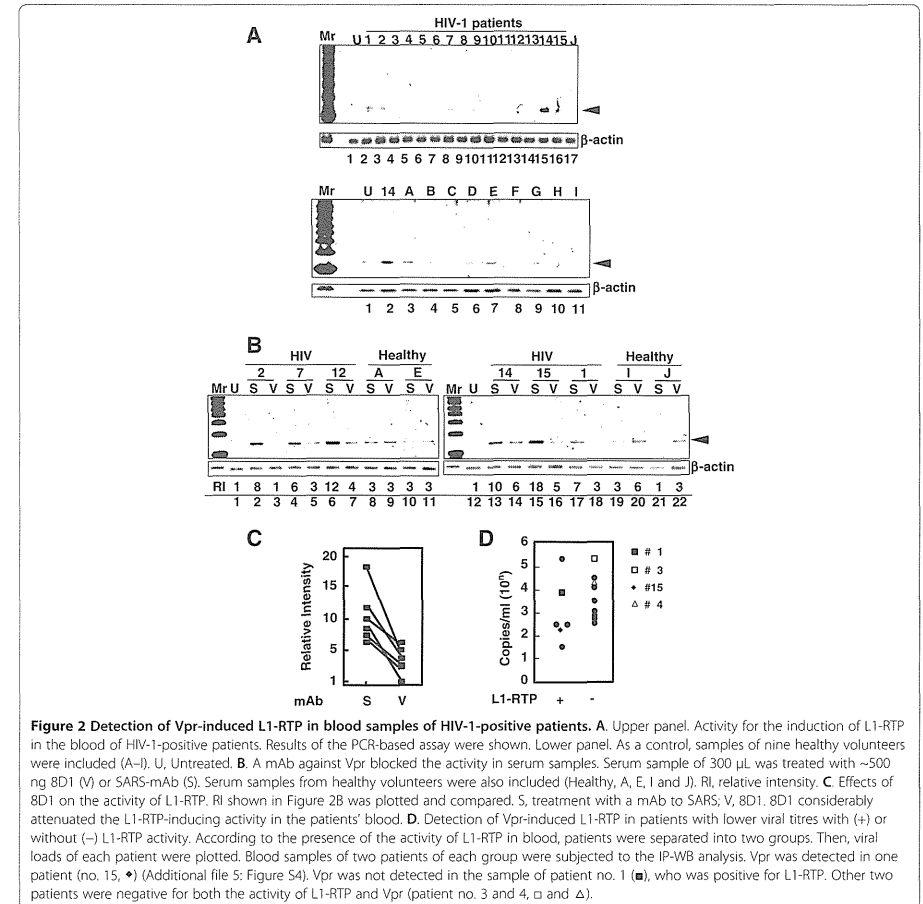
Full list of author information is available at the end of the article



inhibitors of reverse transcriptase (RTIs) [39,40]. As shown in Figure 3C, stavudine (d4T) and tenofovir inhibited the rVpr activity for L1-RTP induction (lanes 3 and 4), but lamivudine (3TC) and azidothymidine (AZT) did not (lanes 1 and 2). The inhibitory effects of d4T on rVpr-induced L1-RTP were potent, and the compound could effectively block the induction of L1-RTP at a concentration of 5 μ M (Additional file 7: Figure S5). We next investigated the effects of 2',3'-dideoxy-3'-deoxy-4'-ethynylthymidine (4'-Ed4T), a stavudine analogue with more specific activity as an RTI and fewer side effects

[41]. As shown in Figure 3D, 50 μ moles of 4'-Ed4T, when administered intraperitoneally 2 h before intravenous administration of 250 ng of rVpr, efficiently attenuated L1-RTP (compare lanes 2 and 3). qPCR analysis also clearly showed the inhibitory effects of 4'-Ed4T (Figure 3E).

By immunohistochemical analysis using α -GFP, we successfully detected cells positive for the induction of L1-RTP after a single injection of 2 μ g or 250 ng of Vpr (Figure 4A). Intriguingly, L1-RTP occurred at a frequency of several cells per 10^4 cells after six administrations of 10 ng of rVpr (Figure 4B, $P < 0.05$). Co-administration



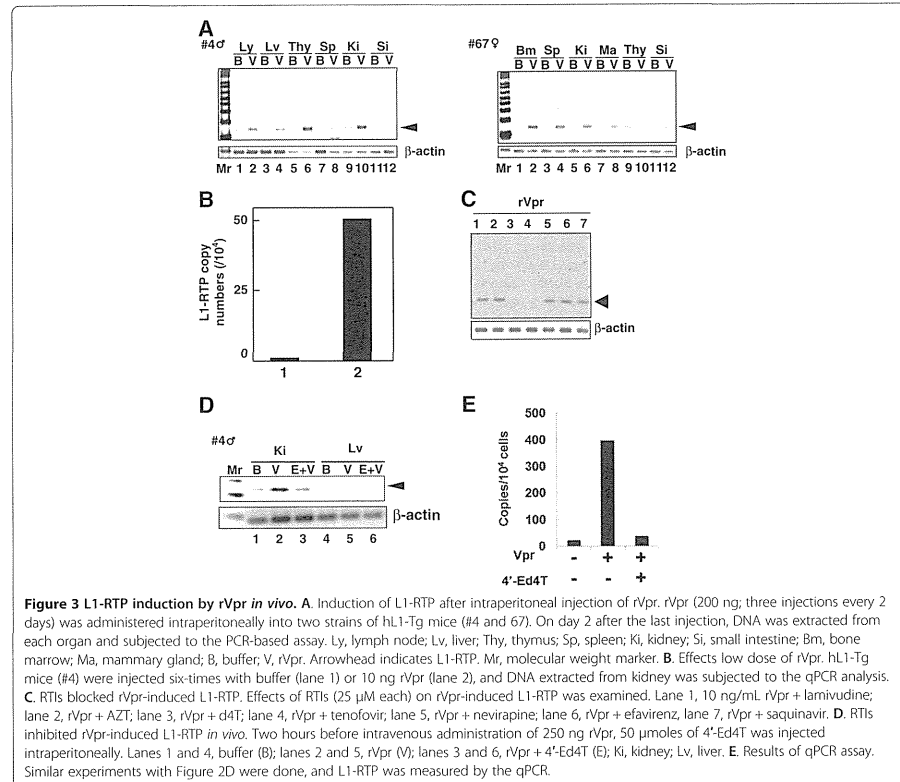
of 4'-Ed4T significantly blocked L1-RTP induced by repetitive injection of 250 ng of rVpr (Figure 4C, column 3). Consistent with the results obtained by hematoxylin-eosin (H/E) and α -GFP staining, dual staining for α -aquaporin-1 or α -phalloidin, which are markers of proximal renal tubular cells [42-44], detected rVpr-induced L1-RTP in renal tubular epithelial cells (RTECs) (Figure 4D).

We also investigated the methylation status of CpG in the L1-5'UTR in the rVpr-treated kidney. Analysis by the COBRA method [45], a method of quantifying CpG methylation, detected no apparent changes in the methylation

status of CpG before or after six administrations of 10 ng of rVpr (Additional file 8: Figure S6).

rVpr-induced L1-RTP depends on an AhR-p38-C/EBP- β cellular cascade

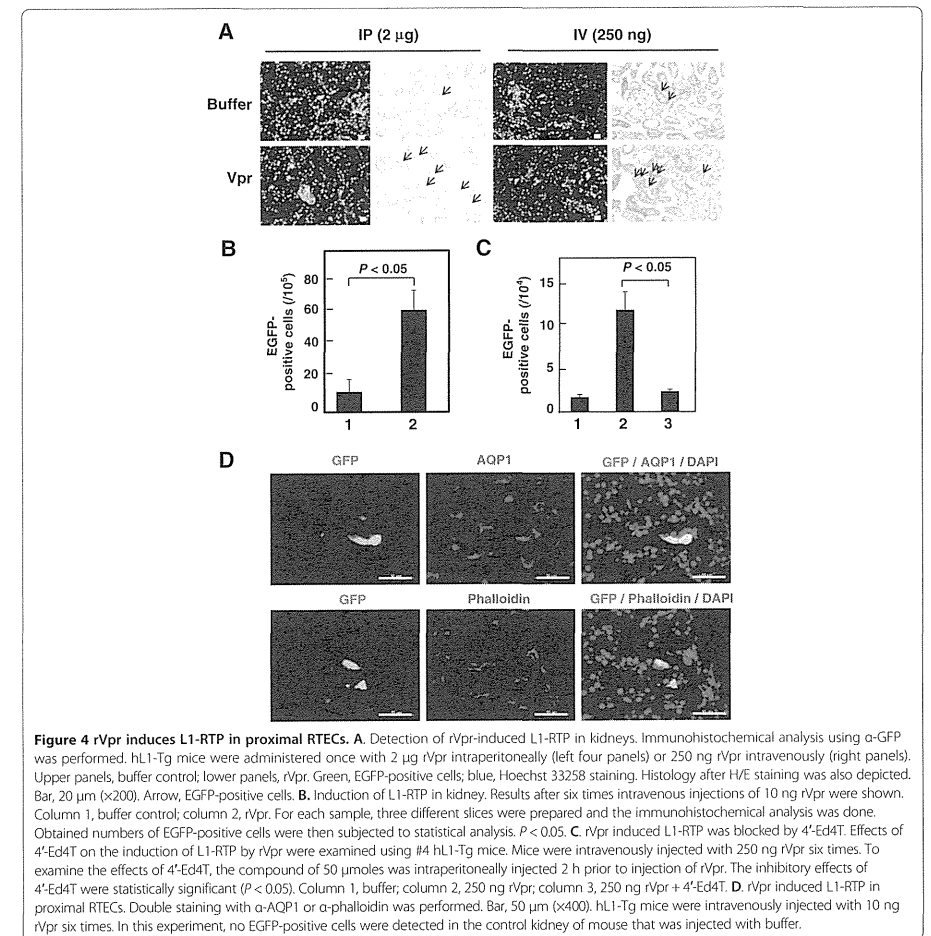
Previously, we reported that various environmental compounds induced L1-RTP in a manner dependent on the aryl hydrocarbon receptor (AhR), which has been shown to associate with other cellular molecules via an LxxLL motif in the counterpart molecule (amino acids denoted by single letters) [46]. Interestingly, Vpr contains



an LQQLL motif at amino acids 64–68 that functions as a sequence motif for binding to host cellular proteins, including p300/histone acetyl transferase [47]. Based on these observations, we hypothesized that AHR functions as a cellular factor responsible for rVpr-induced L1-RTP. To prove this, we first assessed the effects of 3'-methoxy-4'-nitroflavone (MNF), an AHR inhibitor [48], and observed that 10 μM MNF completely blocked rVpr-induced L1-RTP (Additional file 9: Figure S7). Moreover, down-regulation of endogenous Ahr expression by *Ahr* siRNA was accompanied by reduced rVpr-induced L1-RTP (see Figure 5A, lane 4, and 5B for a representative result from experiments using two different *Ahr* siRNAs; see also Additional file 10: Figure S8A and B for data obtained using another *Ahr* siRNA). By contrast, down-regulation of ARNT1 by siRNA (Figure 5C) did not attenuate L1-RTP (Figure 5D, lane 9 and Additional file 10: Figure S8D, lane 9). Ahr and ARNT1 form a heterodimer

(AHR complex) and are involved in the induction of *CYP1A1* mRNA expression in response to environmental pollutants [49]. Both *Ahr* and *ARNT1* siRNAs blocked the induction of *CYP1A1* mRNA expression by 6-formylindolo [3,2-*b*]carbazole (FICZ), a tryptophan photoproduct (Additional file 11: Figure S9), indicating that each siRNA efficiently inhibited the functional properties of the AHR complex, further suggesting that rVpr-induced L1-RTP depends on Ahr, but not ARNT1.

To determine the importance of the LxxLL motif of Vpr for the induction of L1-RTP, we investigated the activity of a Vpr mutant containing AQQAA instead of LQQLL (LA mutant, "LAM" in Figure 5). First, studies of forced expression of wild-type Vpr (WT Vpr) and the LA mutant revealed that the mutant was not active for induction of L1-RTP (Figure 5E, left panel), although comparable levels of each protein were detected (Figure 5E, right panel). Additionally, IP-WB

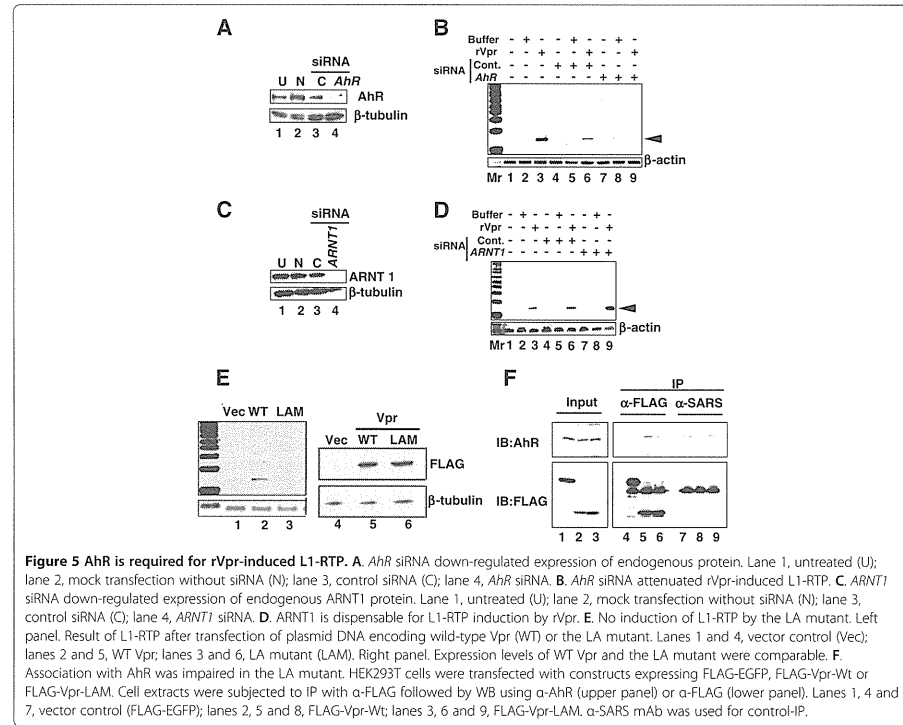


analysis detected an association between WT-Vpr and Ahr (Figure 5E, lane 5), but less interaction of the LA mutant with Ahr (Figure 5E, lane 6). These data suggest that Vpr-induced L1-RTP is dependent on a molecular interaction with Ahr via the LxxLL motif of Vpr.

To identify additional cellular factors involved in rVpr-induced L1-RTP, we investigated the involvement of MAPK, because our previous work revealed that Vpr induced IL-6 production via activation of p38 [7]. First,

qPCR analysis revealed that the MAPK inhibitors attenuated rVpr-induced L1-RTP to the basal level observed after treatment with control buffer (Figure 6A, see also Additional file 12: Figure S10 for representative qPCR data). Data indicate that the tested compounds inhibited the up-regulation of L1-RTP by rVpr.

In a previous study, we showed that p38 and C/EBP-β are important for understanding the cellular response to exogenously applied rVpr [7], implying that these molecules are also involved in the induction of L1-RTP by

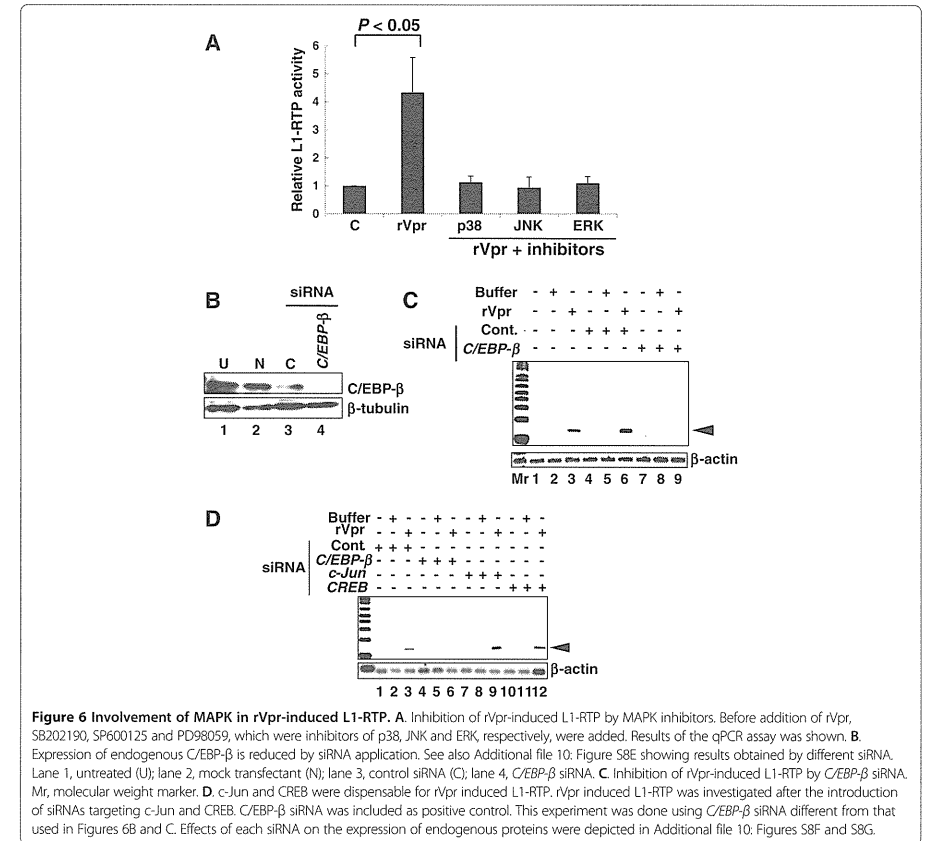


rVpr. To confirm this, we focused on the effect of *C/EBP- β* siRNA on rVpr activity. As shown in Figure 6B, transfection of the *C/EBP- β* siRNA down-regulated the endogenous protein level and attenuated rVpr-induced L1-RTP (Figure 6C, lane 9; see also Additional file 10: Figure S8E for data obtained using another siRNA targeting *C/EBP- β* mRNA, which was used in the experiment shown in Figure 6D). In contrast, siRNAs against *CREB* and *c-Jun* did not attenuate rVpr-induced L1-RTP (Figure 6D), although each siRNA efficiently down-regulated endogenous protein expression (Additional file 10: Figure S8F and G). One possible reason is that MAPK inhibitors are not specific for target molecules [37].

Chromatin recruitment of ORF1 induced by rVpr is dependent on AhR

L1 encodes two proteins, open reading frame-1 (ORF1) and ORF2, which are ~40 and ~150 kDa, respectively, and are present in cytoplasmic ribonucleoprotein complexes

and cytoplasmic stress granules [50,51]. Moreover, L1-RTP is initiated by target-primed reverse transcription within the genome [9], and ORF1 functions as a nucleic acid chaperone during L1-RTP [52]. These observations suggest that ORF1 is recruited to the chromatin fraction in response to rVpr treatment. To demonstrate chromatin recruitment of ORF1, we transfected a plasmid DNA that encodes ORF1 into HuH-7 cells, and then carried out WB analysis of the chromatin fraction of the transfected cells after treatment of rVpr. The rVpr-induced chromatin recruitment of ORF1 was blocked by MAPK inhibitors examined (Figure 7A, lanes 4 and 6) and the *AhR* siRNA (Figure 7B, lane 4; see also Additional file 13: Figure S11 for results from an independent experiment performed using a different *AhR* siRNA). To further show that ORF1 and AhR form a complex, we transfected a plasmid DNA encoding a chimeric protein of ORF1 and EGFP (pORF1-EGFP) into HuH-7 cells, and then performed IP-WB analysis. IP using α -AhR followed by WB analysis



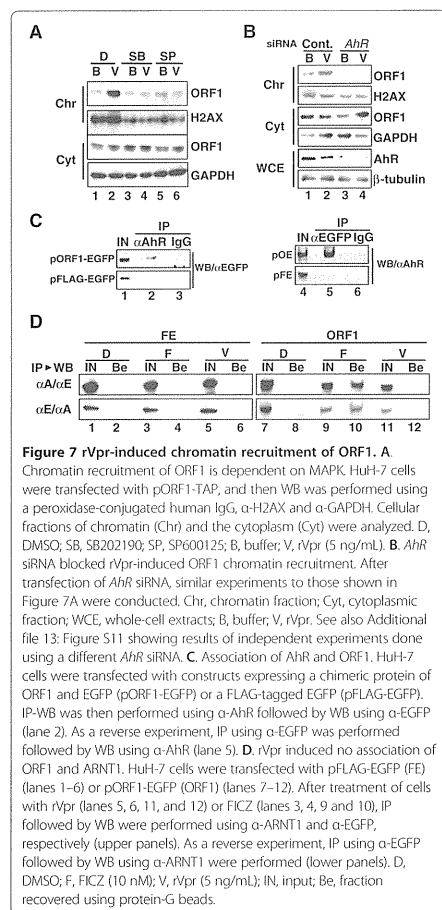
using α -EGFP revealed that ORF1 and AhR were associated (Figure 7C, lane 2). The reverse experiment, in which IP using α -EGFP was followed by WB using α -AhR, confirmed formation of this complex (Figure 7C, lane 5). The interaction between ORF1 and AhR was also detected in cells in which both ORF1 and ORF2 proteins were expressed exogenously (Additional file 14: Figure S12).

Previously, we reported that FICZ is a potent activator of L1-RTP, and that its activity was dependent on ARNT1, but not on AhR [37]. To determine the functional link between ORF1 and ARNT1, we performed IP-WB analysis after transfecting pORF1-EGFP into HuH-7 cells. ORF1 was detected in an extract of cells treated with FICZ and was recovered using α -ARNT1 (Figure 7D, upper panel, lane 10). By contrast, it was not recovered from

extracts of cells treated with rVpr using α -ARNT1 (Figure 7D, upper panel, lane 12). Consistent results were obtained in a reverse experiment, in which WB using α -ARNT1 was performed on a sample recovered by IP using α -EGFP (Figure 7D, lower panel). In this case, the cell extract obtained after FICZ treatment yielded a positive signal (Figure 7D, lower panel, lane 10). These data suggest that the association between ORF1 and ARNT1 is induced by exogenous FICZ but not rVpr.

Discussion rVpr-induced L1-RTP depends on an AhR-p38-C/EBP- β cellular cascade

Here we found that Vpr is a viral protein active for the induction of L1-RTP. Experiments using MNE, siRNAs



targeting *AhR* and *C/EBP- β* mRNAs, and MAPK inhibitors revealed that rVpr-induced L1-RTP depends on an AhR-p38-C/EBP- β cellular cascade (Figures 5 and 6). We confirmed by *in vitro* experiments that rVpr did not increase expression of *L1* mRNA or the splicing efficiency of an immature *EGFP* transcript derived from the reporter L1 construct (Additional file 15: Figure S13). Moreover, no apparent changes in the CpG methylation status were observed in the 5'UTR of the exogenous hL1 gene in the kidneys of hL1-Tg mice that had been

treated with rVpr (Additional file 8: Figure S6). Our data suggest that rVpr-induced L1-RTP is controlled at the post-transcriptional level, although it has been proposed that L1-RTP is influenced at the transcriptional level by the methylation status of the L1-5'UTR [53,54].

In addition to the LA mutant, we investigated the activity of a Vpr mutant lacking the C-terminal 12 amino acids (Δ C12). A PCR-based assay revealed that the Δ C12 mutant was not active for the induction of L1-RTP (Additional file 16: Figure S14). It has been shown that Vpr has an affinity for nucleic acids, which is attributable to the basic moiety in the C-terminal region of Vpr [55]. To exclude the possibility that the induction of AhR-dependent L1-RTP by Vpr depends on binding to nucleic acids, we investigated the interaction between Vpr and AhR after nuclease treatment. IP-WB analysis combined with treatment with benzonase, a nuclease that degrades both DNA and RNA, revealed that their interaction was not reduced (Additional file 17: Figure S15A). Additionally, ORF1 and AhR constitutively formed a complex, and their interaction was also resistant to nuclease treatment (Additional file 17: Figure S15B). Moreover, rVpr triggered chromatin recruitment of ORF1 in an AhR-dependent manner (Figure 7B). Taken together, these data suggest that Vpr functions as an AhR ligand, and activates a cellular cascade for the induction of L1-RTP.

Biologically active Vpr is present in the blood of HIV-1-positive patients

We detected L1-RTP-inducing activity in the blood of HIV-1 patients: 6 of 15 patients were positive for the induction of L1-RTP (Figure 2A). The L1-RTP activity in those six patients was selectively blocked by 8D1, a mAb against Vpr (Figure 2B). Interestingly, we previously examined blood Vpr by IP-WB analysis, and detected Vpr in 20 of 52 blood samples from HIV-1 patients [4]. Interestingly, the positive frequencies observed in these two sets of experiments are comparable, but greater numbers of samples are needed to conclude that blood Vpr is exclusively biologically active. Although it was reported that an antibody against Vpr is present in patients' blood [56], and implied that Vpr activity would be blocked by such autoantibodies, our current experiments proved that blood Vpr is active for the induction of L1-RTP. Because L1-RTP can alter cellular properties by inducing DNA damage and apoptosis [9], it is tempting to speculate that blood Vpr can modify clinical outcomes of AIDS patients.

Consistent with our previous observation that Vpr protein was detectable in blood samples from HIV-1-positive patients with low viral titres [4], we here detected Vpr-induced L1-RTP in samples from patients with low viral titres. As shown in Figure 2, L1-RTP-inducing activity was detected in some blood samples, and IP-WB

analysis successfully detected a Vpr signal (no. 15) (Additional file 4: Table S1 and Additional file 5: Figure S4). Intriguingly, however, the viral titre of patient 15 was 140 copies/mL (Figure 2D, closed diamond and Additional file 4: Table S1). By striking contrast, the viral titres of the blood samples from patients 3, 8 and 4 were $>10^4$ copies/mL, but no apparent L1-RTP-inducing activity was detected. Although it remains completely unknown why Vpr was present in patients with low viral titres, one possible explanation would be that Vpr is secreted into the blood from latent foci in patients. *In vivo* experiments support the notion that Vpr is excreted by infected cells and functions as a soluble protein with bystander effects [57].

rVpr is active for the induction for L1-RTP *in vivo*

Repeated intravenous administration of 10 ng of rVpr, a dose comparable to patients' blood levels [7], induced L1-RTP *in vivo* (Figure 4B). We observed that administration of rVpr induced L1-RTP in various organs, such as the lymph nodes and spleen. Additionally, we found that Vpr also induced L1-RTP in the kidney (Figure 4A and Additional file 6: Table S2). Notably, even a single injection of 250 ng of rVpr into the tail vein induced L1-RTP in the kidneys (Figure 4A, right panels), suggesting that the kidney is a target organ of Vpr-induced L1-RTP. Immunohistochemical analysis showed that Vpr induced L1-RTP in RTECs, especially in proximal RTECs (Figure 4D). Previously, it was reported that Vpr and Nef are candidate mediators of HIVAN: forced expression of these viral genes in mouse podocytes resulted in proteinuria and glomerular diseases [34]. Although it was proposed that renal dysfunction is a direct effect of primary HIV-1 infection in RTECs [58], it remains to be investigated whether repeated administration of rVpr causes renal insufficiency.

HIVAN develops mostly in people of African descent, and shows the strong influence of genetic traits [59-61]. However, its mechanism remained completely unknown. Importantly, HIVAN has no apparent correlation to viral load [31], and, intriguingly, it has been proposed that the kidneys are a latent reservoir of HIV-1 [62,63]. Based on these observations, it is plausible that both blood-circulating Vpr and Vpr secreted locally from a latent reservoir (the kidney, for example) attack RTECs. To prove this, further studies are required to determine whether the kidney is an organ from which Vpr is constitutively secreted.

In addition to their clinical relevance for HIV-1 pathogenesis, our findings should have a general impact on the involvement of L1-RTP in human diseases. By analysis of tumors using second-generation sequencing technology, *de novo* L1 insertions were detected in the vicinity of tumor suppressor genes [21,22], suggesting

that L1 insertion was actively involved in carcinogenesis. Additionally, it was shown that de-regulation of L1-RTP is positively linked to the development of autoimmune diseases [27]. Although these lines of evidence revealed that L1-RTP is induced in somatic cells and is involved in the development of human diseases, it remained unclear how L1-RTP is induced in somatic cells. It was previously reported that 2-amino-1-methyl-6-phenylimidazo[4,5-*b*]pyridine (PhIP), a food-borne carcinogen, induced L1-RTP in the mouse mammary gland, a target organ of carcinogenesis, when it was administered orally to hL1-Tg mice [29]. Given that PhIP is present in broiled meat [64] and has been detected in human breast milk [65], it is plausible that humans are susceptible to the induction of L1-RTP by environmental factors. Further study is required to demonstrate the activity of L1-RTP under pathological conditions, enabling the roles of L1-RTP in disease development to be specified.

Conclusions

Six of the 15 blood samples from HIV-1-positive patients examined were positive for Vpr-induced L1-RTP. L1-RTP-inducing activity was detected in blood samples with low viral titres. Monitoring circulating Vpr in relation to clinical outcomes is important to clarify the roles of Vpr in AIDS symptoms. The present study is the first to show that L1-RTP-inducing activity is present *in vivo*, shedding light on the possible involvement of L1-RTP in human diseases. In further research, it will be important to detect L1-RTP-inducing activity under pathological conditions.

Methods

Chemicals and cells

HuH-7 cells (RCB1366) and HEK293T cells (RCB2202) were obtained from the Riken BioResource Centre Cell Bank. They were cultured in Dulbecco's modified Eagle's medium supplemented with 10% fetal calf serum (Sigma-Aldrich, St. Louis, MI, USA). The transfection efficiencies were ~70 and ~30%, respectively, as determined by fluorescence-activated cell sorting (FACS) on day 2 after transfection of plasmid DNA encoding enhanced green fluorescent protein (EGFP) (data not shown). MNF was kindly provided by Dr. Gabriele Vielhaber (Symrise, Holzminden, Germany). SB20358, SP60012, PD98059 and lipopolysaccharide (L8274) were from Sigma-Aldrich. FICZ was obtained from Enzo Life Sciences (Plymouth Meeting, PA, USA). Protease inhibitors (Roche Diagnostics, Tokyo, Japan) were also purchased.

Antibodies against AhR, (Santa Cruz Biotechnology, Santa Cruz, CA, USA), ARNT1 (Santa Cruz Biotechnology), β -tubulin (Thermo Fisher Scientific, Waltham, MA, USA), H2AX (Millipore, Billerica, MA, USA), C/EBP- β (Cell Signaling Technology Inc., Danvers, MA, USA),

FLAG (Sigma-Aldrich), EGFP (rabbit antibody: Medical & Biological Laboratories, Co., Ltd., Nagoya, Japan; mouse monoclonal antibody: Abcam, Cambridge, United Kingdom), aquaporin 1 (AQP1; Abcam) and glyceraldehyde 3-phosphate dehydrogenase (GAPDH; Trevigen, Gaithersburg, MD, USA) were used as the primary antibodies. A rabbit polyclonal antibody against human ORF1 was generated using the peptide MGKKQNRKTGNSK TQSAC (amino acids denoted by single letters) as an immunogen (Medical & Biological Laboratories). An Alexa Fluor 546-conjugated antibody to phalloidin (Invitrogen, Carlsbad, CA, USA) was purchased. As secondary antibodies, α -mouse IgG (GE Healthcare Bio-Sciences Corp., Piscataway, NJ, USA), α -rabbit IgG (GE Healthcare), and α -goat IgG (Santa Cruz Biotechnology), all of which were conjugated with horseradish peroxidase, were used. For immunohistochemical analysis, Alexa Fluor 555-conjugated goat α -rabbit IgG (Invitrogen) and Alexa Fluor 488 goat α -mouse IgG (Invitrogen) were used as the secondary antibodies. Hoechst 33258 was purchased from Invitrogen.

Based on recent reports that RTIs efficiently blocked L1-RTP [39,40], we used 4'-Ed4T, which has more potent inhibitory activity than d4T and less effect on DNA polymerases, and which is currently undergoing phase IIb clinical trials in HIV-1-infected patients [41]. Two hours before injection of rVpr, 50 μ moles of 4'-Ed4T was injected intraperitoneally to give a final concentration of approximately 25 μ M when most of the compound is transferred to the blood, the estimated volume of which is \sim 2 mL.

Purification of rVpr and assays of L1-RTP

rVpr was expressed using pGEX-6P-1 in *Escherichia coli* BL21 and purified as described previously (Figure 1A) [4]. Purified rVpr was tested for endotoxin using a highly sensitive lipopolysaccharide (LPS) assay with Limulus amoebocyte lysate, the detection limit of which was 0.25 EU/mL (Wako Pure Chemical Ind., Ltd., Osaka, Japan). For L1-RTP assays, we used two reporter constructs, pEF06R [38] and pCEP4/L1mneoI/ColE1 (pL1-Neo^R) [28,35-37], for semi-quantitative and quantitative PCR, and colony formation assays, respectively. Each construct contained all components of human L1 with single transcriptional units with EGFP or Neo^R, which were inserted in reverse orientation. When L1-RTP occurs, the intron within each reporter gene is spliced out, and then pEF06R expresses functional EGFP, whereas pL1-Neo^R expresses a functional neomycin-resistance gene (Neo^R). Cells were transfected with pEF06R or pL1-Neo^R using Lipofectamine 2000 (Invitrogen) or Xfect (Takara Bio Inc., Shiga, Japan). Cells were selected for 2 days with puromycin (Puro, 0.5 μ g/mL) for pEF06R, or with hygromycin (Hygro, 25 μ g/mL) for pL1-Neo^R.

Next, cells were treated for additional 2 or 3 days with the indicated amounts of rVpr.

For the PCR assay, genomic DNA was prepared from harvested cells using a DNA extraction system (QuickGene; Fujifilm, Tokyo, Japan). For semi-quantitative PCR, primers that were designed for each exon would amplify a product of \sim 1040 bp, whereas they would generate a product of \sim 140 bp upon L1-RTP. Thus, occurrence of L1-RTP was determined by evaluating the size of the amplified product [28,29,37]. After staining of amplified DNA with SYBR Green I (LONZA, Basel, Switzerland), signal intensities of the 140 bp bands were measured using a molecular imager (FX-PRO; Bio-Rad, Hercules, CA, USA) and normalized by the signal intensity of the β -actin band, used as the internal control. Relative intensities (RIs) of each 140 bp band were calculated by standardizing the signal of the buffer-treated sample as "1".

For qPCR analysis, 5'-GAA CGG CAT CAA GGT GAA CT-3' and 5'-GGG GTG TTC TGC TGG TAG TG-3', which were designed for each exon of the *EGFP* gene, were used as forward and reverse primers, respectively. A TaqMan-probe (5'-FAM- TGC AG * C TGG CCG AC -MGB-3') (Invitrogen) was used to detect an amplicon of 87 bp in length (* denotes the exon junction). Template DNA was amplified with Eagle Taq Master Mix (Roche Diagnostics) and a CFX Connect Real-Time System (Bio-Rad) using the following amplification conditions: 95°C for 10 min, followed by 45 cycles of 95°C for 15 sec and 64°C for 15 sec. To obtain a standard curve for EGFP-qPCR, *EGFP* DNA generated after the induction of L1-RTP was amplified using the above primers and cloned into the pGEM-T Easy vector (Promega, Madison, USA). After confirmation of the nucleotide sequence, standard samples were prepared by mixing human or mouse genomic DNA with the *EGFP*-containing plasmid to give 1.0, 10⁻¹, 10⁻², 10⁻³ and 10⁻⁴ copies/cell. To normalize the amounts of input DNA, human β -globin or mouse β -actin was quantified by qPCR with SYBR Premix Ex Taq (TaKaRa) and the CFX Connect Real-Time System (Bio-Rad). For human β -globin, the forward primer was 5'-TTG GAC CCA GAG GTT CTT TG-3' and the reverse primer was 5'-GAG CCA GGC CAT CAC TAA AG-3'; for mouse β -actin, the forward primer was 5'-TGA CGT TGA CAT CCG TAA AGA CC-3' and the reverse primer was 5'-AAG GGT GTA AAA CGC AGC TCA-3'.

In the colony formation assay, \sim 2.0 \times 10⁶ cells were transfected with pL1-Neo^R and selected with 25 μ g/mL Hygro, and 1.0 \times 10⁵ cells were re-plated to new plates (Split). Next, cells were treated for 2 days with rVpr and further cultured in the presence of neomycin (800 μ g/mL) [35-37]. In the initial experiment, we used 5–10 ng/mL rVpr because the maximum reported plasma Vpr

concentration in HIV-1-positive patients is \sim 5 ng/mL [4]. To determine Vpr activity for L1-RTP induction, each of the six plates was treated with rVpr or a buffer control for 2 days, and further cultured in the presence of neomycin. After 3–4 weeks, cell aggregates were stained with methylene blue, and colonies were enumerated. To minimize plate-to-plate variation, the colony numbers of the middle four of the six plates were subjected to statistical analysis. At least two independent experiments were performed, representative results of which are shown.

Suppression of rVpr-induced L1-RTP by mAbs against Vpr

The effects of mAbs against Vpr on the induction of L1-RTP were investigated by applying 5 ng of rVpr with 500 ng of 8D1 and C217 [4], giving an approximately 10-fold excess molar amount of rVpr. After 60 min of incubation at room temperature, a 300 μ L reaction mixture was filtrated and added to 1.5 mL of culture medium of cells. As a control, a SARS mAb, an irrelevant mAb that recognizes a spike protein of the severe acute respiratory syndrome corona virus (SARS-CoV), was used.

Effect of down-regulation of endogenous proteins on induction of L1-RTP

For each gene, two small interfering RNAs (siRNAs) were prepared (Applied Biosystems, Foster City, CA, USA or Thermo Scientific), and their functions were evaluated by transfection into cells followed by WB analysis. The nucleotide sequences of each siRNA are shown in Additional file 18: Table S3. To evaluate the inhibitory effects of the siRNAs on L1-RTP induction, each siRNA was introduced on day 3 after initial transfection with pL1-Neo^R or pEF06R. Two days later, the cells were re-plated, incubated for 2 days with rVpr, and subjected to analysis. Silencer Negative Control siRNAs (cat. no. AM4613, AM4637 and AM464; Life Technologies Corporation, Carlsbad, CA, USA) were used as controls.

Effects of MAP kinase inhibitors on rVpr-induced L1-RTP

HuH-7 cells were transfected with pEF06R and selected for 2 days with 0.5 μ g/mL Puro. On day 3 after transfection, cells were re-plated and subjected to an L1-RTP assay. To examine the effects of MAPK inhibitors, SB202190, SP600125 and PD98059 at concentrations of 1, 100 and 20 μ M, respectively, were added 1 h before the addition of rVpr. The cells were exposed to 10 ng/mL rVpr for 3 days and subjected to qPCR analysis. Genomic DNA was isolated using the QuickGene DNA Tissue Kit S and QuickGene-800 (Fujifilm). To selectively detect *EGFP* genes derived from L1-RTP, \sim 250 ng of DNA were used as the qPCR template. To amplify β -globin gene as an internal control, \sim 50 ng of DNA were used as the qPCR template.

Administration of rVpr to hL1-Tg mice and L1-RTP assessment

For *in vivo* experiments, we used two transgenic mouse lines, #4 and #67, in which the L1-DNA fragment of pEF06R had been introduced as a transgene (hL1-Tg mice; Figure 1A, sidebar) [28,29]. These two lines were selected because they display low background L1-RTP during embryogenesis but respond vigorously to environmental compounds [29]. The CpG island of the 5' untranslated region of introduced human L1 (L1-5'UTR) was highly methylated in #4 and #67 mice, as assessed by a PCR-based assay using methylation-specific primers [29]. All animal experiments were approved by the Animal Care and Use Committee at the National Center for Global Health and Medicine (NCGM).

Clinical samples

Fifteen blood samples obtained from anti-retroviral therapy-naïve male patients who presented to the NCGM hospital between October 1996 and October 2003 were subjected to the PCR-based assay. The patients were 21–44 years of age with viral loads and CD4 counts of 50–230,000 copies/mL and 315–795 cells/mL, respectively. Nine healthy volunteers served as controls. To detect L1-RTP-inducing activity, HEK293T cells were first transfected with pEF06R and selected with 0.5 μ g/mL Puro. Then, 150 μ L of each heat-inactivated patient serum sample was added to 1.35 mL of culture medium of HEK293T cells. To show that L1-RTP activity in patients' blood was attributable to Vpr, 100 μ L of serum was reacted for 60 min with 500 ng of 8D1 or SARS-S mAb at room temperature in a 300 μ L reaction volume. The experimental protocol was approved by the institutional review board of NCGM.

L1-RTP activity of the Vpr mutant

The LA mutant, which contains AQQAA at codons 64–68, and wild-type (WT) Vpr were expressed as FLAG-tagged proteins using the pFLAG-CMV2 expression vector (Sigma-Aldrich). To obtain comparable levels of expression of each protein, the molar ratio of 1:4 of plasmid DNA for the wild-type Vpr and the LA mutant were transfected respectively. On the next day of transfection, cells were subjected to the PCR-based assay.

Chromatin recruitment of ORF1 induced by rVpr

We used the pORF1-TAP (tandem affinity purification) construct [66], which encodes a chimeric protein of ORF1, protein A and calmodulin-binding protein. On day 2 after transfection of pORF1-TAP into HuH-7 cells, 5 ng/mL rVpr was added to the culture medium, and cell extracts were prepared on the following day. The chromatin-enriched fraction (chromatin fraction) was

isolated using a Subcellular Protein Fractionation Kit (Thermo Fisher Scientific) with micrococcal nuclease, as described previously [29]. Detection of ORF1-TAP was performed by probing with a horseradish peroxidase-conjugated human IgG (Jackson ImmunoResearch West Grove, PA, USA). H2AX was used as an internal control for the chromatin fraction.

ORF1, AhR, and Vpr complex formation

HuH-7 or HEK293T cells were transfected with the plasmid constructs pFLAG-Vpr-Wt or pFLAG-Vpr-LA mutant, pORF1-EGFP and pFLAG-EGFP, which encode FLAG-tagged Vpr, a chimeric protein of ORF1 and EGFP, and FLAG-tagged EGFP, respectively. On day 2 after transfection, cells were treated with 10 ng/mL rVpr for 1 day to evaluate the dependence of the protein-protein interaction on Vpr. Then, cells were subjected to IP-WB analysis. To analyze the ORF1-AhR association, cells were suspended in a buffer containing 50 mM Tris (pH 7.5), 150 mM NaCl, 1% NP40, 1 mM EDTA and a protease inhibitor cocktail and subjected to brief sonication. For analysis of the Vpr-AhR association, cells were suspended in a buffer containing 25 mM HEPES (pH 7.5), 200 mM NaCl, 0.1% NP40, 10% glycerol and a protease inhibitor cocktail, and were completely lysed by passage through 22 G and 27 G needles (in that order) ten times. Cell extracts (500 to 2000 µg) were pre-cleared with protein G Sepharose beads (GE Healthcare), reacted with 4 µg of α-AhR, α-EGFP, α-FLAG or α-SARS, and then recovered with protein G beads. As an "input" sample, about 5 or 10% of each extract subjected to immunoprecipitation, was assessed simultaneously.

Immunohistochemical analysis of EGFP-positive cells

After perfusion fixation, organs were immersed in 0.1 M phosphate buffer (PB) (pH 7.4) supplemented with 4% paraformaldehyde at 4°C. On the following day, samples were serially immersed at 4°C in PB supplemented with 10% saccharose for 1 h, 20% saccharose until immersed completely, and then 30% saccharose overnight. Next, samples were embedded in Optimal Cutting Temperature compound (Sakura Finetek, Torrance, CA, USA) for cryosectioning. Using a cryostat (Leica Biosystems, Wetzlar, Germany), three slices (5 µm thick) were prepared from different sections of the fixed kidney: a first slice from the middle part of the kidney, a second section is from the part that contained mainly cortex with little amount of medulla, and the third section that is composed mainly of cortex. Samples were washed three times with 0.1 M phosphate-buffered saline (PBS) (10 min per wash), and incubated for 30 min at room temperature in Image-iT Fx signal enhancer (Invitrogen). After rinsing three times with 25 mM Tris-HCl (pH 7.5), 150 mM NaCl,

and 0.05% Tween 20 (TBST) (10 min each), sections were then reacted with rabbit α-EGFP antibody (1:2000; Medical & Biological Laboratories) in TBST supplemented with 1% bovine serum albumin (BSA) at 4°C. On the following day, specimens were rinsed three times with TBST, and then incubated with Alexa Fluor 555-conjugated goat α-rabbit IgG antibody (1:5000; Invitrogen) for 2 h at room temperature. Nuclear DNA was stained with Hoechst 33258 at a final concentration of 0.36 µM. Fluorolabeled sections were examined under a fluorescence microscope (Olympus BX51; Olympus, Tokyo, Japan). Using the cellSens system (Olympus), total cell numbers in each section were first counted automatically. Next, numbers of EGFP-positive cells were counted manually. The frequency of EGFP-positive cells was calculated using the numbers of total and EGFP-positive cells. Three independent sections were prepared from a single specimen and subjected to analysis. The significance of the frequency of EGFP-positive cells was then evaluated statistically.

To identify RTECs positive for L1-RTP, immunohistochemistry was performed as described previously [42] using the following primary antibodies; α-GFP antibody (1:200 dilution) (Abcam, UK), α-AQP1 antibody (1:200 dilution) [43], and Alexa Fluor 546-phalloidin (1:400 dilution) (Invitrogen) [44].

L1-5'UTR methylation status

We performed sodium bisulfite treatment of genomic DNA using the EZ DNA Methylation Kit (Zymo Research, Irvine, CA, USA), according to the manufacturer's instructions. One microlitre of the aliquot was used as the template for combined bisulfite restriction analysis (COBRA) [45]. Primers used for amplification of the L1 transgene promoter region were as follows: forward 5'-GTAAGGGGTTAGGGAGT'TTTT-3' and reverse 5'-CCTTACAATTTAATCTCAAACCTA-3'. The PCR reactions were performed in a volume of 20 µL containing 1 µL of bisulfite-treated genomic DNA, primers (0.3 µM each), and a 10 µL EpiTect MSP Kit (Qiagen, Hilden, Germany). The amplification conditions consisted of 40 cycles of 94°C for 15 sec, 50°C for 30 sec and 72°C for 30 sec. PCR products were digested using the restriction enzyme *Taq* I (New England Biolabs, Ipswich, MA, USA), which is specific for the methylated sequence, after sodium bisulfite treatment. Digested products were resolved by 3% agarose gel electrophoresis and stained with ethidium bromide.

Statistical analysis

Statistical significance was evaluated using the Mann-Whitney U-test. A *P* value < 0.05 was deemed to indicate statistical significance.

Additional file

- Additional file 1: Figure S1.** No cytotoxicity of rVpr.
Additional file 2: Figure S2. Standard curve of qPCR assay with a TaqMan probe.
Additional file 3: Figure S3. L1-RTP induced by low dose of rVpr.
Additional file 4: Table S1. Summary viral titres and L1-RTP activity.
Additional file 5: Figure S4. Detection of Vpr in blood samples of HIV-1 positive patients.
Additional file 6: Table S2. Summary of the PCR-based assay *in vivo*.
Additional file 7: Figure S5. Effects of dAT on rVpr-induced L1-RTP.
Additional file 8: Figure S6. No changes of methylation status of CpG in the L1-5'UTR.
Additional file 9: Figure S7. Inhibitory effects of MNF on rVpr-induced L1-RTP.
Additional file 10: Figure S8. Effects of siRNAs of *AhR*, *ARNT1*, *CREB* and *c-Jun* on expression of endogenous proteins.
Additional file 11: Figure S9. *CYP1A1* expression under down-regulation of *AhR* or *ARNT1*.
Additional file 12: Figure S10. Effects of MAPK inhibitors on rVpr-induced L1-RTP.
Additional file 13: Figure S11. Effects of *AhR* siRNA on chromatin recruitment of ORF1.
Additional file 14: Figure S12. Constitutive association of ORF1 and *AhR* under the conditions competent for the induction of L1-RTP.
Additional file 15: Figure S13. No apparent changes of expression of L1 mRNA after the addition of rVpr.
Additional file 16: Figure S14. L1-RTP by Vpr required a carboxy-terminal region.
Additional file 17: Figure S15. Effects of benzonase on the interaction of *AhR* and ORF1 or Vpr.
Additional file 18: Table S3. Nucleotide sequence of siRNA used in the current study.

Competing interest

All authors declare that they have no competing interest for the current work.

Authors' contributions

NO, MT, YS, KI, MS, AD and SH carried out biochemical analyzes using cell lines, KY, TO and TD, NO, MT, YS, MG, AD and TO performed experiments using hL1-Tg mice, YK, TO, KI and YS established qPCR of L1-RTP, AM and NO analyzed methylation status of CpG in the L1-5'UTR, YS, NO, MT, KI and MY carried out immunohistochemistry of cells positive for rVpr-induced L1-RTP, NO, SH, JT, HG and SO analyzed correlation of the activity of Vpr-induced L1-RTP in blood of HIV-positive patients and clinical manifestations. NO, MB and MT examined the effects of RTIs on rVpr-induced L1-RTP. SK and YI designed experiments. NO, KI, MT, AD, YS and YI were involved in preparation of the manuscript. All authors read and approved the final manuscript.

Acknowledgements

We are grateful to Drs. Elena T. Luning Prak (University of Pennsylvania Medical Center), Gilbert Nicolas (University of Michigan Medical School), and Gabriele Vielhaber (Symrise, Germany) for providing us with pEP06R, pCEP4/L1mneo/ColE1, and MNF, respectively. We thank Ms. Rieko Yanabu-Takanashi for qPCR of the L1 transgenes in the L1-transgenic mice. Mr. Noriyuki Okudaira was an applicant supported by a Grant-in-Aid from the Tokyo Biochemical Research Foundation. This work was supported in part by Grants-in-Aid for Research from the National Center for Global Health and Medicine (22A-113), the Tokyo Biochemical Research Foundation and the Ministry of Health, Labor and Welfare of Japan (09156296).

Author details

¹Department of Intractable Diseases, Research Institute, National Center for Global Health and Medicine, 1-21-1 Toyama, Shinjuku-ku, Tokyo 162-8655, Japan. ²Graduate School of Comprehensive Human Sciences, University of Tsukuba, 1-1-1 Ten-nodai, Tsukuba 305-8577, Japan. ³Department of Laboratory Animal Medicine, Research Institute, National Center for Global Health and Medicine, 1-21-1 Toyama, Shinjuku-ku, Tokyo 162-8655, Japan. ⁴Department of Gastroenterology, Research Center for Hepatitis and Immunology, Research Institute, National Center for Global Health and Medicine, 1-7-1 Kohnodai, Ichikawa, Chiba 272-8516, Japan. ⁵Department of Tropical Medicine and Malaria, Research Institute, National Center for Global Health and Medicine, 1-21-1 Toyama, Shinjuku-ku, Tokyo 162-8655, Japan. ⁶Division of Hematology, Department of Internal Medicine, National Center for Global Health and Medicine, 1-21-1 Toyama, Shinjuku-ku, Tokyo 162-8655, Japan. ⁷AIDS Clinical Center, National Center for Global Health and Medicine, 1-21-1 Toyama, Shinjuku-ku, Tokyo 162-8655, Japan. ⁸Division of Antiviral Chemotherapy, Center for Chronic Viral Diseases, Graduate School of Medical and Dental Sciences, Kagoshima University, Kagoshima 890-8544, Japan. ⁹Department of Nephrology, Graduate School of Medicine, Kyoto University, Shogoin-Kawahara-cho 54, Sakyo-ku, Kyoto 606-8507, Japan. ¹⁰Section of Animal Model, Department of Infectious Diseases, Research Institute, National Center for Global Health and Medicine, 1-21-1 Toyama, Shinjuku-ku, Tokyo 162-8655, Japan. ¹¹Department of Legal Medicine, Hyogo College of Medicine, 1-1 Mukogawa-cho, Nishinomiya, Hyogo 663-8501, Japan. ¹²Kyoto University, Graduate School of Medicine, Medical Innovation Center, Shogoin-Kawahara-cho 53, Sakyo-ku, Kyoto 606-8507, Japan.

Received: 16 November 2012 Accepted: 18 July 2013
Published: 5 August 2013

References

- Cohen EA, Dehni G, Sodroski JG, Haseltine WA: Human immunodeficiency virus vpr product is a virion-associated regulatory protein. *J Virol* 1990, **64**:3097-3099.
- Kogan M, Rappaport J: HIV-1 accessory protein Vpr: relevance in the pathogenesis of HIV and potential for therapeutic intervention. *Retrovirology* 2011, **8**:25.
- Levy DN, Refaeli Y, MacGregor RR, Weiner DB: Serum Vpr regulates productive infection and latency of human immunodeficiency virus type 1. *Proc Natl Acad Sci USA* 1994, **91**:10873-10877.
- Hoshino S, Sun B, Konishi M, Shimura M, Segawa T, Hagiwara Y, Koyanagi Y, Iwamoto A, Mimaya J, Terunuma H, Kano S, Ishizaka Y: Vpr in plasma of HIV-1-positive patients is correlated with the HIV-1 RNA titres. *AIDS Res Hum Retrovir* 2007, **23**:391-397.
- Patel CA, Mukhtar M, Pomerantz RJ: Human immunodeficiency virus type 1 Vpr induces apoptosis in human neuronal cells. *J Virol* 2000, **74**:9717-9726.
- Muthumani K, Choo AY, Premkumar A, Hwang DS, Thieu KP, Desai BM, Weiner DB: Human immunodeficiency virus type 1 (HIV-1) Vpr-regulated cell death: insights into mechanism. *Cell Death Differ* 2005, **12**:962-970.
- Hoshino S, Konishi M, Mori M, Shimura M, Nishitani C, Kuraki Y, Koyanagi Y, Kano S, Itabe H, Ishizaka Y: HIV-1 Vpr induces TLR4/MyD88-mediated IL-6 production and reactivates viral production from latency. *J Leukoc Biol* 2010, **87**:1133-1143.
- Bannert N, Kurth R: Retroelements and the human genome: new perspectives on an old relation. *Proc Natl Acad Sci USA* 2004, **101**:14572-14579.
- Goodier JL, Kazazian HH Jr: Retrotransposons revisited: the restraint and rehabilitation of parasites. *Cell* 2008, **135**:23-35.
- Brouha B, Schustak J, Badge RM, Lutz-Prigge S, Farley AH, Moran JV, Kazazian HH Jr: Hot L1s account for the bulk of retrotransposition in the human population. *Proc Natl Acad Sci USA* 2003, **100**:5280-5285.
- Kazazian HH Jr, Wong C, Youssoufian H, Scott AF, Phillips DG, Antonarakis SE: Haemophilia A resulting from de novo insertion of L1 sequences represents a novel mechanism for mutation in man. *Nature* 1988, **332**:164-166.
- Hancks DC, Kazazian HH Jr: Active human retrotransposons: variation and disease. *Curr Opin Genet Dev* 2012, **22**:1-13.
- Muotri AR, Chu YT, Marchetto MC, Deng W, Moran JV, Gage FH: Somatic mosaicism in neuronal precursor cells mediated by L1 retrotransposition. *Nature* 2005, **435**:903-910.

14. Georgiou I, Noutsopoulos D, Dimitriadou E, Markopoulos G, Apergi A, Lazaros L, Vaxevanoglou T, Pantos K, Syrou M, Tzavaras T: **Retrotransposon RNA expression and evidence for retrotransposition events in human oocytes.** *Hum Mol Genet* 2009, **18**:1221-1228.

15. Kano H, Godoy J, Courtney C, Vetter MR, Gerton GL, Ostertag EM, Kazazian HH Jr: **L1 retrotransposition occurs mainly in embryogenesis and creates somatic mosaicism.** *Genes Dev* 2009, **23**:1303-1312.

16. Coufal NG, Garcia-Perez JL, Peng GE, Yeo GW, Mu Y, Lovci MT, Morell M, O'Shea KS, Moran JV, Gage FH: **L1 retrotransposition in human neural progenitor cells.** *Nature* 2009, **460**:1127-1131.

17. Baillie JK, Barnett MW, Upton KR, Gerhardt DJ, Richmond TA, De Sapio F, Brennan PM, Rizzu P, Smith S, Fell M, Talbot RT, Gustinich S, Freeman TC, Mattick JS, Hume DA, Heutink P, Carninci P, Jeddeloh JA, Faulkner GJ: **Somatic retrotransposition alters the genetic landscape of the human brain.** *Nature* 2011, **479**:534-537.

18. Iskov RC, McCabe MT, Mills RE, Torene S, Pittard WS, Neuwald AF, Van Meir EG, Vertino PM, Devine SE: **Natural mutagenesis of human genomes by endogenous retrotransposons.** *Cell* 2010, **141**:1253-1261.

19. Ting DT, Lipson D, Paul S, Brannigan BW, Akhavanfar S, Coffman EJ, Contino G, Deshpande V, Iafraite AJ, Letovsky S, Rivera MN, Bardeesy N, Maheswaran S, Haber DA: **Aberrant overexpression of satellite repeats in pancreatic and other epithelial cancers.** *Science* 2011, **331**:593-596.

20. Kazazian HH Jr: **Mobile DNA transposition in somatic cells.** *BMC Biol* 2011, **9**:62.

21. Lee E, Iskov R, Yang L, Gokcumen O, Haseley P, Luquette LJ 3rd, Lohr JG, Harris CC, Ding L, Wilson RK, Wheeler DA, Gibbs RA, Kucherlapati R, Lee C, Kharchenko PV, Park PJ, Cancer Genome Atlas Research Network: **Landscape of somatic retrotransposition in human cancers.** *Science* 2012, **337**:967-971.

22. Shukla R, Upton KR, Muñoz-Lopez M, Gerhardt DJ, Fisher ME, Nguyen T, Brennan PM, Baillie JK, Collino A, Ghisletti S, Sinha S, Iannelli F, Radaelli E, Dos Santos A, Rapoud D, Guettier C, Samuel D, Natoli G, Carninci P, Ciccarelli FD, Garcia-Perez JL, Faivre J, Faulkner GJ: **Endogenous retrotransposition activates oncogenic pathways in hepatocellular carcinoma.** *Cell* 2013, **153**:101-111.

23. Gilbert N, Lutz-Prigge S, Moran JV: **Genomic deletions created upon LINE-1 retrotransposition.** *Cell* 2002, **110**:315-325.

24. Symer DE, Connelly C, Szak ST, Caputo EM, Cost GJ, Parmigiani G, Boeke JD: **Human L1 retrotransposition is associated with genetic instability in vivo.** *Cell* 2002, **110**:327-338.

25. Gasior SL, Wakeman TP, Xu B, Deininger PL: **The human LINE-1 retrotransposon creates DNA double-strand breaks.** *J Mol Biol* 2006, **357**:1383-1393.

26. Haouidi A, Semmes OJ, Mason JM, Cannon RE: **Retrotransposition-competent human LINE-1 induces apoptosis in cancer cells with intact p53.** *J Biomed Biotechnol* 2004, **2004**:185-194.

27. Stetson DB, Ko JS, Heidmann T, Medzhitov R: **Trex1 prevents cell-intrinsic initiation of autoimmunity.** *Cell* 2008, **134**:587-598.

28. Okudaira N, Goto M, Yanobu-Takanashi R, Tamura M, An A, Abe Y, Kano S, Hagiwara S, Ishizaka Y, Okamura T: **Involvement of retrotransposition of long interspersed nucleotide element-1 in skin tumorigenesis induced by 7,12-dimethylbenz[*a*]anthracene and 12-O-tetradecanoylphorbol-13-acetate.** *Cancer Sci* 2011, **102**:2000-2006.

29. Okudaira N, Okamura T, Tamura M, Iijima K, Goto M, Matsunaga A, Ochiai M, Nakagama H, Kano S, Fujii-Kuriyama Y, Ishizaka Y: **Long interspersed element-1 is differentially regulated by food-borne carcinogens via the aryl hydrocarbon receptor.** *Oncogene* 2012. in press.

30. Rao TK, Filippone EJ, Nicastri AD, Landesman SH, Frank E, Chen CK, Friedman EA: **Associated focal and segmental glomerulosclerosis in the acquired immunodeficiency syndrome.** *N Engl J Med* 1984, **310**:669-673.

31. Izzedine H, Wirlden M, Launay-Vacher V: **Viral load and HIV-associated nephropathy.** *N Engl J Med* 2005, **353**:1072-1074.

32. Wyatt CM, Mellambro K, Klotman PE: **Recent progress in HIV-associated nephropathy.** *Annu Rev Med* 2012, **63**:147-159.

33. Dickie P, Roberts A, Uwiera R, Wittmer J, Sharma K, Kopp JB: **Focal glomerulosclerosis in proviral and c-fms transgenic mice links Vpr expression to HIV-associated nephropathy.** *Virology* 2004, **322**:69-81.

34. Zhong J, Zuo Y, Ma J, Fogo AB, Jolicœur P, Ichikawa I, Matsusaka T: **Expression of HIV-1 genes in podocytes alone can lead to the full spectrum of HIV-1-associated nephropathy.** *Kidney Int* 2005, **68**:1048-1060.

35. Gilbert N, Lutz S, Morrish TA, Moran JV: **Multiple fates of L1 retrotransposition intermediates in cultured human cells.** *Mol Cell Biol* 2005, **25**:7780-7795.

36. Wei W, Morrish TA, Alish RS, Moran JV: **A transient assay reveals that cultured human cells can accommodate multiple LINE-1 retrotransposition events.** *Anal Biochem* 2000, **284**:435-438.

37. Okudaira N, Iijima K, Koyama T, Minemoto Y, Kano S, Mimori A, Ishizaka Y: **Induction of long interspersed nucleotide element by 6-formylindolo[3,2-*b*]carbazole, a tryptophan photoproduct.** *Proc Natl Acad Sci USA* 2010, **107**:18487-18492.

38. Farkash EA, Kao GD, Horman SR, Prak ET: **Gamma radiation increases endonuclease-dependent L1 retrotransposition in a cultured cell assay.** *Nucleic Acids Res* 2006, **34**:1196-1204.

39. Jones RB, Garrison KE, Wong JC, Duan EH, Nixon DF, Ostrowski MA: **Nucleoside analogue reverse transcriptase inhibitors differentially inhibit human LINE-1 retrotransposition.** *PLoS One* 2008, **3**:e1547.

40. Dai L, Huang Q, Boeke JD: **Effect of reverse transcriptase inhibitors on LINE-1 and Ty1 reverse transcriptase activities and on LINE-1 retrotransposition.** *BMC Biochem* 2011, **12**:18.

41. Yang G, Dutschman EG, Wang CJ, Tanaka H, Baba M, Anderson KS, Cheng YC: **Highly selective action of triphosphate metabolite of 4'-ethynyl DAT: a novel anti-HIV compound against HIV-1 RT.** *Antiviral Res* 2007, **73**:185-191.

42. Asada N, Takase M, Nakamura J, Oguchi A, Asada M, Suzuki N, Yamamura K, Nagoshi N, Shibata S, Rao TN, Fehling HJ, Fukatsu A, Minoguchi N, Kita T, Kimura T, Okano H, Yamamoto M, Yanagita M: **Dysfunction of fibroblasts of extrarenal origin underlies renal fibrosis and renal anemia in mice.** *J Clin Invest* 2011, **121**:3981-3990.

43. Tanaka M, Endo S, Okuda T, Economides AN, Valenzuela DM, Murphy AJ, Robertson E, Sakurai T, Fukatsu A, Yancopoulos GD, Kita T, Yanagita M: **Expression of BMP-7 and USAG-1 (a BMP antagonist) in kidney development and injury.** *Kidney Int* 2008, **73**:181-191.

44. Nürnberger A, Rübiger M, Mack A, Diaz J, Sokoloff P, Mühlbauer B, Luippold G: **Subapical localization of the dopamine D3 receptor in proximal tubules of the rat kidney.** *J Histochem Cytochem* 2004, **52**:1647-1655.

45. Xiong Z, Laird PW: **COBRA: a sensitive and quantitative DNA methylation assay.** *Nucleic Acids Res* 1997, **25**:2532-2534.

46. Flaveny C, Reen RK, Kusnadi A, Perdew GH: **The mouse and human Ah receptor differ in recognition of LXXLL motifs.** *Arch Biochem Biophys* 2008, **471**:215-223.

47. Kino T, Gragerov A, Kopp JB, Stauber RH, Pavlakis GN, Chrousos GP: **The HIV-1 virion-associated protein Vpr is a coactivator of the human glucocorticoid receptor.** *J Exp Med* 1999, **189**:51-62.

48. Fritsche E, Schäfer C, Calles C, Bernsmann T, Bernshausen T, Wurm M: **Lightening up the UV response by identification of the arylhydrocarbon receptor as a cytoplasmic target for ultraviolet B radiation.** *Proc Natl Acad Sci USA* 2007, **104**:8851-8856.

49. Beischlag TV, Luis Morales J, Hollingshead BD, Perdew GH: **The aryl hydrocarbon receptor complex and the control of gene expression.** *Crit Rev Eukaryot Gene Expr* 2008, **18**:207-250.

50. Goodier JL, Mandal PK, Zhang L, Kazazian HH Jr: **Discrete subcellular partitioning of human retrotransposon RNAs despite a common mechanism of genome insertion.** *Hum Mol Genet* 2010, **19**:1712-1725.

51. Doucet AJ, Hulme AE, Sahinovic E, Kulpa DA, Moldovan JB, Kopera HC, Athanikar JN, Hasnaoui M, Bucheton A, Moran JV, Gilbert N: **Characterization of LINE-1 ribonucleoprotein particles.** *PLoS Genet* 2010, **6**:e1001150.

52. Martin SL: **Nucleic acid chaperone properties of ORF1p from the non-LTR retrotransposon, LINE-1.** *BNA Biol* 2010, **7**:706-711.

53. Woodcock DM, Lawler CB, Linsenmeyer ME, Doherty JP, Warren WD: **Asymmetric methylation in the hypermethylated CpG promoter region of the human L1 retrotransposon.** *J Biol Chem* 1997, **272**:7810-7816.

54. Muotri AR, Marchetto MC, Coufal NG, Oefner R, Yeo G, Nakashima K, Gage FH: **L1 retrotransposition in neurons is modulated by MeCP2.** *Nature* 2010, **468**:443-446.

55. Tachiwana H, Shimura M, Nakai-Murakami C, Tokunaga K, Takizawa Y, Sata T, Kurumizaka H, Ishizaka Y: **HIV-1 Vpr induces DNA double-strand breaks.** *Cancer Res* 2006, **66**:627-631.

56. Reiss P, Lange JM, de Ronde A, de Wolf F, Dekker J, Danner SA, Deboucq C, Goudsmit J: **Antibody response to viral proteins U (vpu) and R (vpr) in HIV-1-infected individuals.** *J Acquir Immune Defic Syndr* 1990, **3**:115-122.

doi:10.1186/1742-4690-10-83

Cite this article as: Iijima et al.: **Viral protein R of human immunodeficiency virus type-1 induces retrotransposition of long interspersed element-1.** *Retrovirology* 2013 **10**:83.

Submit your next manuscript to BioMed Central and take full advantage of:

- Convenient online submission
- Thorough peer review
- No space constraints or color figure charges
- Immediate publication on acceptance
- Inclusion in PubMed, CAS, Scopus and Google Scholar
- Research which is freely available for redistribution

Submit your manuscript at
www.biomedcentral.com/submit



Assessment of Antigenemia Assay for the Diagnosis of Cytomegalovirus Gastrointestinal Diseases in HIV-Infected Patients

Yohei Hamada, MD,¹ Naoyoshi Nagata, MD,² Takuro Shimbo, MD, PhD,³ Toru Igari, MD,⁴ Ryo Nakashima, MD,² Naoki Asayama, MD,² So Nishimura, MD,² Hirohisa Yazaki, MD, PhD,¹ Katsuji Teruya, MD, PhD,¹ Hiroyuki Gatanaga, MD, PhD,^{1,5} Yoshimi Kikuchi, MD, PhD,¹ Junichi Akiyama, MD,² Norio Ohmagari, MD,⁶ Naomi Uemura, MD, PhD,⁷ and Shinichi Oka, MD, PhD^{1,5}

Abstract

We conducted a single-center prospective study to evaluate the utility of cytomegalovirus (CMV) antigenemia assay for the diagnosis of CMV-gastrointestinal disease (GID). The study subjects were HIV-infected patients with CD4 count ≤ 200 $\mu\text{L}/\text{cells}$ who had undergone endoscopy. A definite diagnosis of CMV-GID was made by histological examination of endoscopic biopsied specimen. CMV antigenemia assay (C10/C11 monoclonal antibodies), CD4 count, HIV viral load, history of HAART, and gastrointestinal symptoms as measured by 7-point Likert scale, were assessed on the same day of endoscopy. One hundred cases were selected for analysis, which were derived from 110 cases assessed as at high-risk for CMV-GID after endoscopy screening of 423 patients. Twelve patients were diagnosed with CMV-GID. Among the gastrointestinal symptoms, mean bloody stool score was significantly higher in patients with CMV-GID than in those without (2.5 vs. 1.7, $p=0.02$). The area under the receiver-operating characteristic curve of antigenemia was 0.80 (95%CI 0.64–0.96). The sensitivity, specificity, positive likelihood ratio (LR), and negative LR of antigenemia were 75.0%, 79.5%, 3.7, and 0.31, respectively, when the cutoff value for antigenemia was ≥ 1 positive cell per 300,000 granulocytes, and 50%, 92.0%, 5.5, and 0.55, respectively, for ≥ 5 positive cells per 300,000 granulocytes. In conclusion, CMV antigenemia seems a useful diagnostic test for CMV-GID in patients with HIV infection. The use of ≥ 5 positive cells per 300,000 granulocytes as a cutoff value was associated with high specificity and high positive LR. Thus, a positive antigenemia assay with positive endoscopic findings should allow the diagnosis of CMV-GID without biopsy.

Introduction

CYTOMEGALOVIRUS (CMV) IS A MAJOR opportunistic pathogen of gastrointestinal diseases in patients with HIV infection. The incidence of CMV end-organ diseases, including CMV gastrointestinal disease (CMV-GID), has declined significantly following the introduction of highly active antiretroviral therapy (HAART). However, CMV-GID remains an important cause of morbidity and mortality because it can result in massive bleeding and gastrointestinal perforation.^{1–5} There-

fore, diagnosis at an early stage is essential.⁶ Tissue biopsy is invasive and carries the risk of hemorrhage or perforation. Instead, endoscopy with biopsy provides definitive diagnosis.

The CMV blood antigenemia assay is a noninvasive method to detect CMV viremia and its utility has been evaluated previously for the diagnosis of CMV end-organ diseases in patients with HIV infection.^{7–10} However, many of those studies included various types of CMV end-organ diseases such as CMV retinitis and pneumonia. To our knowledge, there are no studies that have investigated the value of

388

CMV antigenemia assay in the diagnosis of CMV-GID, especially in HIV-infected patients.

We conducted a prospective study to assess the utility of the CMV antigenemia assay for the diagnosis of CMV-GID in patients with HIV infection.

Methods

Subjects

We prospectively recruited 423 HIV-infected patients who had undergone endoscopy between 2009 and 2012 at the National Center for Global Health and Medicine (NCGM), a 900-bed hospital located in the Tokyo metropolitan area and the largest referral center for HIV/AIDS in Japan. These patients were generally referred for endoscopy by the attending physician, based on the presence of gastrointestinal symptoms or for asymptomatic screening. Patients with CD4 count ≤ 200 were included in the analysis. We excluded patients who had received endoscopy for follow-up evaluation less than 3 months after treatment of gastrointestinal disease, who were under treatment for other CMV end-organ diseases, and those who were free of antigenemia.

The institutional review board of our hospital approved this study (approval No. 715).

Clinical factors

Gastrointestinal (GI) symptoms, CD4 count, HIV-RNA, history of HAART, and sexual behavior were collected before endoscopy. To evaluate GI symptoms, the modified gastrointestinal symptom rating scale (GSRS) rating on a 7-graded Likert scale was used.^{11,12} The modified GSRS consists of the original GSRS (abdominal pain, heart burn, acid regurgitation, sucking sensation in the epigastrium, nausea and vomiting, borborygmi, abdominal distention, eructation, increased flatus, decreased passage of stools, loose stools, hard stools, urgent need for defecation, feeling of incomplete evacuation), plus odynophagia, chronic diarrhea, and bloody stool. Chronic diarrhea was defined as an episode lasting longer than 4 weeks.

Antigenemia assay

Antigenemia assay using C10/C11 monoclonal antibodies (Mitsubishi Chemical Medience, Tokyo, Japan) was performed as described previously.^{13–15} A positive result of the CMV antigenemia assay was defined as ≥ 1 CMV-positive cell per 300,000 granulocytes applied. The assay was performed on the same day of endoscopy. For patients who were empirically prescribed anti-CMV therapy before endoscopy, CMV antigenemia obtained before initiating the therapy was used for analysis.

Diagnosis of CMV-GID

CMV-GID was suspected based on endoscopic findings, such as patchy erythema, edematous mucosa, multiple erosions, and ulcers.^{16,17} Biopsy was performed when such endoscopic findings were encountered. CMV-GID was defined as the detection of large cells with intranuclear inclusions, alone, or in association with granular cytoplasmic inclusions on histological examination of biopsy specimens.¹ Biopsy sections were stained with hematoxylin and eosin, and also

immunohistochemically stained with anti-CMV. The results were considered positive when the above-mentioned cells showed marked brown coloration in both nuclei and cytoplasm.

Statistical analysis

We divided patients into two groups based on the presence or absence of CMV-GID. Patient characteristics and clinical findings were then compared in the two groups using the Mann-Whitney U test, χ^2 test, and Fisher's exact test for quantitative and qualitative variables, respectively. Area under the receiver-operating characteristic curve (ROC-AUC) analysis was used to quantify the accuracy of CMV antigenemia assay. The sensitivity, specificity, positive predictive value (PPV), and negative predictive value (NPV), positive likelihood ratio (LR), negative LR, and diagnostic odds ratio for the diagnosis of CMV-GID were also calculated for different cutoff values (≥ 1 positive cells per 300,000 granulocytes and ≥ 5 positive cells per 300,000 granulocytes). In a subgroup analysis stratified by patients with and without history of HAART, the sensitivity, specificity, PPV, and NPV were calculated using the cutoff value of CMV-positive cells of ≥ 1 per 300,000 granulocytes. All statistical analyses were performed using Stata software (version 10, Stata Co., USA).

Results

A total of 100 patients were selected for analysis after the application of the aforementioned exclusion criteria (Fig. 1). The majority of patients were males, and the median age was 40. The median CD4 count was 84 [interquartile range (IQR) 33.3–148.8] and 58.0% of the patients had history of HAART. Twelve patients were diagnosed with CMV-GID based on the abovementioned criteria (Fig. 2). In these patients, the median CMV antigenemia value was 4 positive cells per 300,000 granulocytes (range, 0–786). CMV-GID was localized to the upper GI tract in one patient, in the lower GI tract in 11, and in both parts in two.

Table 1 shows the baseline and demographic characteristics of the participating patients. Univariate analysis showed that significantly fewer patients with CMV-GID had history of HAART than those without CMV-GID ($p=0.016$) and median CD4 count was not significantly different between the two groups ($p=0.356$). The number of patients with positive CMV antigenemia was significantly higher in those with CMV-GID than those without ($p<0.01$). The mean bloody stool scores was significantly higher in patients with CMV-GID than in those without CMV-GID ($p=0.021$). In addition, there was a trend toward higher scores for heartburn ($p=0.064$) and chronic diarrhea ($p=0.078$) in patients with CMV-GID. The proportions of patients with the other symptoms were not different between the two groups.

ROC-AUC of the CMV antigenemia assay was 0.80 (95%CI 0.64–0.96). Table 2 lists the data that describe the diagnostic accuracy of CMV antigenemia assay. Using a cutoff value of ≥ 1 positive cell per 300,000 granulocytes for positive CMV antigenemia assay, the sensitivity, specificity, positive LR, and negative LR of antigenemia for CMV-GID were 75.0%, 79.5%, 3.7, and 0.31, respectively. The use of a cutoff value of ≥ 5 positive cells per 300,000 granulocytes yielded 50.0% sensitivity, 90.9% specificity, a positive LR of 5.5, and negative LR of 0.55 for the diagnosis of CMV-GID. Subgroup analysis

¹AIDS Clinical Center, National Center for Global Health and Medicine, Tokyo, Japan.

Departments of ²Gastroenterology and Hepatology, ³Clinical Research and Informatics, International Clinical Research Center Research Institute, ⁴Pathology Division of Clinical Laboratory, ⁵Division of Infectious Diseases, Disease Control and Prevention Center, National Center for Global Health, Tokyo, Japan.

⁶Center for AIDS Research, Kumamoto University, Kumamoto, Japan.

⁷Department of Gastroenterology and Hepatology, National Center for Global Health and Medicine, Kohnodai Hospital, Chiba, Japan.

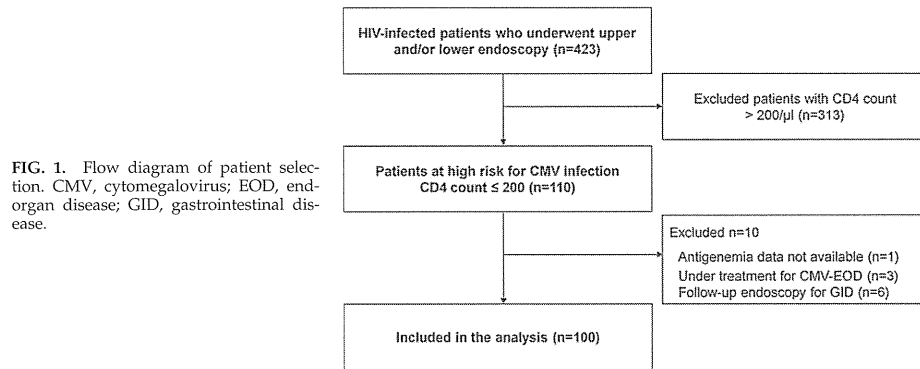


FIG. 1. Flow diagram of patient selection. CMV, cytomegalovirus; EOD, end-organ disease; GID, gastrointestinal disease.

showed a sensitivity of 66.7% and specificity of 83.6% for the assay for patients with history of HAART, while higher sensitivity (77.8%) and lower specificity (72.7%) were noted for those without ART.

Discussion

The present study provides the first prospective analysis of the CMV antigenemia assay in the diagnosis of CMV-GID in HIV-infected patients with 75.0% sensitivity and 79.5% specificity. The antigenemia assay is one of the most widely used methods for detecting reactivation of CMV infection, but only a few studies have examined its diagnostic value for CMV-GID,¹⁸⁻²¹ and all were retrospective in design. Jang et al.²⁰ recently reported that the sensitivity and specificity of

the CMV antigenemia assay for the diagnosis of CMV-GID were 54% and 88%, respectively, in patients with secondary immunodeficiency disease. Nagata et al.²¹ also reported 65.4% sensitivity and 93.6% specificity of the CMV antigenemia assay for CMV-GID in patients with positive endoscopic findings. The present study demonstrated higher sensitivity (75.0%) and lower specificity (79.5%) than those studies. This difference in accuracy could be explained by the difference in the study population since only HIV-infected patients were included in our study, whereas previous studies included a substantial number of patients with immune deficiency due to etiologies other than HIV infection.

The sensitivity of antigenemia assay for the diagnosis of CMV end-organ disease in HIV-infected patients reported in previous studies was generally higher than that in the present

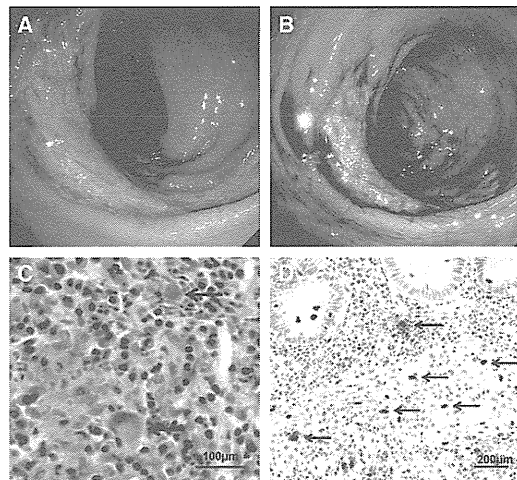


FIG. 2. Endoscopic and pathological features in representative cases. (A) Large distinct ulcer in the sigmoid colon; (B) Ulcer was more clearly observed with indigo carmine; (C) Large cells with intranuclear inclusions or associated with granular cytoplasmic inclusions (hematoxylin and eosin staining); (D) Cytomegalovirus (CMV)-infected cells (arrows) show brown coloration in both nuclei and cytoplasm (immunohistochemical staining with anti-CMV). (Color image can be found at www.liebertonline.com/apc.)

TABLE 1. CLINICAL CHARACTERISTICS OF PATIENTS WITH AND WITHOUT CMV-GID

	CMV-GID (n=12)	Non CMV-GID (n=88)	p Value
Age (IQR)	39 (36-46)	40 (37-51)	0.451
Male gender (%)	11 (91.7)	87 (98.9)	0.227
CD4 count (/μL) (IQR)	68.5 (28.8-123.3)	84 (38.3-151.0)	0.356
HIV viral load (log ₁₀ /mL) (IQR)	4.58 (3.27-5.24)	2.84 (1.60-5.08)	0.084
History of HAART (%)	3 (5.2)	55 (62.5)	0.016
MSM (%)	9 (75.0)	69 (78.4)	0.723
Positive CMV antigenemia (%)	9 (75.0)	18 (20.5)	<0.001
Epigastric pain (SD)	2.5 (2.1)	1.8 (1.3)	0.373
Heartburn (SD)	2.5 (1.5)	1.8 (1.3)	0.064
Nausea and vomiting (SD)	2.4 (1.7)	2.0 (1.5)	0.384
Odynophagia (SD)	2.1 (1.7)	1.7 (1.5)	0.481
Chronic diarrhea (SD)	2.3 (1.3)	1.8 (1.4)	0.078
Bloody stool (SD)	2.5 (2.0)	1.7 (1.5)	0.021

CD4 cell counts within 1 week and HIV-RNA viral load within 1 month were checked at the day of endoscopy. A positive result for real-time HIV RNA was defined as ≥40 copies/mL. History of HAART was collected from the medical records prior to endoscopy. Sexual behavior was defined as men who have sex with men (MSM) or heterosexual.

CMV, cytomegalovirus; GID, gastrointestinal disease; HAART, highly active antiretroviral therapy; IQR, interquartile range; MSM, men who have sex with men; SD, standard deviation.

study.^{8-10,22-26} This difference could be explained by the fact that the current study focused on gastrointestinal disease, while previous studies included various CMV diseases such as retinitis, cholangitis, pneumonia, and encephalitis.^{8-10,22-26} The diagnostic accuracy of CMV antigenemia may vary depending on the site and extent of organ/tissue involvement.

Identification of CMV cells in tissue samples obtained by endoscopic biopsy is considered the gold standard for the diagnosis of CMV-GID.^{1,2,6} The endoscopic findings in CMV-GID include ulcer and mucosal inflammation,^{16,17} however, physicians may not consider it necessary to take a biopsy in patients with only mucosal inflammation without ulceration. Even in cases of severe deep or bleeding ulcers, some physicians may hesitate to perform a biopsy. In such cases, no definite diagnosis of CMV-GID can be made. Our results suggest that the CMV antigenemia assay is to some extent useful for the diagnosis of CMV-GID in patients with endoscopic findings, especially when CMV positive cell counts are high. Considering the high specificity and high positive LR (5.5) of the positive CMV cell count ≥5, the use of this method before endoscopy could potentially avoid complications due to biopsy.

One limitation of this study was the single-center nature of the investigation. Significant differences in independent factors were not detected in the present study probably due to the small number of patients with CMV-GID. For example, we used gastrointestinal symptoms with score of 7 points on the Likert scale, but the differences in most symptoms between patients with or without CMV-GID did not reach statistical significance due to the small number of cases. Further studies based on larger population are needed. Another limitation is a selection bias related to the selection criteria applied in the present study: only patients who underwent endoscopy for such reasons as symptoms and screening were included in the study.

In conclusion, the CMV antigenemia assay showed relatively good sensitivity and specificity for the diagnosis of CMV-GID in patients with HIV infection. Furthermore, specificity and positive LR improved when the cutoff value of CMV cell count was increased from 1 to ≥5 positive cells per 300,000 granulocytes. Considering the high specificity of the test, the use of this method before endoscopy could potentially avoid complications due to biopsy.

TABLE 2. DIAGNOSTIC ACCURACY OF CMV ANTIGENEMIA ASSAY FOR CMV-GID USING DIFFERENT CUTOFF VALUES AND HISTORY OF HAART

	Sensitivity (95%CI)	Specificity (95%CI)	PPV (95%CI)	NPV (95%CI)	LR+ (95%CI)	LR- (95%CI)	OR (95%CI)
CMV antigenemia ≥1 positive cell	75.0% (42.8-94.5)	79.5% (69.6-87.4)	33.3% (16.5-54.0)	95.9% (85.9-99.1)	3.7 (2.2-6.2)	0.31 (0.11-0.84)	11.7 (3.1-44)
CMV antigenemia ≥5 positive cells	50.0% (21.1-78.9)	90.9% (82.9-96.0)	42.9% (17.7-71.1)	93% (85.4-97.4)	5.5 (2.3-13.1)	0.55 (0.31-0.97)	10.0 (2.7-37.1)
History of HAART							
Yes ^a	66.7% (9.4-99.2)	83.6% (71.2-92.2)	18.2% (2.3-51.8)	97.9% (88.7-99.9)	3.7 (2.2-6.2)	0.31 (0.11-0.84)	10.2 (1.2-NA)
No ^a	77.8% (40.0-97.2)	72.7% (54.5-86.7)	43.8% (19.8-70.1)	92.3% (74.9-99.1)	2.9 (1.5-5.5)	0.31 (0.88-1.1)	9.33 (1.79-NA)

^aCutoff value of ≥1 positive cell per 300,000 granulocytes was used in the analysis. CMV, cytomegalovirus; HAART, highly active antiretroviral therapy; LR+, positive likelihood ratio; LR-, negative likelihood ratio; NPV, negative predictive value; OR, odds ratio; PPV, positive predictive value.

Acknowledgments

We are grateful to Hisae Kawashiro (Clinical Research Coordinator) for help with data collection. The authors thank all other clinical staff at the AIDS Clinical Center and all the staff of the endoscopy unit.

This work was supported by Grants-in Aid for AIDS research from the Japanese Ministry of Health, Labor, and Welfare (H23-AIDS-001), and the Global Center of Excellence Program (Global Education and Research Center Aiming at the Control of AIDS) from the Japanese Ministry of Education, Science, Sports and Culture.

Author Disclosure Statement

The other authors declare no conflict of interest.

References

- Goodgame RW. Gastrointestinal cytomegalovirus disease. *Ann Intern Med* 1993;119:924–935.
- Baroco AL, Oldfield EC. Gastrointestinal cytomegalovirus disease in the immunocompromised patient. *Curr Gastroenterol Rep* 2008;10:409–416.
- Toogood GJ, Gillespie PH, Gujral S, et al. Cytomegalovirus infection and colonic perforation in renal transplant patients. *Transpl Int* 1996;9:248–251.
- Almeida N, Romaozinho JM, Amaro P, Ferreira M, Cipriano MA, Leita MC. Fatal mid-gastrointestinal bleeding by cytomegalovirus enteritis in an immunocompetent patient. *Acta Gastroenterol Belg* 2009;72:245–248.
- Frank D, Raicht RF. Intestinal perforation associated with cytomegalovirus infection in patients with acquired immune deficiency syndrome. *Am J Gastroenterol* 1984;79:201–205.
- Korkmaz M, Kunefeci G, Selcuk H, et al. The role of early colonoscopy in CMV colitis of transplant recipients. *Transplant Proc* 2005;37:3059–3060.
- Skies DJ, Crosby C. CMV pp65 antigen testing is of limited utility in the diagnosis of concomitant CMV disease in HIV-infected patients in the HAART era. *J Clin Virol* 2003;28:203–213.
- Podzamczar D, Ferrer E, Garcia A, et al. pp65 antigenemia as a marker of future CMV disease and mortality in HIV-infected patients. *Scand J Infect Dis* 1997;29:223–227.
- Bek B, Boeckh M, Lepenies J, et al. High-level sensitivity of quantitative pp65 cytomegalovirus (CMV) antigenemia assay for diagnosis of CMV disease in AIDS patients and follow-up. *J Clin Microbiol* 1996;34:457–459.
- Wattanamoto P, Clayton JL, Kopicko JJ, et al. Comparison of three assays for cytomegalovirus detection in AIDS patients at risk for retinitis. *J Clin Microbiol* 2000;38:727–732.
- Svedlund J, Sjodin I, Dotevall G. GRS—A clinical rating scale for gastrointestinal symptoms in patients with irritable bowel syndrome and peptic ulcer disease. *Dig Dis Sci* 1988;33:129–134.
- Revicki DA, Wood M, Wiklund I, Crawley J. Reliability and validity of the Gastrointestinal Symptom Rating Scale in patients with gastroesophageal reflux disease. *Qual Life Res* 1998;7:75–83.
- Gondo H, Minematsu T, Harada M, et al. Cytomegalovirus (CMV) antigenemia for rapid diagnosis and monitoring of CMV-associated disease after bone marrow transplantation. *Br J Haematol* 1994;86:130–137.
- Kanda Y, Mineishi S, Saito T, et al. Pre-emptive therapy against cytomegalovirus (CMV) disease guided by CMV antigenemia assay after allogeneic hematopoietic stem cell transplantation: a single-center experience in Japan. *Bone Marrow Transplant* 2001;27:437–444.
- Mori T, Okamoto S, Matsuoka S, et al. Risk-adapted pre-emptive therapy for cytomegalovirus disease in patients undergoing allogeneic bone marrow transplantation. *Bone Marrow Transplant* 2000;25:765–769.
- Rene E, Marche C, Chevalier T, et al. Cytomegalovirus colitis in patients with acquired immunodeficiency syndrome. *Dig Dis Sci* 1988;33:741–750.
- Ljungman P, Griffiths P, Paya C. Definitions of cytomegalovirus infection and disease in transplant recipients. *Clin Infect Dis* 2002;34:1094–1097.
- Mori T, Mori S, Kanda Y, et al. Clinical significance of cytomegalovirus (CMV) antigenemia in the prediction and diagnosis of CMV gastrointestinal disease after allogeneic hematopoietic stem cell transplantation. *Bone Marrow Transplant* 2004;33:431–434.
- Fica A, Cervera C, Perez N, et al. Immunohistochemically proven cytomegalovirus end-organ disease in solid organ transplant patients: Clinical features and usefulness of conventional diagnostic tests. *Transpl Infect Dis* 2007;9:203–210.
- Jang EY, Park SY, Lee EJ, et al. Diagnostic performance of the cytomegalovirus (CMV) antigenemia assay in patients with CMV gastrointestinal disease. *Clin Infect Dis* 2009;48:e121–124.
- Nagata N, Kobayakawa M, Shimbo T, et al. Diagnostic value of antigenemia assay for cytomegalovirus gastrointestinal disease in immunocompromised patients. *World J Gastroenterol* 2011;17:1185–1191.
- Pannuti CS, Kallas EG, Muccioli C, et al. Cytomegalovirus antigenemia in acquired immunodeficiency syndrome patients with untreated cytomegalovirus retinitis. *Am J Ophthalmol* 1996;122:847–852.
- Boivin G, Handfield J, Murray G, et al. Quantitation of cytomegalovirus (CMV) DNA in leukocytes of human immunodeficiency virus-infected subjects with and without CMV disease by using PCR and the SHARP Signal Detection System. *J Clin Microbiol* 1997;35:525–526.
- Wetherill PE, Landry ML, Alcibes P, Friedland G. Use of a quantitative cytomegalovirus (CMV) antigenemia test in evaluating HIV+ patients with and without CMV disease. *J Acquir Immune Defic Syndr Hum Retrovirol* 1996;12:33–37.
- Salzberger B, Franzen C, Fatkenheuer G, et al. CMV-antigenemia in peripheral blood for the diagnosis of CMV disease in HIV-infected patients. *J Acquir Immune Defic Syndr Hum Retrovirol* 1996;11:365–369.
- Pellegrin I, Garrigue I, Binquet C, et al. Evaluation of new quantitative assays for diagnosis and monitoring of cytomegalovirus disease in human immunodeficiency virus-positive patients. *J Clin Microbiol* 1999;37:3124–3132.

Address correspondence to:
Naoyoshi Nagata, M.D.

Department of Gastroenterology and Hepatology
National Center for Global Health and Medicine
1-21-1, Toyama, Shinjuku-ku
Tokyo 162-8655
Japan

E-mail: nnagata_ncgm@yahoo.co.jp

CD8⁺ T Cell Cross-Reactivity Profiles and HIV-1 Immune Escape towards an HLA-B35-Restricted Immunodominant Nef Epitope

Chihiro Motozono^{1,2}, John J. Miles^{1,3,4}, Zafrul Hasan², Hiroyuki Gatanaga^{2,5}, Stanley C. Meribe², David A. Price¹, Shinichi Oka^{2,5}, Andrew K. Sewell^{1*9}, Takamasa Ueno^{2*9}

1 Institute of Infection and Immunity, Cardiff University School of Medicine, Heath Park, Cardiff, United Kingdom, **2** Center for AIDS Research, Kumamoto University, Kumamoto, Japan, **3** Australian Centre for Vaccine Development, Human Immunity Laboratory, Queensland Institute of Medical Research, Brisbane, Australia, **4** School of Medicine, The University of Queensland, Brisbane, Australia, **5** AIDS Clinical Center, National Center for Global Health and Medicine, Tokyo, Japan

Abstract

Antigen cross-reactivity is an inbuilt feature of the T cell compartment. However, little is known about the flexibility of T cell recognition in the context of genetically variable pathogens such as HIV-1. In this study, we used a combinatorial library containing 24 billion octamer peptides to characterize the cross-reactivity profiles of CD8⁺ T cells specific for the immunodominant HIV-1 subtype B Nef epitope VY8 (VPLRPMTY) presented by HLA-B*35:01. In conjunction, we examined naturally occurring antigenic variations within the VY8 epitope. Sequence analysis of plasma viral RNA isolated from 336 HIV-1-infected individuals revealed variability at position (P) 3 and P8 of VY8; Phe at P8, but not Val at P3, was identified as an HLA-B*35:01-associated polymorphism. VY8-specific T cells generated from several different HIV-1-infected patients showed unique and clonotype-dependent cross-reactivity footprints. Nonetheless, all T cells recognized both the index Leu and mutant Val at P3 equally well. In contrast, competitive titration assays revealed that the Tyr to Phe substitution at P8 reduced T cell recognition by 50–130 fold despite intact peptide binding to HLA-B*35:01. These findings explain the preferential selection of Phe at the C-terminus of VY8 in HLA-B*35:01⁺ individuals and demonstrate that HIV-1 can exploit the limitations of T cell recognition *in vivo*.

Citation: Motozono C, Miles JJ, Hasan Z, Gatanaga H, Meribe SC, et al. (2013) CD8⁺ T Cell Cross-Reactivity Profiles and HIV-1 Immune Escape towards an HLA-B35-Restricted Immunodominant Nef Epitope. *PLoS ONE* 8(6): e66152. doi:10.1371/journal.pone.0066152

Editor: Paul A. Goepfert, University of Alabama, United States of America

Received: January 10, 2013; **Accepted:** May 1, 2013; **Published:** June 17, 2013

Copyright: © 2013 Motozono et al. This is an open-access article distributed under the terms of the Creative Commons Attribution License, which permits unrestricted use, distribution, and reproduction in any medium, provided the original author and source are credited.

Funding: This research was supported by a grant-in-aid for scientific research and a Global COE Program (Global Education and Research Center Aiming at the Control of AIDS) from the Ministry of Education, Science, Sports, and Culture (MEXT), and by a grant-in-aid for AIDS research from the Ministry of Health, Labor, and Welfare of Japan (to T.U.). ZH and SCM are supported by scholarships from The International Priority Graduate Programs, MEXT. JJM is a National Health and Medical Research Council (NHMRC) Career Development Fellow. The authors' studies of TCR binding degeneracy were made possible by generous support from the Biotechnology and Biological Sciences Research Council (grant BB/H001085/1 to AKS and DAP). The funders had no role in study design, data collection and analysis, decision to publish, or preparation of the manuscript.

Competing Interests: The authors have declared that no competing interests exist.

* E-mail: uenotaka@kumamoto-u.ac.jp (TU); sewellak@cardiff.ac.uk (AKS)

9 These authors contributed equally to this work.

Introduction

Hypervariable viruses such as HIV-1 can escape from human leukocyte antigen class I (HLA-I)-restricted CD8⁺ T cell responses by acquiring viral genomic mutations within or near immunogenic epitopes. Such immune escape pathways can be extremely reproducible and broadly predictable based on host HLA-I alleles at a population level [1,2]. Somewhat paradoxically, however, antigen cross-reactivity is an inbuilt feature of the T cell compartment [3,4]. Indeed, a single autoimmune T cell receptor (TCR) has recently been shown to recognize more than a million different peptides within a broad cross-reactivity profile encompassing unrelated amino acid substitutions [5]. Furthermore, several lines of evidence suggest that certain CD8⁺ T cell subsets with the capacity to cross-recognize naturally occurring viral variants are advantageous for viral control *in vivo* [6–11]. However, the true extent of HIV-1-specific T cell cross-reactivity remains elusive. In the present study, we characterized the cross-reactivity footprints of HIV-1-specific CD8⁺ T cells using combinatorial peptide library (CPL) scanning to cover all possible amino acid variations at each position of an octamer epitope.

Additionally, we analyzed antigenic variation within the targeted epitope region of HIV-1 subtype B. Our investigations focused on CD8⁺ T cell responses specific for the immunodominant HIV-1 Nef epitope VY8 (VPLRPMTY) presented by HLA-B*35:01 [12,13].

Materials and Methods

Ethics Statement

All study participants provided informed, written consent at the AIDS Clinical Center, National Center for Global Health and Medicine, Japan. The study was approved by the Institutional Review Board of Kumamoto University and National Center for Global Health and Medicine.

Sequence Analysis of Autologous HIV-1

Treatment-naïve individuals (n = 336) with chronic HIV-1 infection (>90% subtype B) attending the AIDS Clinical Center (International Medical Center of Japan) were enrolled for autologous HIV-1 sequence analysis. The median [IQR] plasma viral load was 95,000 [31,000–350,000] copies/ml; the median

Table 1. TCR β composition of CD8⁺ T cell lines.

Patient	β chain			
	V gene	J gene	CDR3 sequence	Frequency
Pt-100	BV2*01	BJ2-7*01	CASSGEGNVEQYF	1/31
			CASITDRVVEQYF	1/31
	BV3-1*01	BJ2-5*01	CASSTSSVTETQYF	2/31
		BJ2-7*01	CASSQDIAGVHEQYF	1/31
	BV4-1*01	BJ2-1*01	CASSQTSGSYNEQFF	1/31
	BV6-1*01	BJ1-5*01	CASSEASGIYEQYF	1/31
		BJ2-7*01	CASSEASGIYEQYF	1/31
	BV10-1*01	BJ2-1*01	CASSAAGVEVNEQFF	1/31
	BV11-2*01	BJ1-1*01	CASSFDIVNTEAFF	1/31
		BJ2-1*01	CASSPDLVDNEQFF	4/31
		BJ2-5*01	CASSGAWTGGGETQYF	2/31
		BJ2-7*01	CASSLDLVSYEQYF	1/31
			CASSLGIGRAYEQYF	1/31
	BV12-3*01	BJ1-4*01	CASSRFATNKLFF	1/31
	BV27*01	BJ2-5*01	CASSFDTNQETQYF	1/31
		BJ2-7*01	CASSLDTNGYEQYF	1/31
			CASSFQLAGVHGQYF	1/31
			CASSPRLDDEQYF	2/31
			CASSLDTSGYEQYF	2/31
			CASSDRDRESHEQYF	2/31
Pt-168	BV28*01	BJ2-2*01	CASSSTDAIPNTGELFF	1/31
		BJ2-3*01	CASSLPLDSTDTQYF	1/31
		BJ2-7*01	CASSEGGRYEQYF	1/31
	BV2*01	BJ2-7*01	CASSESLAGGPYEQYF	7/31
	BV3-1*01	BJ2-3*01	CASSQEGADTQYF	2/31
	BV3-1*02	BJ2-3*01	CASSQEGAGTQYF	1/31
	BV6-2*01	BJ1-1*01	CASSGGRDTEAFF	1/31
		BJ2-1*01	CASSYERDSENGEQFF	1/31
	BV11-2*01	BJ2-7*01	CASSLDVAGSYEQYF	1/31
			CASSLDIVSYEQYF	1/31
	BV11-3*03	BJ2-3*01	CASSLVLTGTDTQYF	1/31
	BV12-3*01	BJ2-3*01	CASSWDSISTDTQYF	1/31
		BJ2-7*01	CASSSDGYEQYF	3/31
	BV12-5*01	BJ2-2*01	CASSGLAMVSGELFF	1/31
	BV15*02	BJ2-1*01	CATSRLDVEDEQFF	2/31
BV20-1*05	BJ2-2*01	CSARDPRTDRGNTGELFF	1/31	
BV24-1*01	BJ2-3*01	CATSVRDLDTGPNQDTQYF	2/31	
BV27*01	BJ2-3*01	CASSLDLRPDTQYF	1/31	
BV28*01	BJ2-5*01	CASSLLGETRETQYF	4/31	
BV30*01	BJ2-5*01	CAWHTVRVQETQYF	1/31	

doi:10.1371/journal.pone.0066152.t001

[IQR] CD4⁺ T cell count was 242 [64.5–367.5] cells/mm³. We determined autologous *nef* sequences from plasma viral RNA using a previously reported direct sequencing method [13].

Table 2. TCR β composition of CD8⁺ T cell clones.

Patient	Clone	β chain		
		V gene	J gene	CDR3 sequence
Pt-19	19-136	BV7-2*03	BJ2-1*01	CASSPTPGQDYEQFF
	19-139	BV11-2*01	BJ1-1*01	CASSLDLVSTEAFF
	33-S1	BV4-2*01	BJ2-3*01	CASSQAADAAITDADTQYF
Pt-100	100-K51	BV27*01	BJ2-5*01	CASSFDTNQETQYF
	100-K105	BV11-2*01	BJ1-1*01	CASSFDIVNTEAFF
	100-K810	BV27*01	BJ2-7*01	CASSFQLAGVHGQYF

doi:10.1371/journal.pone.0066152.t002

Generation and Maintenance of CD8⁺ T cell Lines and Clones

The CD8⁺ T cell clones (19-136, 19-139 and 33-S1) were established previously [13]. Additional CD8⁺ T cell lines and clones were generated by VY8 peptide stimulation of peripheral blood mononuclear cells (PBMCs) isolated from *HLA-B*35:01*⁺ individuals with chronic HIV-1 infection (Pt-100 and Pt-168) with 10 nM of VY8 (VPLRPMTY) peptide. The Institutional Review Board of the National Center for Global Health and Medicine approved both taking samples and generating cell lines, and patients provided the written informed consent. All CD8⁺ T cell lines and clones were maintained in RPMI 1640 supplemented with 10% fetal calf serum, 10 IU recombinant human interleukin (IL)-2, antibiotics and L-glutamine.

Analysis of TCR-encoding Genes

TCR-encoding genes of CD8⁺ T cell lines and clones were obtained by using a SMART PCR cDNA synthesis kit (Clontech) and analyzed with reference to the ImmMunoGeneTics database (<http://imgt.cines.fr>) as described previously [14].

T cell Sensitivity Assay

Secretion of cytokines and chemokines by virus-specific CD8⁺ T cells in response to specific antigen provides a useful tool for quantitative assessment of antigen recognition [15,16]. MIP-1β was used as a functional readout in this study since it is one of the most sensitive means to assess functional avidity of human CD8⁺ T cells as previously described [15–17]. Briefly, 3 × 10⁴ T cells were mixed with 6 × 10⁴ HLA-B*35:01-expressing C1R cells (C1R-B3501), either unpulsed or pulsed with cognate peptide across a range of concentrations. After overnight incubation at 37°C, the supernatant was harvested and assayed for MIP-1β content by ELISA as described previously [5,17]. The amount of MIP-1β released in the absence of the peptide was subtracted as background. It should be noted that the VY8 peptide titration experiments of T cell clones 136 and 139 exhibited comparable results when IFN-γ [13] and MIP-1β were used as readouts (data not shown).

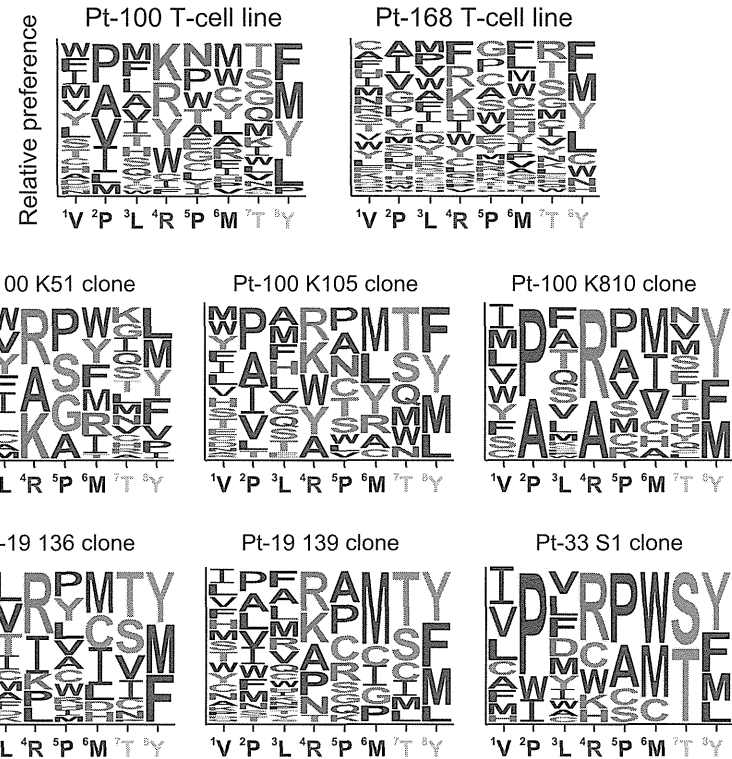


Figure 1. Amino acid residues preferentially recognized by VY8-specific CD8⁺ T cells. Graphical representation showing relative preference for amino acid residues recognized by VY8-specific T cell lines and clones based on the CPL scan data shown in Figure S1. Responses >20% were included. A web-based application, WebLogo 3 (<http://weblogo.threeplusone.com/>), was used to generate the graphic. Colours represent physicochemical properties: polar (G, S, T, Y and C), green; neutral (Q and N), purple; basic (K, R and H), blue; acidic (D and E), red; hydrophobic (A, V, L, I, P, W, F and M), black. The index residues at each position are outlined in yellow. Residue size is proportional to T cell recognition preference. doi:10.1371/journal.pone.0066152.g001

Octamer Combinatorial Peptide Library (CPL) Scan

The octamer CPL contained a total of 2.4 × 10¹⁰ different peptides (PepScan) divided into 160 sub-mixtures in positional scanning format as described previously [4,18]. Target C1R-B3501 cells (6 × 10⁴ cells/well) were pre-incubated in the absence or presence of CPL sub-mixtures (100 μg/ml). Effector T cells (3 × 10⁵ cells/well) were then added and incubated overnight at 37°C. Supernatant was collected and analyzed for MIP-1β content by ELISA as described previously [5,17]. Background-subtracted results were expressed as % response, normalized with respect to the VY8 index residue. A response >20% was considered positive.

Results and Discussion

Clonotypic Characterization of VY8-specific T cells

CD8⁺ T cell lines were established from two *HLA-B*35:01*⁺ individuals with chronic HIV-1 infection (Pt-100 and Pt-168).

Analysis of TCR β usage by these T cell lines revealed multiple clonotypes, with 23 and 17 distinct TCR β sequences for Pt-100 and Pt-168, respectively (Table 1). This observation is consistent with previous studies showing the oligoclonal nature of immunodominant HIV-1-specific CD8⁺ T cell populations [19,20]. The CD8⁺ T cell clones K51, K105 and K810 were generated from patient Pt-100 by limiting dilution of VY8-specific T cell lines. Monoclonality was confirmed by TCR β analysis and all three sequences were encompassed within the TCR repertoire of the parental T cell lines (Table 2). Additional CD8⁺ T cell clones (136, 139, and S1) previously established from two separate *HLA-B*35:01*⁺ HIV-1-infected individuals [12,13] showed distinct TCR β chain usage (Table 2) and were also used for cross-reactivity studies.